Summer 8-31-2020

A Synthesis Program: Reducing Uncertainties of the Terrestrial Biosphere Carbon Cycle at Various Spatio Temporal Scales

Xinyuan Wei
University of Maine, xinyuan.wei@maine.edu

A SYNTHESIS PROGRAM: REDUCING UNCERTAINTIES OF THE TERRESTRIAL BIOSPHERE CARBON CYCLE AT VARIOUS SPATIO-TEMPORAL SCALES

By

Xinyuan Wei

B.E. Nanjing Forest University, 2013

M.S. University at Buffalo, SUNY, 2015

A DISSERTATION

Submitted in Partial Fulfillment of the

Requirements for the Degree of

Doctor of Philosophy

(in Forest Resources)

The Graduate School

The University of Maine

August 2020

Advisory Committee:

Daniel Hayes, Assistant Professor of Geospatial Analysis & Remote Sensing, Advisor

Aaron Weiskittel, Professor of Forest Biometrics and Modeling

Ivan Fernandez, Professor of Soil Science

Nathaniel Brunsell, Professor of Natural Sciences and Mathematics

Shawn Fraver, Associate Professor of Forest Ecology

A SYNTHESIS PROGRAM: REDUCING UNCERTAINTIES OF THE TERRESTRIAL BIOSPHERE CARBON CYCLE AT VARIOUS SPATIO-TEMPORAL SCALES

By Xinyuan Wei

Dissertation Advisor: Dr. Daniel Hayes

An Abstract of the Dissertation Presented
in Partial Fulfillment of the Requirements for the
Degree of Doctor of Philosophy
(in Forest Resources)
August 2020

The terrestrial biosphere plays an important role in the global carbon cycle, and disturbance fire and climate extreme drought have strong direct and indirect impacts on the carbon fluxes. In addition, the lateral dissolved organic carbon (DOC) flux from soils to inland waters represents an important component of the terrestrial biosphere carbon cycle.

Fires play an important role in the terrestrial biosphere carbon cycle, not only through direct carbon release but also contributing to a potential long-term storage as pyrogenic carbon (PyC). PyC is formed through fires, and because it may resist further biological and chemical degradation, is more stable in soil and sediment than original biomass. The chapter 1 presents estimates of global PyC production.

Worldwide, droughts are becoming more frequent with increasing weather extremes, resulting in substantial impacts on land-atmosphere carbon exchange. However, the patterns of carbon fluxes in response to droughts differ across biomes and time scales due to variations in the adaptation and resilience of different plant species, soil properties, and

available water and nutrients. In chapter 2, I examined the biome-scale spatial patterns in the response of carbon fluxes to droughts at different time scales.

The export of dissolved organic carbon (DOC) from a watershed is a critical flux of terrestrial biosphere carbon cycles. Advanced understanding of how environmental factors drive the temporal patterns of this biogeochemical process and their relative magnitudes of impacts is necessary to accurately model and evaluate terrestrial carbon storage and fluxes. In chapter 3, I examined the impacts of environmental factors on the temporal patterns of DOC export and their relative magnitudes, as well as the autocorrelation of DOC export. The lateral flux of dissolved organic carbon (DOC) from soils to inland waters and ultimately delivered to the ocean represents a fundamental component of the global carbon cycle. To estimate the production, delivery and potential fates of DOC flux from terrestrial through aquatic ecosystems to the ocean, I developed a process-based terrestrial-aquatic DOC fluxes model (TAF-DOC), which has the ability to estimate the spatial and temporal dynamics of DOC flux through incorporating various environmental factors.

DEDICATION

I would like to dedicate my thesis to my beloved parents.

ACKNOWLEDGEMENTS

I would like to express my gratitude to my advisor, Daniel Hayes, for his continuous support, patience, and encouragement throughout my studies. His guidance has given me room and encouragement to explore many bizarre research paths.

I also owe thanks to Aaron Weiskittel, Shawn Fraver, Ivan Fernandez, and Nathaniel Brunsell. They have provided me with innumerable assistance in my research. They helped me with problems large and small, and have consistently been my greatest advocates.

Finally, I would also like to thank the many researchers who have made their field and data available to me.

TABLE OF CONTENTS

LIST OF TABLES

LIST OF FIGURES

LIST OF EQUATIONS

CHAPTER 1

1. GLOBAL PYROGENIC CARBON PRODUCTION DURING RECENT DECADES HAS CREATED THE POTENTIAL FOR A LARGE, LONG-TERM SINK OF ATMOSPHERIC CO_2

1.1 Introduction

Fires, as worldwide ecological disturbances, appeared in the geological record soon after the appearance of terrestrial plants. Fires strongly influence the terrestrial carbon cycle across a broad range of spatial and temporal scales by transferring carbon between ecosystem pools and the atmosphere, as well as through the legacy effects of resetting succession (Giglio et al., 2013; Wei and Larsen, 2019). Fires directly convert carbon stored in biomass, including litter and soil organic matter, to gaseous and particulate forms, which are released to the atmosphere (Forbes et al., 2006; Wei and Larsen, 2018). These gases consist primarily (>90%) of CO_2, but also include CO, CH_4, and CH_3Cl (Crutzen and Andreae, 1990). At the same time, a portion of organic carbon is thermochemically converted to recalcitrant pyrogenic carbon (PyC, also named as black carbon, charred biomass, soot, or colloquially as charcoal), which is formed from the combustion of organic matter through biomass burning (Bird et al., 2017; Wagner et al., 2018).

PyC includes a range of particle sizes, from mainly macroscopic charcoal and partially charred vegetation material that remains on site, to small particles in smoke that may remain in the atmosphere for over a week and thus transported far from the site of origin

(Cooke and Wilson, 1996). Due to its more chemically and biologically stable properties, when compared to original biomass (Kuzyakov et al., 2014; Santín et al., 2015), PyC may have a relative long residence time (e.g. Cotrufo et al., 2016; Singh et al., 2014). Assuming the post-fire carbon can recover to the pre-fire status, PyC may thus serve as a long-term, stable sink that is distributed globally via fluvial and atmospheric transport to become a ubiquitous component in soil, lacustrine, and marine sediment (Santín et al., 2016).

Fuel type, fire intensity, and weather conditions codetermine PyC production during fires (Czimczik et al., 2005; Schmidt and Noack, 2000). Previous studies have explored PyC production rates across various biomes; these rates may be estimated in one of the three ways: (1) the ratio of carbon contained in PyC to that directly released as CO_2 through a burning event (PyC/CO_2) (e.g. Hao et al., 1990; Kuhlbusch and Crutzen, 1996); (2) the ratio of carbon contained in PyC to the carbon exposed to the fire (PyC/C exposed) (e.g. Santín et al., 2015); or (3) the ratio of carbon contained in PyC to the carbon consumed through burning (PyC/C consumed) (e.g. Forbes et al., 2006; Santín et al., 2016). If these ratios were relatively constant within a biome, and the denominators were reasonably estimated, PyC production from fires could be quantified at the biome-, continental-, and global-scale (e.g. Crutzen and Andreae, 1990; Forbes et al., 2006; Kuhlbusch et al., 1996; Preston and Schmidt, 2006; Santín et al., 2016).

Given the substantial impact of fires on the global carbon cycle (van der Werf et al., 2017), improved estimates of PyC production are necessary to better understand, quantify and model the global carbon cycle. Several previous studies have estimated PyC production at the

global scale (e.g. Bird et al., 2015; Kuhlbusch and Crutzen, 1995; Santín et al., 2016), but none have incorporated the full set of biome-specific conversion ratios to characterize and quantify the temporally- and spatially-explicit patterns of PyC production from global vegetation burning. The objectives of our study were to (1) update the estimate of PyC produced by global fires using detailed, biome-scale PyC-carbon ratios obtained from previous studies, and (2) present the spatio-temporal and inter-annual variations of CO_2 emissions and PyC production from global fires in the period of 2000-2016.

1.2 Materials and Methods

1.2.1 Estimates for Fire-caused CO_2 Emissions

The magnitude and rate of carbon emissions to the atmosphere from fires over large regions has been quantified and extrapolated based on inventories and ecosystem models (e.g. French et al., 2011; Kasischke et al., 2013). Using the inventory-based burned area data along with meteorological information, vegetation characteristics, and emission factors for different land ecosystems, such approaches can estimate the CO_2 released from global fires (van der Werf et al., 2017). Here we use existing estimates of fire emissions from previous simulation results from two distinct, process-based carbon cycle models, namely the Global Fire Emissions Database (van der Werf et al., 2017) and the Terrestrial Ecosystem Model (Hayes et al., 2011). Because neither model directly estimates PyC production from fires, we used the CO_2 emissions estimates provided by these model results, along with published biome-specific PyC/CO_2 ratios, to estimate the spatial and temporal patterns of global PyC production.

The Global Fire Emissions Database version 4 (GFED4; Giglio et al., 2013; van der Werf et al., 2010) provides a framework for assessing the impact of fires on the terrestrial biosphere carbon cycle, including global burned area and monthly emissions during 1997-2016. The monthly emissions are estimated based on observed burn area data and active fire information classified from MODIS imagery, land cover characteristics, and meteorological data (Giglio et al., 2013). Carbon in biomass and soil organic matter representing fuels in combustion are simulated with a revised version of the Carnegie-Ames-Stanford Approach (CASA) biogeochemical model (van der Werf et al., 2017). In the latest version, GFED4s (van der Werf et al., 2017), "s" means that burned area caused by small fires estimated by models is included in this database, which provides global CO_2 emissions at monthly time step and 0.25° spatial resolution. In our analysis, the worldwide monthly CO_2 emissions from 2000 to 2016 were used to estimate PyC resulting from fires.

The Terrestrial Ecosystem Model version 6 (TEM6; Chen et al., 2017; Hayes et al., 2011) is within the class of process-based terrestrial biosphere models (McGuire et al., 2000) that simulate the dynamics of carbon, nitrogen, and water through plants and soils as determined by climate, atmospheric chemistry, land use and disturbances (Huntzinger et al., 2017; McGuire et al., 2000). TEM6 has been used to examine terrestrial carbon dynamics at various spatial scales and monthly temporal resolution (e.g. Hayes et al., 2011). It was modified by Balshi et al. (2007) to simulate the changes of carbon pools resulting from fires in pan-boreal region, and further modified and applied to estimate the carbon fluxes and storage from burning over large regions (e.g. Chen et al., 2017). In our study, TEM6 provided

CO_2 emissions released from fires at monthly time step and 0.5^0 spatial resolution from 2000 to 2010 based on the global simulation results developed for the Multi-Scale Synthesis and Terrestrial Model Intercomparison Project (Huntzinger et al., 2013; Wei et al., 2014).

1.2.2 PyC Estimation

The two modeling approaches used here estimated carbon directly released by fires as CO_2. Published relationships between PyC and CO_2, specific to each biome of interest, are described below and used to estimate PyC from fires in this analysis. Because several published studies did not present the conversion ratio PyC/CO_2, we calculated it from their results, using Equation 1.1.

$$\mathrm{PyC/CO_2} = \frac{PosF\_PyC - PreF\_PyC}{[(PosF\_C + PosF\_PyC) - (PreF\_C + PreF\_PyC)] * EF}$$

Equation 1.1

where PreF_C is the total Pre-fire carbon, PreF_PyC is the total Pre-fire PyC, PosF_C is the total Post-fire carbon, PosF_PyC is the total Post-fire PyC, and EF is a constant emission factor, representing the percentage of C in released CO_2 of total released carbon. Given that the EF is ~90% (e.g. Crutzen and Andreae, 1990; Forbes et al., 2006), we used 0.9 in the calculation.

Based on the set of PyC/CO_2 ratios that we synthesized across various land ecosystems, we divided the global terrestrial biosphere into seven biomes (Figure 1.1). The biome information was obtained using the Terrestrial Ecoregions of the World Map (Olson et al., 2001; http://www.worldwildlife.org/science/data/item1875.html), and was resampled at both 0.25×0.25 (GFED4s) and 0.5×0.5 (TEM6) degree resolutions to estimate the PyC

production from CO_2 emissions. In addition, we further aggregated biome regions to five continents, including Africa, Australia, Eurasia, North America, and South America.

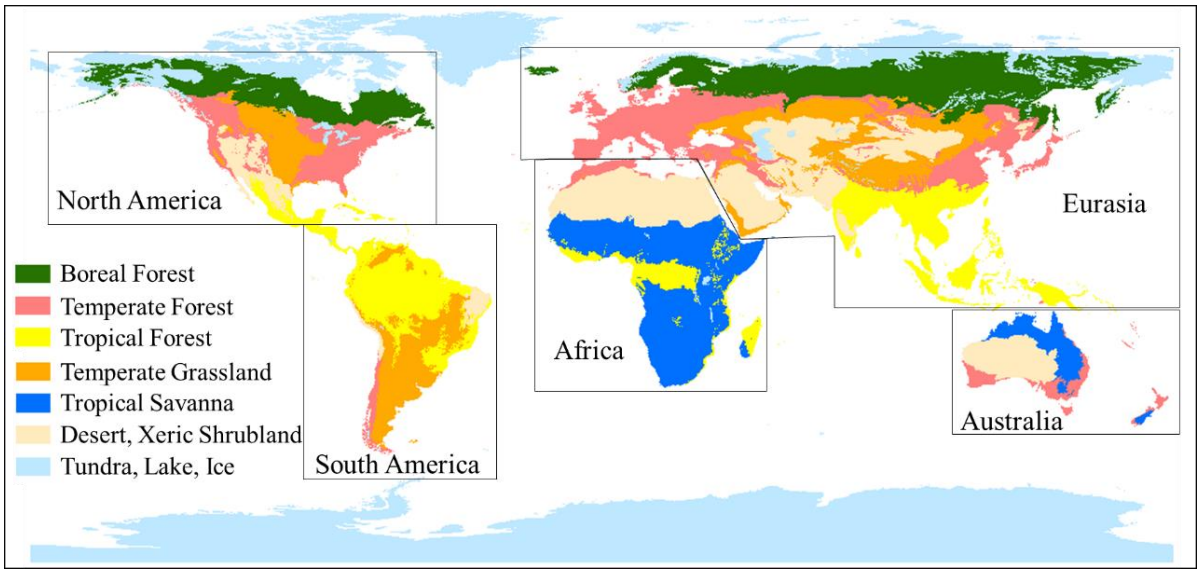

Figure 1.1. The seven global biomes used in this study, aggregated to five continental-scale regions.

Santín et al. (2015) quantified the prefire and postfire fuel and PyC in the boreal forest under the experimental fire, then they concluded that the PyC/CO_2 ratio was 38.1%. Thompson et al. (2016) used laboratory burning for masticated wood fuel particles collected from the boreal forest and concluded a PyC/CO_2 ratio of 0.3-1.4%. Czimczik et al. (2003) analyzed elemental concentrations in both unburned and burned samples from a naturally occurring boreal surface fire in west Siberian, concluding that the PyC/CO_2 ratio was 1.9%. Kuhlbusch and Crutzen (1995) sampled organic materials from various biomes and combusted them in the laboratory to measure the PyC/CO_2 ratios in various biome regions. Their laboratory analyses of boreal forest determined a PyC/CO_2 ratio of 5.0-7.0%. It should

be noted that this study focussed on particles with an average diameter of 40 μm, meaning that smaller PyC particles may have been omitted.

Table 1.1. PyC conversion ratios (PyC/CO_2) from published studies.

Study location	PyC/CO_2 (%)	Type of fire	Fuel type	Type of PyC	Reference
Boreal Forest					
Canada	38.1	Experimental	All fuels	Charred mass	Santín et al. (2015)
Canada	0.3-1.4	Laboratory	Masticated fuel	Total	Thompson et al. (2016)
Siberia	1.9	Wildfire	Forest floor	Total	Czimczik et al. (2003)
Global	5.0-7.0	Laboratory	All fuels	≥40μm	Kuhlbusch and Crutzen (1995)
Temperate Forest					
Australia	6.4-11.3	All[¶]	Surface fuel	Total	Graetz and Skjemstad (2003)
Australia	5.1	Prescribed	Surface fuel	Charcoal, ash	Jenkins et al. (2016)
Arizona, USA	1.1-5.1	Prescribed	Slash pile	Total	Finkral et al. (2012)
California, USA	4.1	Wildfire	All fuels	Total	Miesel et al. (2018)
Florida, USA	9.9	Prescribed	Surface fuel	Visual charcoal	Comery (1981)
Idaho, USA	11.8-12.7	Laboratory	All fuels	Charcoal, ash	Brewer et al. (2013)
Oregon, USA	1.1-8.9	Prescribed	Woody fuels	>2000μm	Pingree et al. (2012)
Germany	8.9	Experimental	Slash pile	≥1 mm	Eckmeier et al. (2007)
Global	5.0-7.0	Laboratory	All fuels	≥40 μm	Kuhlbusch and Crutzen (1995)
Tropical Forest					
Amazon	10.8	Prescribed	Slash pile	Visual charcoal	Fearnside et al. (1993)
Amazon	2.9	Prescribed	Slash pile	Visual charcoal	Barbosa and Fearnside (1996)
Amazon	3.3	Prescribed	Slash pile	Visual charcoal	Fearnside et al. (1999)
Amazon	4.5	Prescribed	Slash pile	Visual charcoal	Fearnside et al. (2001)
Amazon	4.6	Prescribed	Slash pile	Visual charcoal	Fearnside et al. (2007)
Amazon	10.2	Experimental	Slash pile	Charcoal, ash	Graça et al. (1999)

Table 1.1 continued.

Amazon	8.4-19.7	Prescribed	Woody debris	Ash	Kauffman et al. (1995)
Amazon	14.0	Prescribed	Slash pile	Visual charcoal	Righi et al. (2009)
Global	5.0-7.0	Laboratory	All fuels	≥40μm	Kuhlbusch and Crutzen (1995)
Temperate Grassland					
America	3.7	Wildfire	Surface fuel	Visual charcoal	Hao et al. (1990)
Asia	0.3	Wildfire	Surface fuel	Visual charcoal	Hao et al. (1990)
UK	5.0	Prescribed	Surface fuel	Total	Clay and Worrall (2011)
UK	3.0	Laboratory	Surface fuel	Total	Worrall et al. (2013)
Global	6.0	Laboratory	Surface fuel	Ash	Lobert et al. (1991)
Global	1.3	Laboratory	All fuels	Total	Kuhlbusch et al. (1996)
Global	1.3-2.9	Laboratory	All fuels	≥40μm	Kuhlbusch and Crutzen (1995)
Tropical Savanna					
Africa	11.8	Wildfire	Surface fuel	Visual charcoal	Delmas et al. (1991)
Africa	11.6	Wildfire	Surface fuel	Visual charcoal	Hao et al. (1990)
Africa	15.4	Wildfire	Surface fuel	Visual charcoal	Kuhlbusch et al. (1996)
Africa	6.2	Wildfire	Surface fuel	Visual charcoal	Lacaux et al. (1993)
Africa	1.6	Wildfire	Surface fuel	Visual charcoal	Menaut et al. (1991)
Australia	4.0	Wildfire	Surface fuel	Total	Graetz and Skjemstad (2003)
Australia	2.0	Wildfire	Surface fuel	Visual charcoal	Hao et al. (1990)
Australia	1.3	Wildfire	Surface fuel	Visual charcoal	Hurst et al. (1994)
Australia	21.2	Experimental	Surface fuel	Visual charcoal	Saiz et al. (2014)
Global	1.3-2.9	Laboratory	All fuels	≥40μm	Kuhlbusch and Crutzen (1995)

¶Managed and unmanaged forest fires.

In an Australian temperate forest, Graetz and Skjemstad (2003) applied a quantitative framework of charcoal redistribution to estimate the PyC ratios. By monitoring the quantity of PyC in situ and moved by water before and after managed and unmanaged fires, they estimated a PyC/CO_2 ratio of 6.4-11.3% (Table 1.1). However, their calculations ignored the small PyC particles, because they assumed this to be a very small component. Jenkins et al. (2016) investigated both the charcoal and ash created by planned burning in an Australian forest, and reported a PyC/CO_2 ratio of 5.1%. Finkral et al. (2012) sampled the slash pile before and after a prescribed burning in northern Arizona, USA, and measured the char particles. Their results indicated a PyC/CO_2 ratio of 1.1-5.1%. Miesel et al. (2018) quantified the PyC production and carbon losses by five wildfires in the California mixed-conifer forest. They reported a PyC/CO_2 ratio of 4.1%. Comery (1981) analyzed residues from a temperate conifer forest in Florida before and after prescribed burning, reporting a PyC/CO_2 ratio of 9.9%. Brewer et al. (2013) used laboratory fire to burn masticated fuels collected from Idaho, USA, and measured the post-fire charred residues. This analysis suggested a PyC/CO_2 ratio of 11.8-12.7%. Pingree et al. (2012) compared the charcoal quantity in pre- and post-wildfire soil and fuel in southwest Oregon, USA, and their results suggested a PyC/CO_2 ratio of 1.1-8.9%. Eckmeier et al. (2007) used experimental fires to burn slash of a temperate deciduous forest in Germany, then analyzed the fire-created charcoal. Their analysis suggested a PyC/CO_2 ratio of 8.9%. Kuhlbusch and Crutzen (1995) applied the lab-based method to measure the PyC conversion ratio for the temperate forest biome, reporting that the PyC/CO_2 ratio ranged from 5.0% to 7.0%.

Fearnside et al. (1993) sampled PyC materials after a slash-and-burn deforestation fire in the Amazon rainforest, mainly by visually assessing charcoal content, and reported a PyC/CO_2 ratio of 10.8% (Table 1). Fearnside and Barbosa (1996) resampled the post-fire residues in

Amazon fires and updated this ratio to 2.9%. Then, Fearnside et al. (1999) reported a ratio of 3.3% in the Amazon. In another study, Fearnside et al. (2001) updated this ratio to 4.5%. In a later study, Fearnside et al. (2007) estimated a similar ratio of 4.6%. Graça et al. (1999) measured post-fire residues in the soil after a slash-and-burn deforestation fire in the Amazon rainforest, and estimated the PyC/CO_2 ratio to be 10.2%. Kauffman et al. (1995) quantified the total above-ground biomass and charcoal before and after a slash-and-burn deforestation fire in an Amazon tropical moist forest, and their analysis suggested a PyC/CO_2 ratio of 8.4-19.7%. Righi et al. (2009) measured the total aboveground biomass and charcoal in each plot before and then again after prescribed burning, reporting a PyC/CO_2 ratio of 14.0%. Kuhlbusch and Crutzen (1995) used laboratory analyses to determine that the PyC/CO_2 ratio ranged from 5.0 to 7.0% for tropical forest at the global-scale.

Using the inventory data provided by the Food and Agriculture Organization of the United Nations (FAO), Hao et al. (1990) reported a PyC/CO_2 ratio of 0.3% (Table 1) across the Asian steppe; however, this ratio increased to 3.7% in North American grassland. Clay and Worrall (2011) investigated char production from a series of prescribed burns from moorland in the Peak District, UK. Their results indicated a PyC/CO_2 ratio of 5.0%. Worrall et al. (2013) applied the same method and updated this ratio to 3.0% for this area. Lobert et al. (1991) sampled organic materials from temperate grassland, and burned them in the laboratory. They estimated a PyC/CO_2 ratio of 6.0%. In temperate grasslands, based on lab experiments, Kuhlbusch and Crutzen (1995) estimated the PyC/CO_2 ratio to be in the range from 1.3 to 2.9% globally. In a later study, Kuhlbusch and Crutzen (1996) updated this ratio to 1.3%.

Delmas et al. (1991) and Lacaux et al. (1993) reported PyC/CO_2 ratios of 11.8% and 6.2%, respectively, through measuring the char particles in both pre- and post-fire residues in

Africa (Table 1). With the the inventory data, Hao et al. (1990) reported a PyC/CO_2 ratio of 11.6% in African tropical savanna ecosystems, and this ratio decreased to 2.0% in Australian tropical savanna. Kuhlbusch et al. (1996) quantified the PyC formed in the residues of savanna fires on six experimental sites in southern Africa, and determined a PyC/CO_2 ratio of 15.4%. Menaut et al. (1991) measured the visual char created from savanna fires in West Africa, and concluded a PyC/CO_2 ratio of 1.6%. Hurst et al. (1994) used physical separation of PyC particles following a tropical savanna fire to obtain a PyC/CO_2 ratio of 1.3% in Australia. Saiz et al. (2014) used controlled field burning experiments in four savanna sites in northeastern Australia, and quantified the production of visual PyC. Their results suggested a PyC/CO_2 ratio of 21.2%. Kuhlbusch and Crutzen (1995) estimated a PyC/CO_2 ratio of 1.3-2.9% globally through their laboratory-based experiment.

The fuel type and fire weather in desert, xeric shrubland ecosystems differ substantially from those of other terrestrial ecosystems. Perhaps partly due to the unique vegetation types found in desert shrublands, which mainly consist of prostrate shrubs and short-stature woody trees, there are no published studies of PyC production in these ecosystems. Therefore, we simply applied a global temperate grassland PyC/CO_2 ratio to estimate the PyC production in these regions. Similarly, the tundra regions have no available quantitative information on PyC production or conversion rates, although the presence of charcoal in tundra soils can be abundant (e.g. Qi et al., 2017). Recent climatic warming has caused pronounced environmental changes, including shrub expansion and vegetation type change in the tundra region (Myers-Smith et al., 2011), but the paucity of available information on PyC limits our ability to assess the impact of these changes on PyC production. Therefore, as with desert ecosystems, we simply employed the same PyC/CO_2 ratio for temperate grassland to calculate the PyC production in tundra areas.

In this study, we used a Monte Carlo approach to obtain the PyC/CO_2 conversion ratio for each biome region, as follows. First, for each biome region, five conversion ratios from published studies were randomly selected (boreal forest had four, see below). If there were insufficient studies for a given region, conversation ratios from a similar biome were selected to construct the estimate. If the published conversion ratio appeared as a range, a number within this range (to one decimal or 0.1%) was randomly generated. For example, the conversion ratio 5.0-7.0% was used to generate a list of ratios: 5.0% 5.1%, 5.2% ... 7.0%; a ratio was then randomly selected from this list. Second, one conversion ratio was calculated as the mean of the five selected ratios (boreal forest had four). Third, this process was repeated 100 times to produce a set of conversion ratios, from which means and standard deviations were calculated.

Selecting five PyC/CO_2 conversion ratios for each biome presented a challenge, given the dearth of published studies from several biomes (Table 1). For the boreal forest biome, all four ratios obtained from the literature were used here. For temperate forest in North and South America, the five published ratios in USA were used. For temperate forest in Australia, the conversation ratios for Australian and global temperate forest with two randomly selected ratios from the other six temperate forest studies were used. For temperate forest in Eurasia, conversation ratios for Germany and global studies were selected with three randomly selected ratios from the other seven studies were used. For tropical forest, all the nine ratios were used. For temperate grassland in Eurasia, the published ratios in Asia and UK were used with other two randomly selected from the three global studies. For temperate grassland in North and South America, the published ratio in America was used with other four randomly selected ratios. For tropical savanna in Africa, four conversion ratios randomly selected from five African studies with one global ratio were used. For tropical savanna in Australia, four studies in Australia and

one from the other six studies were used. For desert, xeric shrubland and tundra, five randomly selected ratios for temperate grassland were used.

1.3 Results

1.3.1 PyC Conversion Ratio

Through these Monte Carlo estimates, overall, the highest PyC conversion ratio was in boreal forest, having a value of 11.7±0.2 (Figure 1.2). In temperate forest regions, North and South America had the lowest ratio of 6.9±0.5%, and Australia had a similar ratio of 7.1±0.8%, but Eurasia had the highest ratio of 7.4±1.0%. In tropical forest, the ratio was 7.8±1.3%. Globally, the lowest PyC conversion ratio was in Eurasian temperate grassland, having a value of 2.9±0.4%, while the ratio was increased to 3.1±0.4% in North and South American temperate grassland. African tropical savanna had a value of 7.8±0.9%, while it decreased to 7.2±1.0% in tropical savanna of Australia. The PyC conversion ratio in desert, xeric shrubland and tundra, was 3.1±0.5%.

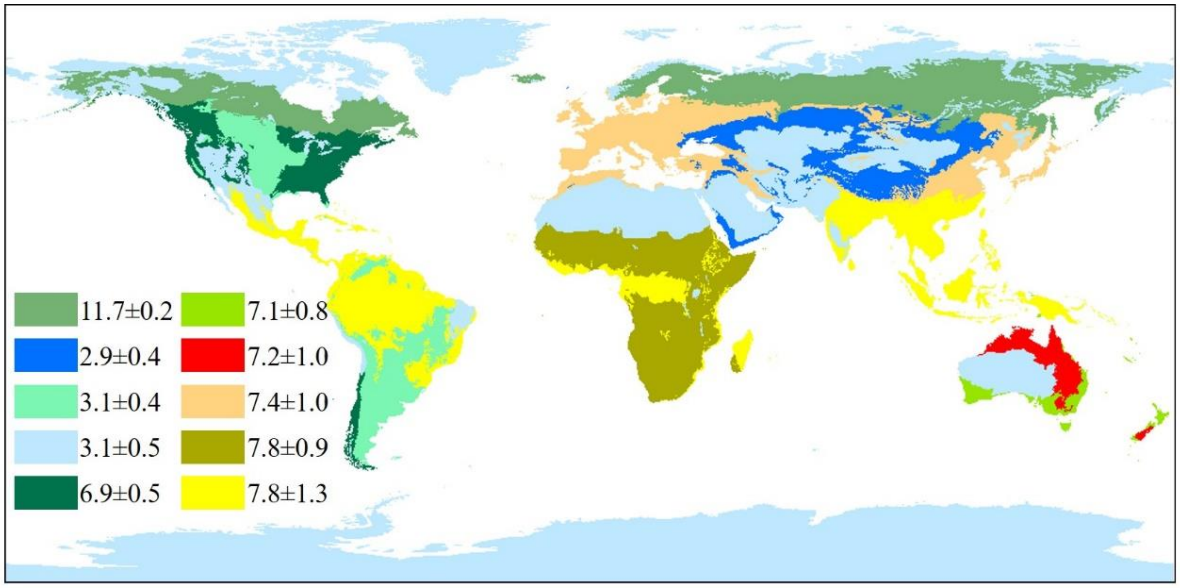

Figure 1.2. The spatial distribution of PyC conversion ratio by biome.

1.3.2 CO_2 Emissions

The CO_2 emissions from GFED4s had been reported by van der Werf et al. (2017) and summarized here according to the biome and continent regions used in this study. Over the 2000-2010 study period, GFED4s estimated that, on average, 2086 Tg C yr^{-1} was released to the atmosphere as direct CO_2 emissions from global fires (Table 1.2), with a minimum in 2009 (1838 Tg C) and a maximum in 2002 (2314 Tg C). By comparison, TEM6 estimated direct CO_2 emissions from global fires as an average of 643 Tg C yr^{-1} over the same time period, with a minimum in 2010 (492 Tg C) and maximum in 2003 (898 Tg C). The GFED4s results suggested that fires in African ecosystems were responsible for more than half (1126 Tg C yr^{-1}) of the global fire-related CO_2 emissions, and 90% (1010 Tg C yr^{-1}) of this estimate was contributed by savanna fires. In contrast, TEM6 results suggested that fires in Eurasian ecosystems were responsible for approximately 50% (310 Tg C yr^{-1}) of its estimated global total. GFED4s results indicate that North American ecosystems produced the least amount of CO_2 from fires (82 Tg C yr^{-1}) during the 2000 to 2010 time period, while TEM6 results identify the least amount from Australian ecosystems (10 Tg C yr^{-1}). At the global scale, results from both models suggested that grassland fires (including temperate grassland and tropical savanna) emitted the largest amount of CO_2 (1258 Tg C yr^{-1} from GFED4s, and 187 Tg C yr^{-1} from TEM6; Table 1.3). In tropical forest regions, GFED4s estimated CO_2 emissions from fires to be 569 Tg C yr^{-1}, compared to 172 Tg C yr^{-1} estimated by TEM6. GFED4s estimated a 102 Tg C yr^{-1} release of CO_2 from fires across global temperate forest regions during this time period, which was larger than the TEM6 estimate (73 Tg C yr^{-1}). Although their estimates differ among the four temperate forest regions, both models identify the Eurasian temperate forest as producing the greatest amount of CO_2 (52 Tg C yr^{-1} and 61 Tg C yr^{-1}), while the South American temperate forest

released the least amount (2 Tg C yr^{-1} and 1 Tg C yr^{-1}). In addition, GFED4s results suggested that CO_2 amounts released from global desert and tundra fires were 34 Tg C yr^{-1} and 15 Tg C yr^{-1}, respectively, and both are similar to the TEM6 estimates (34 Tg C yr^{-1} and 21 Tg C yr^{-1}).

During the period 2000-2016, the global fire CO_2 emissions estimated from GFED4s results was 2041 Tg C yr^{-1}. While TEM6 results were only available up to 2010, we analyzed the GFED4s results from 2011 to 2016, which estimated direct CO_2 emissions during this time period to be 1959 Tg C yr^{-1} globally as a result of fires. During this later time period, African land ecosystems again produced the greatest amount of CO_2, responsible for more than 50% of the global emissions. Compared to the 2000-2010 time period, CO_2 released from South American tropical forest decreased by 33% (73 Tg C yr^{-1}), having the largest absolute reduction of all biomes. CO_2 released from the North American boreal forest increased by 76% (31 Tg C yr^{-1}), having the largest percentage increase. CO_2 released from tropical savannas decreased by 6% (68 Tg C yr^{-1}), having the minimum rate of change.

Table 1.2. Modeled estimates of the average annual CO_2 emissions and PyC production.

Shaded rows indicate sums (Tg C yr^{-1}).

	GFED4s				TEM6	
	2000-2010		2011-2016		2000-2010	
	CO_2	PyC	CO_2	PyC	CO_2	PyC
Africa	1125.8	87.8±10.6	1051.2	82.0±9.9	141.0	11.0±1.4
Tropical Forest	115.7	9.0±1.5	111.0	8.7±1.4	37.4	2.9±0.5
Tropical Savanna	1010.0	78.8±9.1	940.0	73.3±8.5	103.6	8.1±0.9
Desert, Xeric Shrubland	0.1	0.0±0.0	0.2	0.0±0.0	0.0	0.0±0.0
Australia	124.6	8.3±1.1	128.0	8.3±1.1	10.4	0.8±0.1
Temperate Forest	30.2	2.2±0.2	26.2	1.9±0.2	6.5	0.5±0.1
Tropical Savanna	77.4	5.6±0.8	79.5	5.7±0.8	3.8	0.3±0.0
Desert, Xeric Shrubland	16.9	0.5±0.1	22.2	0.7±0.1	0.0	0.0±0.0
Eurasia	388.4	30.0±3.7	402.6	32.8±3.8	309.8	24.5±1.7
Boreal Forest	67.2	7.9±0.1	93.0	10.9±0.2	128.9	15.1±0.3
Temperate Forest	52.4	3.9±0.5	41.0	3.0±0.4	60.7	4.5±0.6
Tropical Forest	213.3	16.6±2.8	228.2	17.8±3.0	27.7	2.2±0.4
Temperate Grassland	42.0	1.2±0.2	29.2	0.8±0.1	60.0	1.7±0.2
Desert, Xeric Shrubland	13.5	0.4±0.1	11.2	0.3±0.1	32.5	1.0±0.2
North America	81.6	7.5±0.4	114.3	11.2±0.4	36.9	3.7±0.1
Boreal Forest	40.6	4.8±0.1	71.5	8.4±0.1	28.2	3.3±0.1
Temperate Forest	17.8	1.2±0.1	20.9	1.4±0.1	4.6	0.3±0.0
Tropical Forest	18.5	1.4±0.2	17.1	1.3±0.2	1.7	0.1±0.0
Temperate Grassland	3.7	0.1±0.0	3.5	0.1±0.0	1.1	0.0±0.0
Desert, Xeric Shrubland	1.0	0.0±0.0	1.3	0.0±0.0	1.3	0.0±0.0
South America	350.4	19.0±3.4	251.4	15.0±2.3	124.5	8.9±1.5
Temperate Forest	1.5	0.1±0.0	2.2	0.2±0.0	0.9	0.1±0.0
Tropical Forest	221.4	17.3±2.9	148.3	11.6±1.9	105.0	8.2±1.4
Temperate Grassland	124.9	3.9±0.5	98.7	3.1±0.4	18.4	0.6±0.1
Desert, Xeric Shrubland	2.7	0.1±0.0	2.1	0.1±0.0	0.2	0.0±0.0
Tundra	15.0	0.5±0.1	11.0	0.3±0.1	20.7	0.6±0.1
Total	2085.7	153.0±19.3	1958.5	149.6±17.7	643.3	49.5±4.9

Table 1.3. Modeled estimates of the CO_2 and PyC produced from fires and summarized at the global biome scale (Tg C yr^{-1}).

	GFED4s				TEM6	
	2000-2010		2011-2016		2000-2010	
	CO_2	PyC	CO_2	PyC	CO_2	PyC
Boreal Forest	107.8	12.7±0.2	164.4	19.2±0.3	157.0	18.4±0.4
Temperate Forest	101.9	7.4±0.8	90.4	6.5±0.7	72.7	5.3±0.7
Tropical Forest	568.8	42.7±7.4	504.6	39.4±6.6	171.9	13.4±2.2
Temperate Grassland	170.6	4.4±0.7	131.4	4.0±0.5	79.5	2.3±0.3
Tropical Savanna	1087.4	84.4±9.9	1019.6	79.1±9.3	107.4	8.4±1.0
Desert, Xeric Shrubland	34.2	1.0±0.2	37.1	1.1±0.2	34.1	1.1±0.2
Tundra	15.0	0.4±0.1	11.0	0.3±0.1	20.7	0.6±0.1
Total	2085.7	153.0±19.3	1958.5	149.6±17.7	643.3	49.5±4.9

1.3.3 PyC Production

During the 2000-2010 analysis period, the average global PyC production from fires was 153.0±19.3Tg C yr^{-1}, as estimated from the GFED4s results (PyC_{GFED4s}), ranging from 139.6±16.4 Tg C in 2008 to 173.5±20.6 Tg C in 2002 (Table 1.2). In comparison, the average global PyC production from fires as estimated from the TEM6 results (PyC_{TEM6}) was 49.5±4.9 Tg C yr^{-1}, ranging from 37.1±4.1 Tg C (2010) to 73.1±5.6 Tg C (2003). PyC_{GFED4s} suggested the largest amount of PyC (58.3±6.2% of total) was produced in African land ecosystems, while PyC_{TEM6} suggested 22.3±2.4% was produced there. (Note that the percent difference between two distributions was estimated by a Monte Carlo approach. Initially, 100 paired samples, that is, one from each distribution, were randomly selected from the two distributions, and the percent difference for each pair was calculated. Finally, mean and standard deviation were obtained from the 100 percentages.) PyC_{TEM6} suggested the largest amount of PyC (50.2±4.2% of total) was produced in Eurasian land ecosystems, while PyC_{GFED4s} suggested 19.0±2.1% was produced there. PyC_{GFED4s} suggested that North American land ecosystems produced the least amount at

37.5±0.4 Tg C yr^{-1}, but PyC_{TEM6} suggested Australian land ecosystems produced the least amount at 0.8±0.1 Tg C yr^{-1}. PyC_{GFED4s} suggested that tropical savanna fires created the greatest amount at 84.4±9.9 Tg C yr^{-1}, while PyC_{TEM6} suggested that boreal forest fires created the greatest amount at 18.4±0.4 Tg C yr^{-1} (Table 3). PyC_{GFED4s} suggested that 28.1±4.0% (42.7±7.4 Tg C yr^{-1}) of the global PyC total was produced in tropical forests, while PyC_{TEM6} suggested 28.2±3.4% (13.4±2.2 Tg C yr^{-1}) was produced there. In temperate forest ecosystems, PyC_{GFED4s} estimated the PyC production at 7.4±0.8 Tg C yr^{-1}, which was higher than PyC_{TEM6} estimate (5.3±0.7 Tg C yr^{-1}). However, in boreal forest ecosystems, PyC_{GFED4s} estimated the PyC production at 12.7±0.2 TgC yr^{-1}, which was lower than PyC_{TEM6} estimate (18.4±0.4Tg C yr^{-1}). In desert and tundra regions, PyC_{GFED4s} estimated 1.0±0.2 Tg C yr^{-1} and 0.4±0.1 Tg C yr^{-1}, respectively, of PyC formed through fires, which are very close to estimates from PyC_{TEM6} (1.1±0.2 Tg C yr^{-1} and 0.6±0.1 Tg C yr^{-1}, respectively).

During the period 2000-2016, global PyC production was estimated as 153.4±18.7 Tg C yr^{-1} based on the GFED4s results. Because TEM6 results were only available up to 2010, we analyzed the PyC results from GFED4s during the period 2011-2016, which indicated an average of 149.6±17.7 Tg C yr^{-1} PyC produced by fires. Fires in African ecosystems still produced the greatest amount of PyC (82.0±9.9 Tg C yr^{-1}), and 89.3±8.0% resulted from African savanna burning. Compared with the period 2000-2010, PyC produced from African tropical savanna decreased by 7.4±6.5% (5.5±3.6 Tg C yr^{-1}), having the largest absolute reduction. PyC produced from North American boreal forest increased by 77.0±2.2% (3.56±0.2Tg C yr^{-1}), having the largest percentage increase. PyC produced from South American tropical forest decreased by 26.4±4.5% (4.15±1.7 Tg C yr^{-1}), having the largest percentage reduction.

1.4 Discussion

We improved current PyC estimations (e.g. Bird et al., 2015; Kuhlbusch and Crutzen, 1995; Santín et al., 2016) in three aspects. First, we used estimates of fire-induced CO_2 emissions from two ecosystem models (GFED4s and TEM6), along with published biome-specific PyC/CO_2 ratios, to estimate the PyC production. To the best of our knowledge, ours is the first attempt to estimate PyC production from fires at a global scale, based on detailed biome-specific PyC production rates.

Second, we depicted the spatial distributions and dynamics of global fire produced CO_2 and PyC, which made it possible to compare PyC production in biome- and continental-scales. GFED4s identified Africa as the largest source of fire-produced CO_2 (Figure 3a); in contrast, TEM6 identified Eurasia as the largest source (Figure 3b). GFED4s suggested that African tropical savanna fires released the largest amount of CO_2; however, TEM6 suggested that Eurasian boreal forest released the largest amount. Using the detailed biome-specific PyC conversion ratios with the two modelling results, both PyC_{GFED4s} and PyC_{TEM6} suggested that African savanna fires produced the largest amount of PyC (Figure 1.4a and 1.4b).

Third, our results provided the interannual variations of fire produced CO_2 emissions and PyC production. They varied among continental regions and among biomes. Both GFED4s and TEM6 indicated that this variation was greatest in tropical forests. Interannual variation of CO_2 emissions and PyC production among other biomes was markedly lower. The higher interannual variability in the tropics may be attributable to ever-changing patterns in slash-and-burn agriculture (Marle et al., 2017), leading to varying CO_2 emissions and PyC production. Extreme weather (e.g., drought, El Niño) may be another contributor to this significant interannual variability (Chen et al., 2017). Alencar et al. (2006) reported that El Niño can significantly

increase the annual fire frequency and burning area in Amazon tropical forest. Sloan et al. (2017) concluded that droughts induced by El Niño can magnify the frequency and severity of fire activity in South Asia.

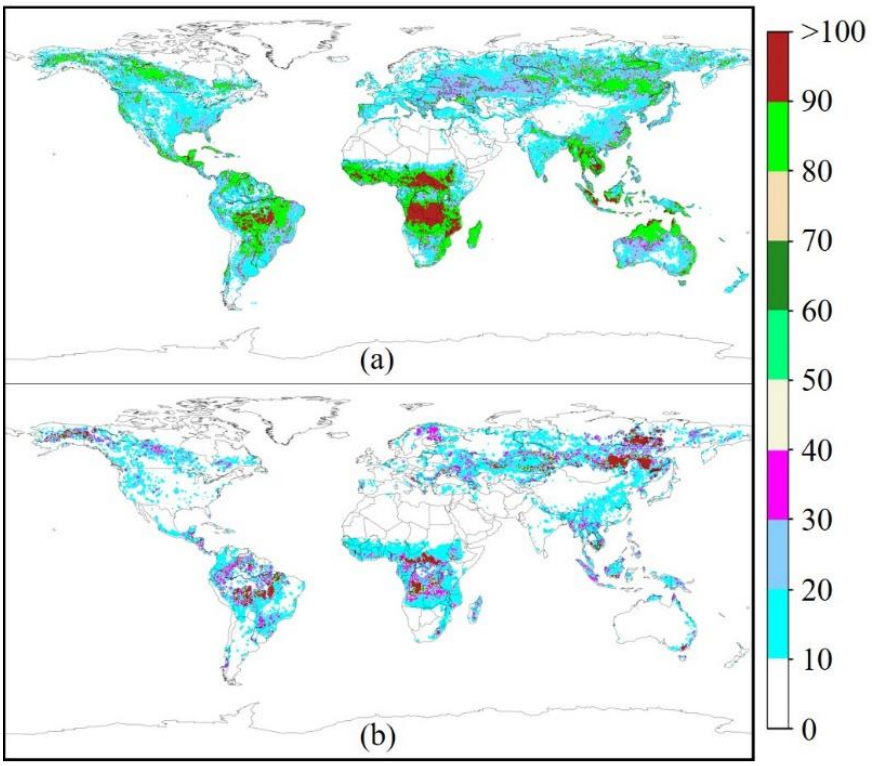

Figure 1.3. The mean of grid-weighted average annual CO_2 (g C m^{-2} yr^{-1}) released from fires resulting from (a) GFED4s in the period of 2000-2016, and (b) TEM6 in the period of 2000-2010.

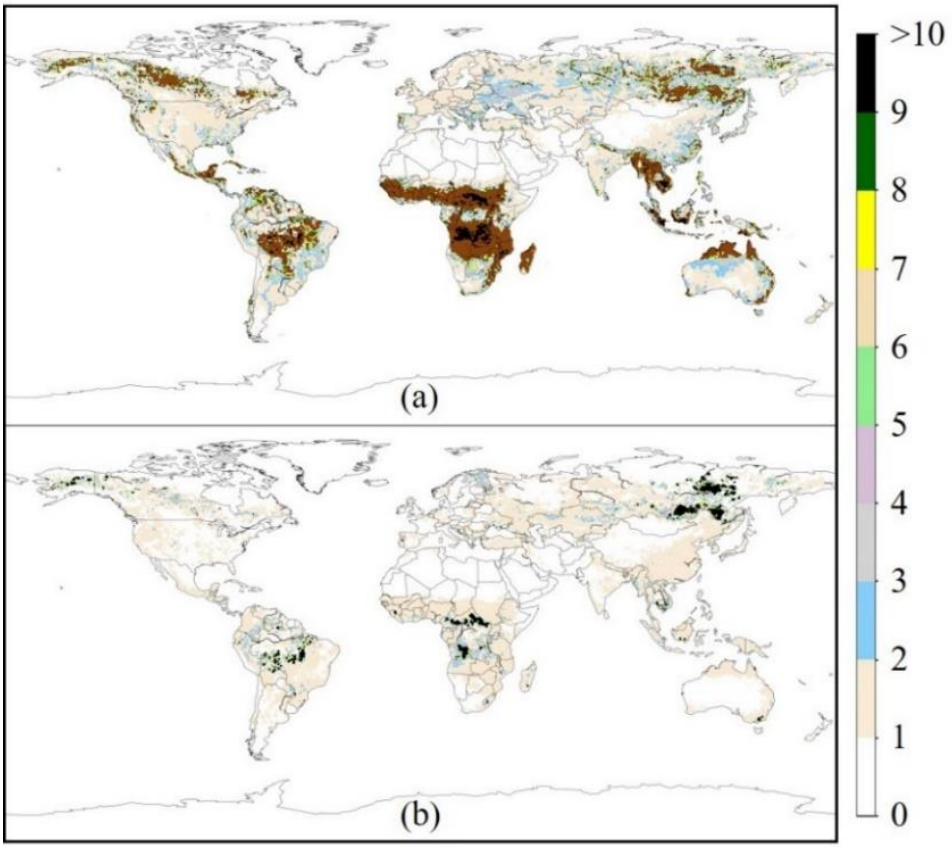

Figure 1.4. The mean of grid-weighted average annual PyC (g C m^{-2} yr^{-1}) produced by fires, which were calculated from CO_2 emissions estimated by (a) GFED4s in the period of 2000-2016, and (b) TEM6 in the period 2000-2010.

PyC production from fires may represent approximately 0.2-0.6% of annual global net primary production (Huston and Wolverton, 2009). Though this percentage is relatively small, we emphasize that PyC is more recalcitrant than original biomass (Bird et al., 2017), meaning that it accumulates in terrestrial and marine ecosystems. Using the central reburning loss rate 7.8% and decomposition rate 0.5% of PyC (Landry and Matthews, 2017) over the study period, PyC_{GFED4s} suggested that a total of 1415±171 Tg C of PyC accumulated during the period 2000-2016 (Figure 5a), while PyC_{TEM6} suggested that 354±35 Tg C accumulated during the period 2000-2010 (Figure 5b). These estimates suggested that PyC from fires may be a significant sink

of atmospheric CO_2 when considered over longer time periods, assuming the post-fire carbon can recover to the pre-fire status.

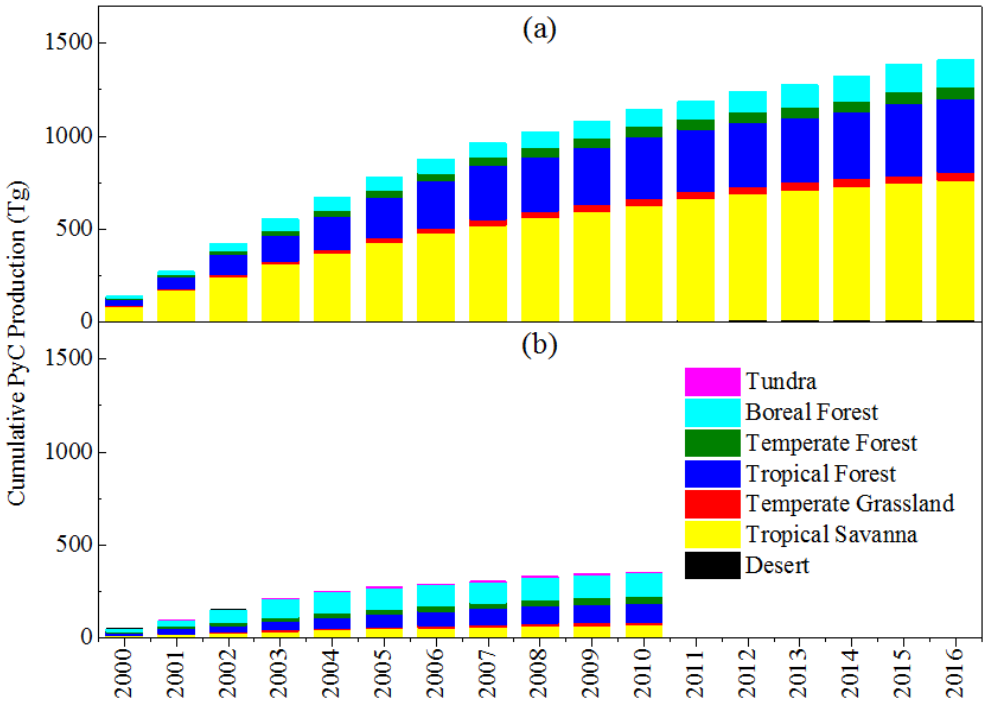

Figure 1.5. The mean of cumulative PyC production estimated from CO_2 emissions provided by (a) GFED4s from 2000 to 2016, and (b) TEM from 2000 to 2010.

The CO_2 emitted and PyC produced by global fires were first discussed by Seiler and Crutzen (1980). They estimated the total amount of global biomass affected by fires using data on fuel burning efficiency along with global transfer rates of CO_2 and PyC in natural and agricultural ecosystems. They estimated global PyC production from biomass burning ranged from 500 to 1700 Tg C yr^{-1}, and CO_2 emissions from 2000 to 4000 Tg C yr^{-1}. Crutzen and Andreae (1990) later estimated that global PyC production from fires ranged from 200 to 600 Tg C yr^{-1}, and CO_2 emissions from 2700 to 6800 Tg C yr^{-1}. However, challenges in measuring PyC conversion rates and CO_2 emissions in diverse land ecosystems results in high uncertainties around these estimates (Crutzen and Andreae, 1990). Kuhlbusch and Crutzen (1995) attempted

to reduce these uncertainties by measuring PyC in the residue after fires in laboratory-based measurements, and clarified the relationships between PyC production and gaseous emissions. Using these refinements, they estimated global PyC production to be approximately 50 to 270 Tg C yr^{-1}. Kuhlbusch and Crutzen (1996) then synthesized previous PyC conversion ratios across coarsely-defined biome regions and concluded that global PyC production ranged from 50 to 200 Tg C yr^{-1}. However, none of these estimates were conducted for specific time periods nor provided PyC spatio-temporal dynamics. Bird et al. (2015) synthesized current knowledge of PyC production, stocks, and fluxes, and estimated a production of 56-123 Tg C yr^{-1} as char. Santín et al. (2016) used a global PyC conversion ratio with the GFED4s for the 1997-2014 time period to estimate that average annual PyC production ranged from 114 to 383 Tg C globally. In our study, the global CO_2 emitted annually from fires was estimated to be 2041 TgC yr^{-1} during the period 2000-2016 obtained from GFED4s, and 643 Tg C yr^{-1} from TEM6 during 2000-2010. The corresponding global PyC production estimated from the GFED4s results was 153±12 Tg C yr^{-1}, and 50±5 Tg C yr^{-1} by TEM6, which roughly correspond with estimates of Bird et al. (2015).

Our study revealed large differences between GFED4s and TEM6 results at both the biome-level and the continental-scale. In many cases the two models produced quite different estimates of both CO_2 and thus PyC production. They often differed in the relative ranking of continental regions and biomes with respect to CO_2 and PyC production. Both models use similar area burned data from satellite image sources but, unlike GFED4s, TEM6 does not incorporate small fires or agricultural burning in its estimates. When the small fires are excluded, GFED4 estimates 1500 Tg C yr^{-1} of CO_2 emissions in the period 1997-2016 (van der Werf et al., 2017). The greatest difference between the two model estimates was in the tropical savanna biome,

which was responsible for 69.4±4.5% of the total difference. The second was the tropical forest biome consisting of 27.9±2.9% of the total difference. These uncertainties could arise from the input data, simulated biochemical processes, and model parameters. In addition, these differences in estimates of the carbon impacts of fire between the two modeling approaches are a function of how each simulates the carbon pools that are exposed to fire, and the fire severity parameters that transfer carbon among them. Therefore, future improvement for the input data (e.g., burn area, burn severity, climate data, fuel load, and vegetation map), simulated biochemical processes (e.g., photosynthesis, respiration, and biomass decomposition), and related parameters (e.g., combustion completeness, combustion efficiency, and emission factors) can enhance their estimation abilities.

In this study, we used conversion ratios from simulated distributions (constrained by published ratios) to estimate annual global PyC production from fires. Because weather conditions, fuel loads, fuel types, and fire types influence these PyC conversion ratios, their use contributes to the uncertainties in our results. Given the factors that influence the PyC production, our estimate could be improved in at least three regards. First, Kuhlbusch and Crutzen (1995) summarized the PyC/CO_2 conversion ratios in various fire types (e.g., wildfire, prescribed fire, deforestation fire), and concluded that fire types could influence the conversion ratio. Miesel et al. (2018) reported that intense fire type (e.g., prescribed fire) could significantly increase PyC production, thereby increasing the PyC/CO_2 conversion ratio. Thus, the lack of fire type information can underestimate the PyC production. Although we employed a sensitivity test with published conversion ratios, detailed fire type information along with corresponding released carbon could decrease the fire-type uncertainties in PyC estimates.

Second, the paucity of fuel type information in various biomes precludes further refinements in our calculations. Using before-vs-after fire inventories, Tinker and Knight (2000) concluded that the presence of coarse fuel biomass can increase PyC production. Similarly, Ward et al. (2017) found that coarse fuel biomass significantly increased PyC production during burning. However, in our study, the influence of coarse fuel loads on PyC production was not considered, which may have led to underestimates of PyC production; the magnitude of this underestimate is unknown. Therefore, fuel type and fuel load information could improve the calibration of PyC conversion ratios, thereby improving estimates.

Third, although we employed biome- and continental-scale PyC conversion ratios to improve existing the PyC estimates, agricultural fire was not considered as one special class. Thus, improved PyC estimates for agricultural fire would decrease the uncertainties in our estimates. Seiler and Crutzen (1980) reported agricultural fire had a different PyC conversion ratio from that of its biome (the PyC/CO_2 was not presented in their study), and agricultural fire produced 53% of the total burned carbon. Through summarizing published studies, Kuhlbusch and Crutzen (1995) also reported that the PyC conversion ratio for agricultural fire differed from that of its biome.

Though unrelated to our modelling approach, we note that authors have chosen different fuel types (see Table 1, e.g. forest floor, slash pile, woody debris), carried out the burning in different fire conditions (e.g. experimental, laboratory, wildfire), and used various size criteria to define PyC types (size of visual charcoal are defined differently in various studies). All of these differences presumably influence PyC conversion ratios. Future modelling approaches aimed at global carbon accounting could benefit from a standardized measurement for PyC in order to increase predictive confidence of such models.

1.5 Conclusions

Our approach – based on biome-specific PyC/CO_2 ratios – represents an improved estimate of global PyC emissions from fires. These fires represent a large carbon source to the atmosphere by releasing CO_2 and other gaseous carbon compounds; however, they also create PyC in the form of charred material that remains on site or small particles that are transported far from the site of origin (Bird et al., 2015; Cotrufo et al., 2016). Because PyC is more recalcitrant to decay than original biomass, the accumulated PyC may serve as a potentially growing, stable carbon sink that is distributed globally. We believe the size of this carbon pool and the processes responsible for its formation merit further research attention.

CHAPTER 2

2. BIOME CORRELATION AND TIME-DEPEND RESPONSE OF TERRESTRIAL ECOSYSTEM CARBON FLUXES TO LONG-LASTING DROUGHTS

2.1 Introduction

The terrestrial biosphere acts as a major sink for atmospheric carbon dioxide (CO_2) (Le Quéré et al., 2009) by taking up and storing carbon in vegetation biomass, soil organic matter, and other ecosystem pools (Dixon et al., 1994; Pan et al., 2011). Through modifying both carbon uptake by photosynthesis and carbon release by total ecosystem respiration (Heimann and Reichstein, 2008; Stocker et al., 2019), as well as introducing time-lagged impacts such as fire, insect outbreak and soil erosion (Chen et al., 2019; Wei et al., 2018; Zhang et al., 2019), droughts can greatly affect terrestrial biosphere carbon fluxes and storage (van der Molen et al., 2011). These effects occur from regional to continental scales, and can persist for long time periods (Dai et al., 2004; van der Molen et al., 2011). Currently, because the area affected by droughts is increasing globally (Huang et al., 2017), droughts can strongly regulate current, biome-scale net ecosystem carbon exchange between terrestrial ecosystems and the atmosphere (Frank et al., 2015).

Each terrestrial biome has distinctive vegetation, climate, edaphic and other environmental conditions, and all of these determine its particular drought response of land-atmosphere carbon exchange over different time scales. To understand the relationship between carbon fluxes and droughts at the biome-scale, several techniques have been applied. One primary approach is using Terrestrial Biosphere Models (TBMs) (e.g. Schwalm et al., 2017; Zscheischler et al., 2014), which estimate past, present, and future land-atmosphere carbon

exchange through simulating biogeochemical processes controlling net carbon exchange (Fisher et al., 2014). Atmospheric Inversion Models (AIMs) represent another modeling approach whereby atmospheric transport models are combined with atmospheric CO_2 concentrations to spatially infer the magnitude and spatial patterns of land-atmosphere carbon exchange (Boese et al., 2019). In addition, by linking remote sensing data with appropriate models, time-series carbon flux information can be obtained to study the drought impact on terrestrial biosphere carbon exchange (e.g. Gouveia et al., 2017; Zhao and Running, 2010). Finally, at the site-level, tower-based eddy covariance techniques provide continuous measurements of land-atmosphere carbon fluxes during drought extremes (e.g. Ciais et al., 2005). Other methods based on biomass inventory use a combination of field surveys to estimate the net land-atmosphere carbon exchange from regional to continental scales with and without droughts and for various time periods (e.g. Klesse et al., 2016; Liski et al., 2006).

Previous studies have demonstrated that the impacts of drought on carbon fluxes will vary among different ecosystems and at different time scales. Using FLUXNET, a global network of eddy covariance towers, Schwalm et al. (2010) analyzed the functional relationships between carbon fluxes and droughts. They found that drought induces an increase of both gross primary production and ecosystem respiration in evergreen forests and wetlands during the growing season; however, drought events overall reduce terrestrial carbon uptake at monthly scales. Zhao and Running (2010) modeled global annual net primary production from MODIS observations, and reported that continued, large-scale drought extremes decrease global terrestrial biosphere carbon uptake. An analysis of carbon flux estimates from ten TBMs conducted by Zscheischler et al. (2014) suggest that carbon fluxes in tropical forests are more likely driven by water availability at a 3-month scale, whereas temperature plays a more

important role in boreal forests at a monthly scale. Mekonnen et al. (2017) used a comprehensive process model to study the impacts of major droughts on terrestrial biosphere carbon fluxes in North America at annual time scale. They concluded that warming in northern ecosystems during drought periods generally increases carbon uptake because of longer growing seasons; however, in several sub-regions, frequent droughts reduce carbon uptake.

The frequency and intensity of droughts are projected to increase under climate change (Solomon et al., 2007) and land-atmospheric carbon exchange in response to droughts remains largely uncertain at different timescales. In addition, differences in ecosystem resilience will result in varying responses to droughts at different time scales (He et al., 2018), and droughts in turn can slow the pace of ecosystem recovery (Kolus et al., 2019; Schwalm et al., 2017). Therefore, we examined the biome-scale patterns in the correlation of land-atmosphere carbon exchange with droughts at different time scales, and examined the time scales at which carbon flux variables are most highly correlated with droughts. To characterize the magnitude and direction of drought on biome-scale net carbon exchange we developed a new categorical Drought Response Index (DRI), which allowed us to analyze the full range of various carbon source / sink responses.

2.2 Materials and Methods

2.2.1 Carbon Fluxes Data

Terrestrial Biosphere Models (TBMs) are advanced in their sensitivities to climate change and have the ability to estimate land-atmospheric carbon fluxes for a long-term, including net ecosystem exchange (NEE) and its component fluxes gross primary production (GPP), total ecosystem respiration (TR), as well as other fluxes (e.g. fire, harvesting, land cover change) (equation 2.1). In addition, disturbances associated with droughts such as fire can be included in

their estimates. Therefore, global-scale carbon flux estimates based on the simulation outputs from eight state-of-the-art TBMs (Table 2.1) that participated in the North American Carbon Program (NACP) Multi-scale Synthesis and Terrestrial Model Intercomparison Project (MsTMIP; Huntzinger et al., 2013) were selected in our analysis. In these eight models, temperature and water stress limit photosynthesis, moisture and temperature influence heterotrophic respiration. In addition, fire disturbance and land use change are included in their estimates of land-atmospheric carbon fluxes (Huntzinger et al., 2013).

$$NEE = -GPP + TR + "Other\ Fluxes"$$

Equation 2.1

The eight models were all driven with the same environmental and meteorological forcing data sets, including climate, land cover, land-use history, atmospheric CO_2 concentration, and atmospheric nitrogen deposition for the period of 1901-2010, and the model outputs were standardized to a monthly time scale and 0.5 degree grid size (Huntzinger et al., 2013; Wei et al., 2014). All of the TBMs in the MsTMIP ensemble were run with a common spin-up procedure; biome boundaries were fixed across all models during their simulations; and both water and temperature stress limit photosynthesis in all eight models (Huntzinger et al., 2014). By successively turning on different time-varying forcing data sets, simulation scenarios were designed to explore the influence of driving factors on their carbon flux estimates and other outputs (Huntzinger et al., 2013; Wei et al., 2014).

Table 2.1. Description of the eight TBMs from the MsTMIP study.

Model	Simulation Scenario	Simulated processes in NEE	Reference
CLASS-CTEM-N	BG1	land cover change	Huang et al. (2011)
CLM4	BG1	fire, land cover change	Mao et al. (2013); Mao et al. (2012)
CLM4VIC	BG1	fire, land cover change	Li et al. (2011)
GTEC	SG3	land cover change	Post et al. (1997)
LPJ-wsl	SG3	fire, land cover change	Sitch et al. (2003)
SiBCASA	SG3	land cover change	Schaefer et al. (2008); Schaefer et al. (2009)
TEM6	BG1	fire, land cover change	Hayes et al. (2011)
VISIT	SG3	land cover change	Ito (2010)

These carbon flux variables (i.e. GPP, TR, NEE) estimated by simulation scenario BG1, which turned on all the driving forces, were used. Since nitrogen cycle were not included in all the eight TBMs, for these models, estimates from SG3 (nitrogen cycle was not included) were used. Given that environmental drivers are better constrained by observations for the most recent 30-year estimates (Zscheischler et al., 2014), our analysis included the estimated carbon fluxes for the period of 1981-2010. Both GPP and TR are expressed as positive values, while a negative value of NEE represents carbon uptake on land (terrestrial carbon sink) and a positive value represents carbon release to the atmosphere (source). The eight model estimates for the carbon fluxes were integrated using the mean value. Schwalm et al. (2015) reported that naïve ("one model - one vote" where each model is weighted equally) integration is statistically indistinguishable from the more complex optimal integration, where weights are derived using reliability ensemble averaging. Therefore, we integrated each carbon flux estimate on a grid-by-grid basis with the mean value of the eight estimates calculated at the monthly time scale. Carbon fluxes are expressed as sums for various time periods.

2.2.2 Drought Metric

Drought and its impacts on vegetation require a specific time period for evaluation, because drought initiation, intensity, duration, and magnitude are all dependent on timescale (McKee et al., 1993). In this study, the response of biome carbon fluxes to droughts was examined at time scales of 3, 6, 12, 24, and 48 months, which are commonly-used time periods to analyze long-lasting droughts (e.g. McKee et al., 1993; Zscheischler et al., 2014). Drought was quantified using the standardized precipitation evapotranspiration index (SPEI), which integrates both precipitation and temperature at different time scales to represent the cumulative water balance (Vicente-Serrano et al., 2010). The SPEI was obtained from SPEIbase v.2.5 and resampled to 0.5 degree (Beguería et al., 2014) (http://hdl.handle.net/10261/153475). SPEI is a drought indicator of deviations from the average water balance, and represents the cumulative water balance over the previous scaled *n* months (Vicente-Serrano et al., 2010; Vicente-Serrano et al., 2013). It has advantages in that it can identify drought at various time scales, and is also sensitive to changes in evaporative demand. However, it is weak in representing soil properties, as water extractability is not incorporated (Bachmair et al., 2015; Blauhut et al., 2016; Vicente-Serrano et al., 2010). SPEI has been adjusted to a log-logistic probability distribution and is expressed as a standardized index, with negative values indicating drought over a given time scale (Vicente-Serrano et al., 2010).

2.2.3 Soil Moisture Metric

Because the eight models were different in their numbers of soils layers (ranging from 1 to 14 layers) and the rooting zone depths of their various vegetation types, it was impossible to directly compare the soil moisture estimates of the eight models. We therefore used an independent model data set to assess the relationship between drought and soil moisture and

further explain the biome response to drought at different time scales. Global, half-degree gridded estimates of monthly soil moisture obtained from the National Oceanic and Atmospheric Administration (NOAA) Climate Prediction Center (CPC; https://www.cpc.ncep.noaa.gov/soilmst/leaky_glb.htm) (Van den Dool et al., 2003) were used to evaluate the relationships between SPEI and soil moisture at time scales of 3, 6, 12, 24, and 48 months. Note that the soil moisture estimates at various time scales were recalculated as the monthly mean of the period.

2.2.4 Biome Aggregation

To compare the sensitivity and response of carbon fluxes to droughts among the biomes at different time scales, we grouped the global terrestrial biosphere into six biomes: tundra (TUN), boreal forest (BOF), temperate forest (TEF), tropical forest (TRF), temperate grassland (TEG) and tropical savanna (TRS). Since the biome data used by the MsTMIP project only has the grid vegetation type information (e.g. forest, shrub, grassland), but the physical climate boundary was not provided, so the biome information was obtained using the Terrestrial Ecoregions of the World Map (Olson et al., 2001) (http://www.worldwildlife.org/science/data/item1875.html) (Figure 2.1), and was resampled to 0.5×0.5 degree spatial resolution.

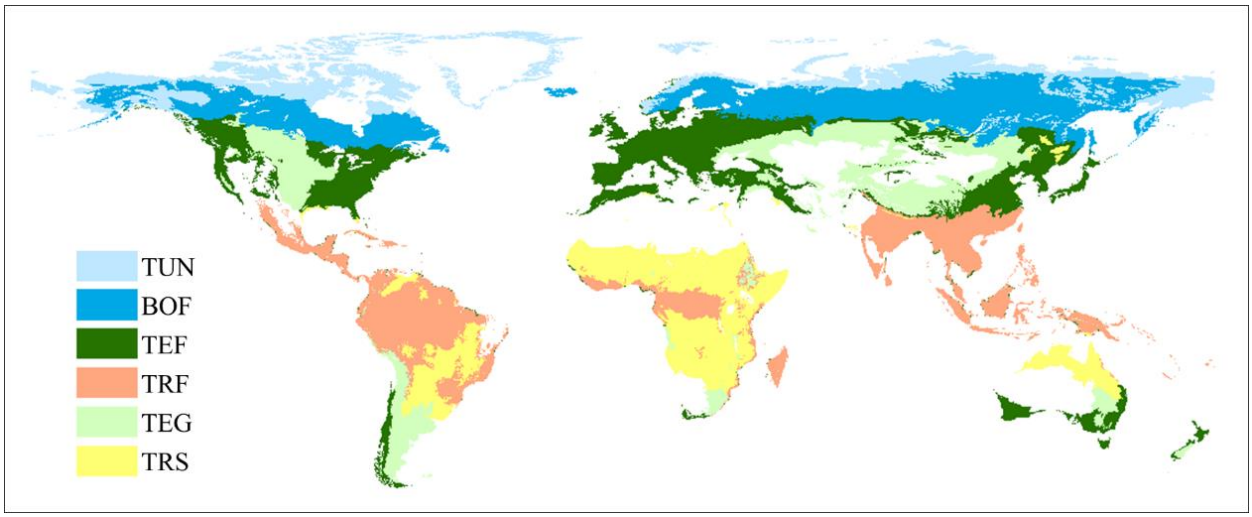

Figure 2.1. The six global biomes, including tundra (TUN), boreal forest (BOF), temperate forest (TEF), tropical forest (TRF), temperate grassland (TEG) and tropical savanna (TRS).

2.2.5 Correlation Analysis

To assess the correlation strength between droughts and carbon fluxes at different time scales, the Pearson's coefficient (Pearson's *r*) was used as the statistical measure to represent the strength of their linear relationship. To overcome the seasonal influence on carbon fluxes, the anomalies of carbon fluxes at all time scales were used in estimating the Pearson's *r*, which was calculated for each half-degree grid cell. A negative Pearson's *r* value indicates a negative linear correlation between the SPEI and the flux, while a positive value indicates a positive linear correlation. Accordingly, a positive Pearson's *r* means that increasing droughts correspond to a decreasing value of GPP, TR or NEE, while a negative Pearson's *r* means that increasing droughts correspond to an increase in the value of GPP, TR or NEE (*Figure A1*).

Because the numbers of paired SPEI and carbon flux anomalies (i.e. GPP, TR, and NEE) or soil moisture at the five time scales were different, a bootstrapping method was used to eliminate the sample size impact on calculating the Pearson's *r*. The bootstrapping was conducted as follows: 100 paired SPEI and carbon-flux anomalies or soil moisture estimates

were randomly selected for each grid cell, and a Pearson's *r* was calculated from them. This process was repeated 100 times, and the mean value of these values was used as the correlation score for that grid cell. Because the standard deviation had a very small value (normally < 0.01), it was not reported in our results.

We further explored the time scale at which the SPEI had the highest correlation with the flux anomaly for each grid cell. The same analysis method was used to assess the correlation strength between droughts and soil moisture at different time scales. Here, the absolute value magnitude of the Pearson's *r* was calculated to assess the strength of their relationship.

2.2.6 Biome-level Response to Droughts

Since the positive and negative values of NEE represent terrestrial carbon uptake (sink) and release (source), respectively, the Pearson's *r* alone could not characterize the patterns of net carbon exchange in response to drought. Therefore, to investigate the biome-scale net carbon exchange in response to droughts at different time scales, we developed a categorical Drought Response Index (DRI) (Table 2.2), representing six possible outcomes between terrestrial ecosystem carbon uptake and release during drought (SPEI < 0) and normal (non-drought, SPEI ≥ 0) periods:

(1) Droughts are associated with an increase in terrestrial carbon uptake (IU), which occurs when the average NEE estimates of both normal and drought periods correspond to carbon uptake (negative value), and the difference in NEE values between the two periods is positive.

(2) Droughts are associated with a decrease in terrestrial carbon release (DR), which occurs when the average NEE of both normal and drought periods corresponds to terrestrial carbon release (positive value), and the difference in the NEE values between the two

periods is positive.

(3) Droughts are associated with a decrease in terrestrial carbon release and an increase in carbon uptake (DRIU), which occurs when the average NEE of normal periods corresponds to terrestrial carbon release (positive value), the NEE of drought periods corresponds to uptake (negative value), and the difference in the NEE values between the two periods is positive.

(4) Droughts are associated with an increase in terrestrial carbon release (IR), which occurs when the average NEE of both normal and drought periods corresponds to terrestrial carbon release (positive value), and the difference in the NEE values between the two periods is negative.

(5) Droughts are associated with a decrease in terrestrial carbon uptake (DU), which occurs when the average NEE of both normal and drought periods corresponds to terrestrial carbon uptake (negative value), and the difference in the NEE values between the two periods is negative.

(6) Droughts are associated with a decrease in terrestrial carbon uptake and an increase in carbon release (DUIR), which occurs when the average NEE of normal periods corresponds with terrestrial carbon uptake (negative value), the NEE of drought periods corresponds with release (positive value), and the difference in the NEE values between the two periods is negative.

Table 2.2. The Drought Response Index (DRI) in terms of increasing or decreasing NEE during normal (N) and drought (D) periods.

	DRI	N	D	N - D	Description
(1)	IU	-	-	+	Droughts increase carbon uptake.
(2)	DR	+	+	+	Droughts decrease carbon release.
(3)	DRIU	+	-	+	Droughts decrease carbon release and increase uptake.
(4)	IR	+	+	-	Droughts increase carbon release.
(5)	DU	-	-	-	Droughts decrease carbon uptake.
(6)	DUIR	-	+	-	Droughts decrease carbon uptake and increase release.

Note that the positive value of NEE represents carbon release, while the negative value represents carbon uptake).

2.3 Results

2.3.1 Correlations of Carbon Fluxes with Droughts

GPP, TR and NEE were all strongly correlated with SPEI over large areas at the biome-scale. Globally, these carbon flux variables had stronger correlations with SPEI at 12-, 24-, and 48- month time scales than 3- and 6- month time scales (Figure 2.2). The tropical regions, including forest and savanna, showed stronger correlations than the other biomes. In contrast, most tundra areas showed the weakest correlation. Overall, both GPP and TR had strong positive correlations with SPEI, which suggests that increasing droughts were coincident with reductions of both of these major components of NEE. On the other hand, NEE had a strong negative correlation with SPEI, which suggests that increasing droughts were coincident with increases in NEE (i.e., decreased terrestrial carbon uptake, increased terrestrial carbon release to the atmosphere).

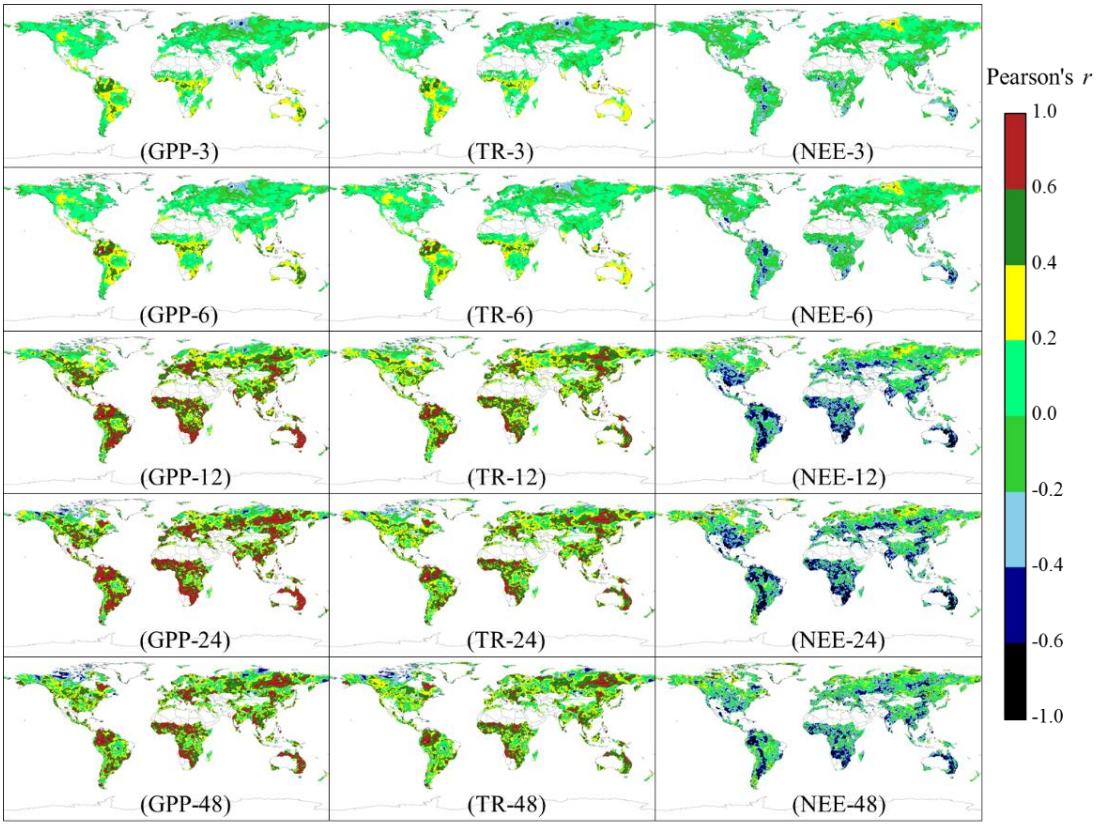

Figure 2.2. Geographical patterns of the correlation (Pearson's *r*) between drought (SPEI) and carbon flux anomaly (i.e., GPP, TR, NEE) at different time scales.

Overall, from the summarized correlation results, the six biomes differed in their correlation strength between carbon fluxes and SPEI at varying time scales (Figure 2.3). When the time scale increased from 3- to 12-month, the correlation strength of these six biomes became stronger, and then relatively stable. GPP had the most robust correlation across all biomes, and NEE had the weakest correlation with SPEI. Carbon fluxes in the tundra biome were more strongly correlated with 48-month SPEI, while all other biomes were more strongly correlated with the SPEI at 12- and 24- month time scales.

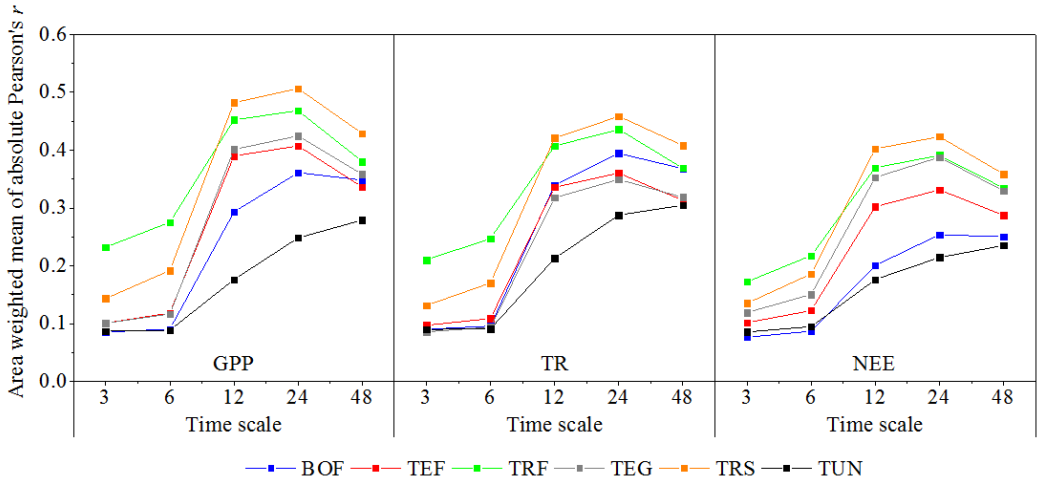

Figure 2.3. The area-weighted average absolute Pearson's *r* on each biome between carbon flux anomaly and SPEI.

2.3.2 The Highest Correlated Time Scale

GPP and TR had similar spatial patterns regarding the highest correlated time scale; however, NEE showed a somewhat different pattern (Figure 2.4). Overall, this correlation was highest when SPEI was assessed at the 24- and 48- month periods; however, several exceptions were found. The central Siberian tundra area was strongly correlated with SPEI at the 3-month time scale. Central North America and most of the Eurasian boreal forest were strongly correlated with SPEI at the 12-month time scale. Western North American temperate forest was strongly correlated with SPEI at the 12-month time scale. The central African tropical savanna was strongly correlated with SPEI at the 6-month time scale. The southern Amazon tropical forest was strongly correlated with SPEI at the 12-month time scale.

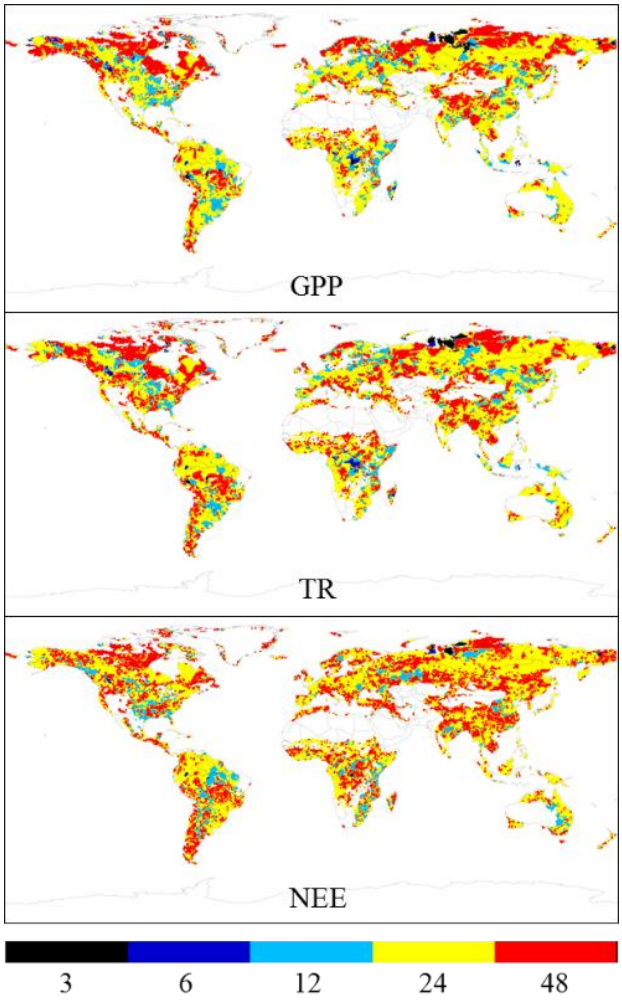

Figure 2.4. The global pattern of the time scale of each grid, at which SPEI had the highest correlation with GPP, TR, and NEE.

From the summarized results of the most correlated time scale, the GPP, TR and NEE had similar patterns across the six biomes in terms of their highest correlated time scales (Figure 5). Overall, the 12-, 24-, and 48- month time scales were dominant across all biomes. GPP and TR in a small portion of the six biomes were both highly correlated with SPEI at 3- and 6- month time scales. However, NEE exhibited higher correlation with SPEI on longer time scales.

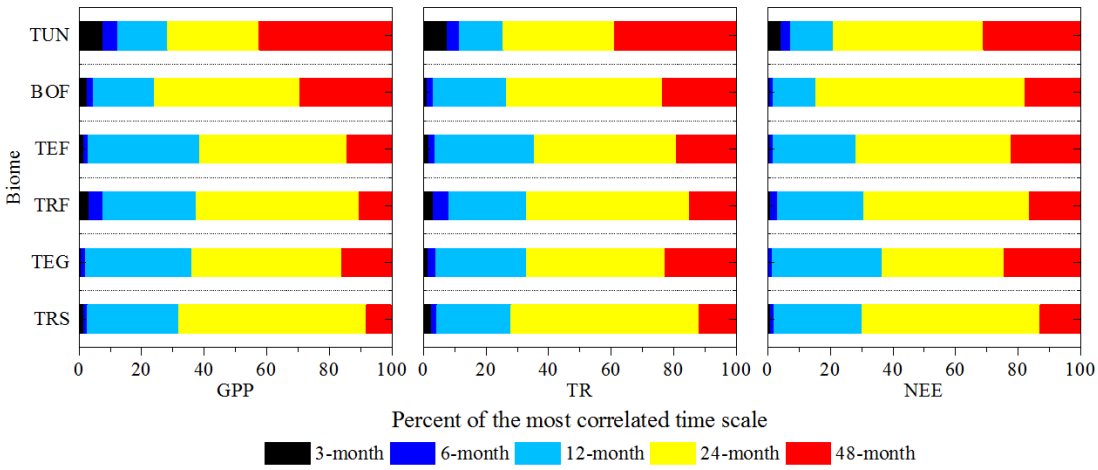

Figure 2.5. The percent of the highest correlated time scale on the six biomes for GPP, TR and NEE.

2.3.3 Net Carbon Exchange Response to Droughts

Geographically, the patterns of net carbon exchange in response to SPEI were similar at 3- and 6- month time scales (Figure 2.6). When the time scale of SPEI increased from 6- to 12-month, the net carbon exchange patterns in response to SPEI were greatly changed. These changes mostly occurred in the boreal forest and tundra biomes. Otherwise, the response patterns were similar at the 12-, 24-, and 48- month time scales. IU (droughts increase carbon uptake) was the dominant response in the Eurasian tundra, boreal and northern temperate forests, as well as parts of the temperate grasslands at 3- and 6- month time scales, but when the time scale increased to 12-month, the response of these regions shifted to DU (droughts decrease carbon uptake) response. DUIR (droughts decrease carbon uptake and increase release) was the dominant response pattern in North American tundra and boreal forest at 3- and 6- month time scales, but when the timescale increased to 12-month, the response of these regions were mostly changed to IR (droughts increase carbon release). Globally, DUIR, IR and DU (droughts decrease carbon uptake) were the dominant responses at all five time scales.

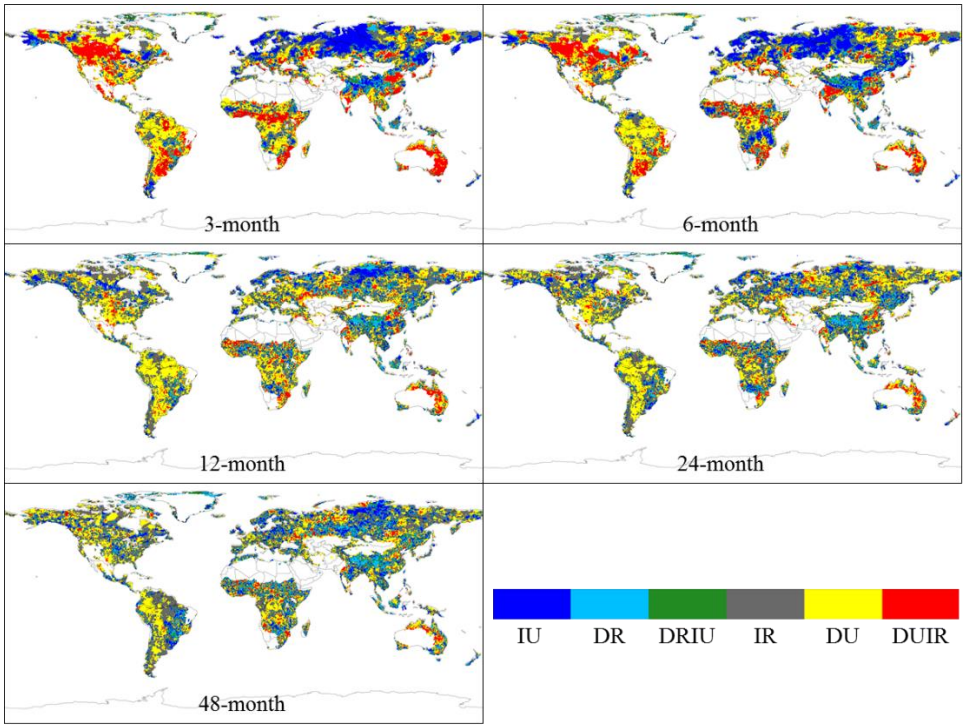

Figure 2.6. Geographical patterns of net carbon exchange in response to drought extremes shown as a map of grid cells categorized by the Drought Response Index (DRI).

From the summarized results of the biome net carbon exchange response to SPEI (Figure 7), in the tundra biome, the area with IU (droughts increase carbon uptake) response decreased with increasing time scale from 3- to 12-month, but the area with IR (droughts increase carbon release) response increased. The area of the other four responses remained stable across the different time scales. In the boreal forest biome, when the time scale increased from 3- to 12-month, the area with IU response increased, while the area with IR and DU (droughts decrease carbon uptake) responses decreased. When the time scale increased from 12- to 48-month, the area of each response was relatively stable. In the temperate forest, with the increasing time scale from 3- to 12-month, the area with DUIR (droughts decrease carbon uptake and increase release) response decreased and then became relatively stable. But, DU response was the dominant response at all time-scales. In the tropical forest, with the increasing time scale from 6- to 12-

month, the area of DUIR response greatly decreased. At all time scales, DU response was the dominant response. In the temperate grassland biome, the response patterns changed until the time scale reached 24-month. DUIR and DU were the dominant responses at the five time scales. In the tropical savanna, DUIR response was the dominant response at all time scales. With the increasing time scale, decreasing area with DRIU (droughts decrease carbon release and increase uptake) response was coincident with an increase area with DU response.

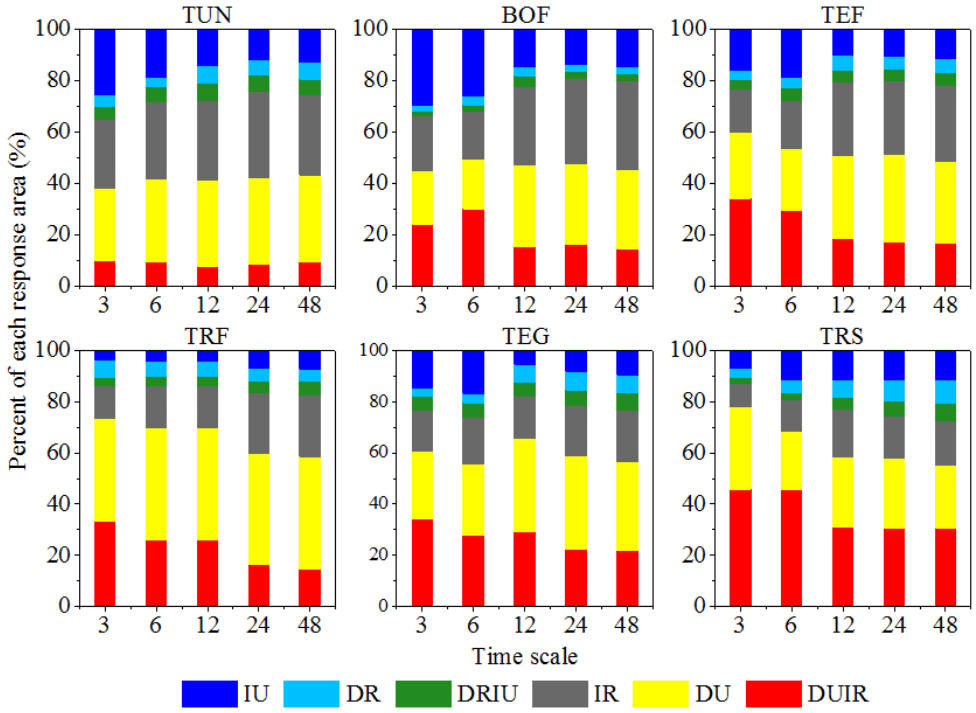

Figure 2.7. The percent of area of each Drought Response Index (DRI) for the six biomes.

2.3.4 Relationship between Soil Moisture and Droughts

Globally, the strength of the relationship between soil moisture and SPEI was different across the six biomes, where temperate forest had the strongest relationship with a mean of 0.5 at the five time scales, but the tundra biome had the weakest relationship with a mean of 0.33 at the five time scales (Figure 8). Overall, with increasing time scale, the strength of relationship between SPEI and soil moisture increased in all of the biomes. In tropical forest, the strength of

the relationship between SPEI and soil moisture was least changed by the time scale (ranged from 0.20 to 0.40), whereas temperate grassland was greatly changed (ranged from 0.28 to 0.61).

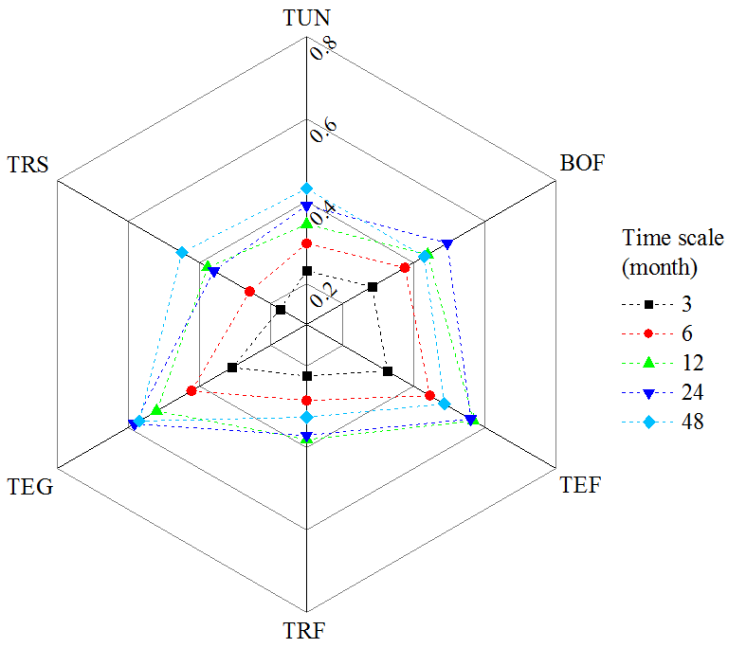

Figure 2.8. The correlation (absolute Pearson's *r*) between drought (SPEI) and soil moisture in each biome region.

2.4 Discussion

2.4.1 Biome Difference in Correlation Strength

The results suggest that terrestrial biosphere carbon fluxes are strongly correlated with droughts. However, the strength of their correlations differs among six global biomes. This is because different plant traits, soil characteristics, available nutrients, and species-specific responses can all influence the strength of the relationship between drought and biome-scale carbon flux (Ciais et al., 2005). Drought stress on vegetation occurs when the available water drops below a critical threshold, and this threshold changes according to plant species (Granier et al., 2007). In addition, the amount of water actually available to plants strongly depends on the root depth and type (Tolk, 2003). Therefore, the plant species assemblages in an ecosystem can

greatly influence the strength of the correlation between carbon flux variables and droughts. In addition, soil type along with other local surface and subsurface characteristics can influence the available water for plants, such as the depth to groundwater or bedrock (Tolk, 2003). Furthermore, mycorrhizal associations influence the response of ecosystem-scale carbon fluxes (i.e., GPP, TR) to changes in temperature and precipitation, where ectomycorrhizal-dominated ecosystems are primarily controlled by interannual variation in mean annual temperature, while arbuscular mycorrhizal-dominated ecosystems are primarily controlled by interannual variation in precipitation (Vargas et al., 2010). In addition, plants may respond to droughts by structural or physiological adjustments such as decreased leaf area, changes in the root-shoot ratio, internal carbohydrate concentration, or changes in osmolyte concentration, which may also increase the vegetation adaptation ability to droughts (Adams et al., 2017; Teuling et al., 2006).

Our results suggest that, among the six biomes, tundra shows the weakest relationship between carbon fluxes and droughts; this is consistent with the fact that warming increases the availability of soil water from snowmelt and thus mitigate droughts (Oechel et al., 1993). In some dry grassland and forest ecosystems, drought and GPP response may not be strongly correlated because photosynthesis can only increase if nutrients are available to support them (Peñuelas et al., 2007). In temperate forests, the carbon flux variables are not strongly correlated with drought likely, because in these ecosystems decreased GPP and autotrophic respiration are observed when relative root-extractable soil water drops below 40% (Granier et al., 2007) and so droughts with low severity may not greatly impact their carbon fluxes.

2.4.2 Spatial Similarity and Difference of Carbon Fluxes

The results of our model-ensemble analysis indicate that droughts are typically coincident with decreases in both GPP and TR. Droughts decrease photosynthetic and respiration rates

through reducing stomatal and mesophyll conductance, as well as the activity and concentrations of enzymes (Keenan et al., 2010). At the ecosystem-scale, droughts generally have a greater impact on photosynthesis than on respiration (Atkin and Macherel, 2008; Schwalm et al., 2010). Therefore, the net effect of droughts is primarily to reduce the rate of carbon uptake by an ecosystem. In addition, drought suppresses photosynthesis, and trees thus reduce investment in their tissue maintenance (Doughty et al., 2015), which can lead to high mortality rates (Greenwood et al., 2017; Phillips et al., 2010) and therefore lower rates of carbon uptake by live biomass and higher rates of release from dead and decaying organic matter. In addition, fires resulting from time-lagged drought effects can directly release carbon to the atmosphere and indirectly reduce the carbon uptake and storage in ecosystems (Frank et al., 2015).

GPP and TR have similar spatial patterns of their correlation strengths with drought, but the spatial patterns of NEE in a biome are different from its patterns of GPP and TR fluxes. This is because droughts can directly affect photosynthesis and respiration (e.g. reducing the activity of enzymes and soil microbes) (Keenan et al., 2010). For example, low photosynthetic rates are typically associated with low costs in autotrophic maintenance respiration (Meir et al., 2008). But, at the biome-scale, the patterns of carbon release and uptake can be influenced by time-lagged impacts (e.g. the changing composition of plant species, frequency of fires, and soil microbial community structure and activity), which are indirectly caused by droughts and substantially promote ecosystem carbon release to the atmosphere (Frank et al., 2015).

2.4.3 Response Similarity and Difference

Our results suggest that in portions of particular biomes, increasing droughts are coincident with increasing GPP and TR resulting in an increase in carbon uptake or a decrease in carbon release. In tundra and boreal forest ecosystems, drought is associated with longer and

warmer growing seasons, which can promote photosynthetic rates as well as respiratory losses (Black et al., 2000; Jager et al., 2009). In tropical forest ecosystems, droughts can also promote GPP and TR because, in radiation-limited environments, relatively drier conditions and the associated decreased cloudiness and higher insolation can accelerate carbon uptake (Huete et al., 2006; Scott et al., 2009). In temperate forest and grassland regions, droughts may induce plant activity earlier and thus increase the carbon uptake, which has been observed at biome scales with remote sensing (Myneni et al., 1997; Pilegaard et al., 2011).

Our results suggest that the net carbon exchange in response to droughts is strongly influenced by biome type and time scale. When the time scale is increased from 6-month to 12-month, the response patterns changed dramatically in part of the boreal forest and tundra area, where temperature represents the major control on carbon fluxes (Oechel et al., 1993; Welp et al., 2007). Short episodes of drought in late winter and spring may extend the growing seasons and thus reduce the carbon release or increase the carbon uptake (Jager et al., 2009). In contrast, droughts with longer time scales are associated with warmer summers, which can greatly reduce GPP and further decrease carbon uptake or increase carbon release (Welp et al., 2007).

In water-limited regions such as the tropical biomes, plant species are adapted to water shortage, droughts with shorter time scales may not impact their carbon uptake or release patterns as much as in other biomes. In contrast, plant species of humid biomes are not well-adapted to drought, so droughts with shorter time scales may significantly change their response patterns (Maherali et al., 2004). This is in agreement with our results that suggest the drought response patterns of each biome are relatively stable within shorter time scales (3- and 6- month time scales) while much more highly impacted at the 6-month to 12-month time scale. The time-

lagged impacts may occur at the end of drought events on a longer time scale (Yin et al., 2013) and influence the patterns of carbon fluxes.

2.4.4 Effect of Soil Moisture on Drought Response

Because the SPEI is weak in representing soil properties and could not measure water extractability, the impact of soil porosity and moisture on biome carbon fluxes was not examined. However, soil moisture greatly affects the land-atmospheric carbon exchange in response to drought (e.g. Bartlett et al., 2012; Prentice et al., 1992). Our results suggest that soil moisture is correlated to drought and the strength becomes stronger with increasing time scale, which means that drought events with longer time scales can further change the patterns of carbon fluxes. The strength of the relationship between soil moisture and drought is strongly influenced by biome type and by time scale, both of which influence the dynamic drought response patterns of carbon fluxes. In the tundra biome, where soil moisture is weakly correlated to drought, the patterns of carbon fluxes are weakly influenced by drought. In temperate forests, because soil moisture is strongly correlated with drought format the 3- to 12-month time scale, the patterns of carbon fluxes are highly influenced by the response to drought. In tropical forests, since the strength of relationship between SPEI and soil moisture is least influenced by the time scale, the response patterns of carbon fluxes are also not greatly changed. In both temperate grassland and tropical savanna, the strengths of the relationships between SPEI and soil moisture are influenced by the time scale, which significantly changes the temporal patterns of carbon fluxes in response to drought.

2.5 Conclusions

Our study used an ensemble of terrestrial biosphere model outputs to examine the biome-scale relationship and magnitude of ecosystem carbon fluxes in response to droughts in different

biomes and at varying time scales. Our results suggest that tropical regions, including both forest and savanna, have the most robust correlation with drought whereas the tundra biome has the weakest. In addition, the time-scale at which drought most affects carbon fluxes is useful to understand and therefore predict how biome-scale carbon fluxes may respond to future climate change. Globally, the patterns of biome carbon fluxes vary according to time scale, and are most highly correlated to drought at the 24-month scale. The drought response index suggest that carbon uptake / release patterns are influenced by the biomes and time scales. Overall, drought primarily decreased carbon uptake or increased carbon release; however, they may increase carbon uptake or reduce the carbon release in particular portions of each biome.

CHAPTER 3

3. EFFECTS OF ENVIRONMENTAL FACTORS ON REGULATING TEMPORAL PATTERNS OF DISSOLVED ORGANIC CARBON EXPORT

3.1 Introduction

An advanced understanding and accurate accounting of the terrestrial carbon cycle is required to predict future climate change and ecosystem response (Chapin et al., 2006; Cox et al., 2000). Carbon budget estimation and scaling efforts have typically focused on comparing "bottom-up" estimates of carbon stock change from field inventories and process models with "top-down" estimates of land-atmosphere carbon exchange from inversion modeling frameworks (King et al., 2015). Increasingly recognized, however, is the important role that lateral transfer of carbon through the aquatic system plays in the overall dynamics of the terrestrial ecosystem (Battin et al., 2009; Regnier et al., 2013), and that these "sideways" fluxes must be better characterized in order to balance the carbon budget and reconcile differences between top-down and bottom-up estimates (Hayes et al., 2018). Current carbon budget estimation and scaling approaches may only implicitly include these lateral fluxes or ignore them altogether, thus making it difficult or impossible to compare among estimates (Hayes and Turner, 2012).

Dissolved organic carbon (DOC), which is primarily formed by the incomplete decomposition of soil organic carbon and exuded by plants (Michalzik et al., 2003), can be moved from the soils to inland waters by surface runoff and subsurface lateral flow, and serve as an important component of the lateral terrestrial-aquatic carbon flux (Cole et al., 2007; Tank et al., 2018). In aquatic ecosystems, DOC can be subject to sedimentation in water bodies or be biotically or abiotically oxidized into CO_2 and released to the atmosphere, with the remaining

DOC exported to the ocean (Cole et al., 2007). Therefore, including the terrestrial-aquatic DOC flux is necessary to improve estimates of broad-scale ecosystem carbon dynamics; however, this flux is excluded or not well represented in some carbon flux estimation methods. Eddy-covariance measurements have the ability to capture carbon fluxes from aquatic ecosystems within the tower footprint (Foken et al., 2012; Zhao et al., 2019). Atmospheric inversion models are a type of top-down method that estimates vertical, terrestrial-atmosphere carbon exchange including carbon outgassing from aquatic ecosystems within the modeling domain (Peters et al., 2007; Schuh et al., 2019). However, neither of these methods are able to explicitly account for the fate of carbon exported to aquatic ecosystems. Inventory-based methods may indirectly estimate fluxes from carbon stock changes in the major carbon pools (Hayes et al., 2012; Pan et al., 2011); however, they do not track the direction of carbon transfers among these carbon pools.

To estimate this terrestrial-aquatic DOC flux, numerous modeling methods including empirical and process-based models have been applied at various spatial and temporal scales. Ludwig et al. (1996) presented an empirical model using drainage intensity, landscape and soil organic carbon content to estimate DOC flux from terrestrial to aquatic ecosystems. Aitkenhead and McDowell (2000) developed a linear empirical model based on soil carbon to nitrogen ratios and estimated the global DOC export from land to oceans. Neff and Asner (2001) developed a runoff-based layered soil model, which is driven by the water fluxes, to estimate the DOC transported from terrestrial to aquatic ecosystems. Michalzik et al. (2003) developed a process-based model that used precipitation, air and soil temperature to drive the DOC flux process in forest soil. Harrison et al. (2005) proposed an empirical modelling method using runoff, wetland area, and consumptive water use to assess determine DOC export. Futter et al. (2007) used land cover, air temperature, and precipitation to estimate the DOC flux from soil to stream.

Kicklighter et al. (2013) improved and applied the Terrestrial Ecosystem Model (TEM) to estimate the DOC loading from terrestrial ecosystems to the river networks in pan-Arctic region. Ren et al. (2016) improved the Dynamic Land Ecosystem Model (DLEM) to simulate the DOC export from the Mississippi River to the ocean. Lauerwald et al. (2017) added the DOC flux estimation module with the existing Organising Carbon and Hydrology in Dynamic Ecosystems (ORCHIDEE) model, which has the ability to estimate the DOC production, leaching from soils to inland waters, and decomposition. Li et al. (2019) developed a process-based model, TRIPLEX-hydrological routing algorithm (TRIPLEX-HYDRA), which has the ability to simulate the fate of DOC in terrestrial and aquatic ecosystems.

Many environmental factors interact to control DOC export from watersheds, and various combinations of these factors have been used in existing modelling methods. Recent studies have suggested that the export rate is primarily related to air temperature (Raymond and Saiers, 2010; Winterdahl et al., 2016), precipitation (Raymond et al., 2016), sulfur deposition (Meyer-Jacob et al., 2015; SanClements et al., 2012), nitrogen deposition (Chen et al., 2015), and land cover (Sawicka et al., 2016; Webster and McLaughlin, 2010). At the subcontinental watershed-scale, there remains considerable uncertainty as to the relative importance of these environmental factors in determining the rate and temporal patterns on DOC export. Investigating these factors and understanding their relative importance in determining intra-annual variability as well as temporal patterns in DOC export are critical for adequately assessing and modelling terrestrial biosphere carbon cycle dynamics at regional and global scales. In this synthesis study, we integrated the data sets for DOC export from 14 watersheds at the subcontinental scale within the conterminous United States and analyzed the influence of major potential environmental factors

governing DOC export, including air temperature, precipitation, nitrogen deposition, sulfur deposition and land cover on a multi-decadal time scale.

3.2 Data and Methods

3.2.1 Watershed DOC Export Data

The watershed DOC export data for each of 14 watersheds was obtained from the long-term observational data of DOC concentration and water discharge provided by the US Geological Survey (USGS) National Water Information System (NWIS; waterdata.usgs.gov/nwis/, Figure 1, Figure S1). The 14 watersheds were selected based on two criteria: (1) that they were located entirely within only one climate division as defined by the National Oceanic and Atmospheric Administration (NOAA) data set (esrl.noaa.gov/psd/data/usclimdivs/) to better represent their climate information, with one exception being Suwannee River Watershed (which had 43% area located in Georgia south central climate division and 57% in Georgia southeast, so that the weighted average air temperature and precipitation of the two climate divisions were used as its climate information); (2) included at least 200 records of organic carbon concentration and all daily hydrological discharge in the analyzed time period (These two conditions were required to realize the DOC export calculation in section 2.3.), mean annual and monthly air temperature, total annual precipitation, and total annual atmospheric sulfur and nitrogen deposition. Since the organic carbon concentration measured from unfiltered water samples included all organic matter (i.e. both dissolved and particulate organic carbon), the organic carbon concentrations measured from the unfiltered water samples were adjusted as DOC concentration estimates via a linear regression model (y=0.60x+0.63, R^2=0.91, *Figure B2*).

The boundary and stream flow of each watershed were obtained from the USGS Watershed Boundary Dataset (WBD) and National Hydrography Dataset (NHD) of the National Geospatial Program (NGP; usgs.gov/core-science-systems/ngp/national-hydrography) (*Table B1*). The 14 watershed varied greatly in size, and ranged from 6 km^2 (McDonalds Branch) to 2927 km^2 (Suwannee River). To assess the impact of watershed size on DOC export, the linear relationship between annual DOC export from a watershed and watershed size as well as the linear relationship between coefficient of variation of annual DOC export from a watershed (an indicator of the magnitude of interannual changes) and watershed size were analyzed.

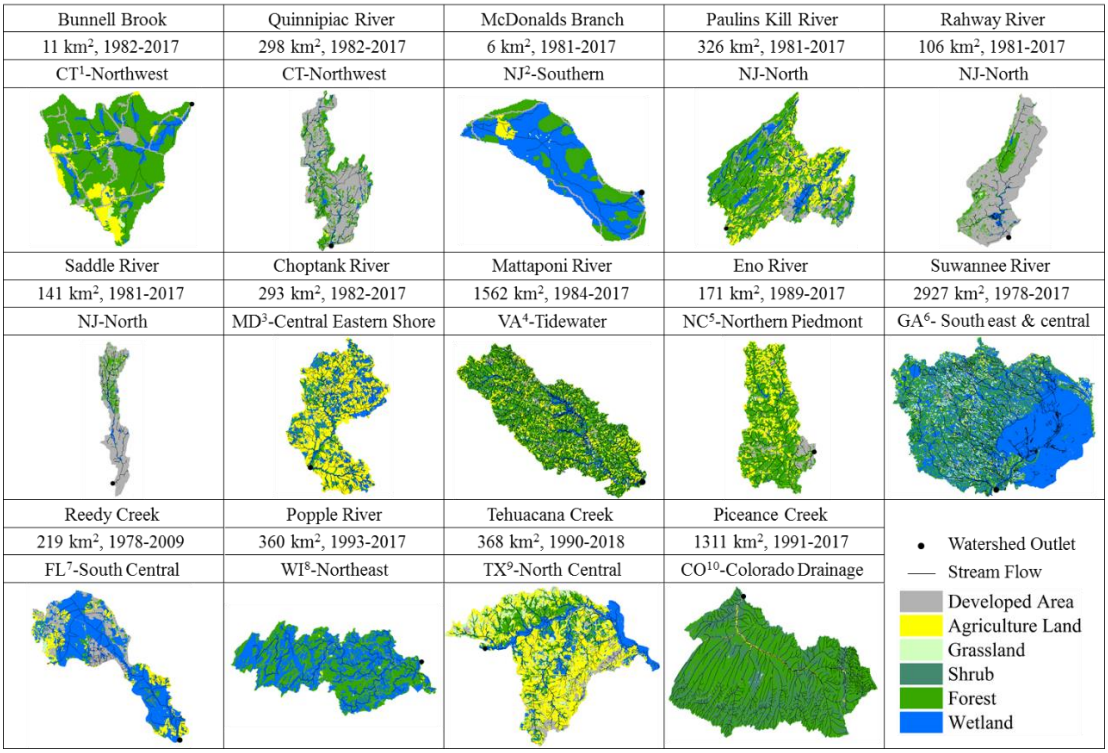

[1]Conneticut, [2]New Jersey, [3]Maryland, [4]Virginia, [5]North Carolina, [6]Georgia, [7]Florida, [8]Wisconsin, [9]Texas, [10]Colorado

Figure 3.1. Maps of the 14 watersheds, as well as the size, time period of available data sets, climate division, stream flow, location of the watershed outlet, and land cover composition.

3.2.2 Environmental Factors

The climate data for each watershed including mean annual and monthly air temperature (°C) and annual and monthly total precipitation (cm) were obtained from NOAA's National Centers for Environmental Information (NCEI; ncdc.noaa.gov/cag/divisional). The wet sulfur (SO_4^{2-} deposition, g/m^2 per year as sulfur) and total inorganic nitrogen (NH_4^+ and NO_3^- deposition, g/m^2 per year as nitrogen) deposition were obtained from the National Trends Network (NTN) of National Atmospheric Deposition Program (NADP; nadp.slh.wisc.edu/data/) (NADP, 2019). NTN provided annual gradient raster maps of atmospheric deposition from 1985 to 2017. We used the boundary of each watershed to extract its annual gradient raster maps, and calculated the mean value (g/m^2 per year) to represent the annual watershed sulfur and nitrogen deposition. NTN also provided site recorded atmospheric deposition data, which has longer records (started from 1978 and end in 2018). To extend the length of atmospheric deposition data for a watershed, we used the annual records from a site that was within the watershed (or the closest site), as well as the mean values obtained from the gradient maps of the watershed to build a linear regression model. The model was then used to extend the length of atmospheric deposition records for that watershed.

The most recent National Land Cover Database 2016 (NLCD2016) (Yang et al., 2018), provided by the Multi-Resolution Land Characteristics (MRLC) Consortium (mrlc.gov), was used to characterize each watershed for its proportional land cover (Figures 2). For this analysis, we aggregated the 16 classes of the original NLCD2016 into six land cover types (*Table S2*): developed area, agriculture land, grassland, shrub, forest, and wetland.

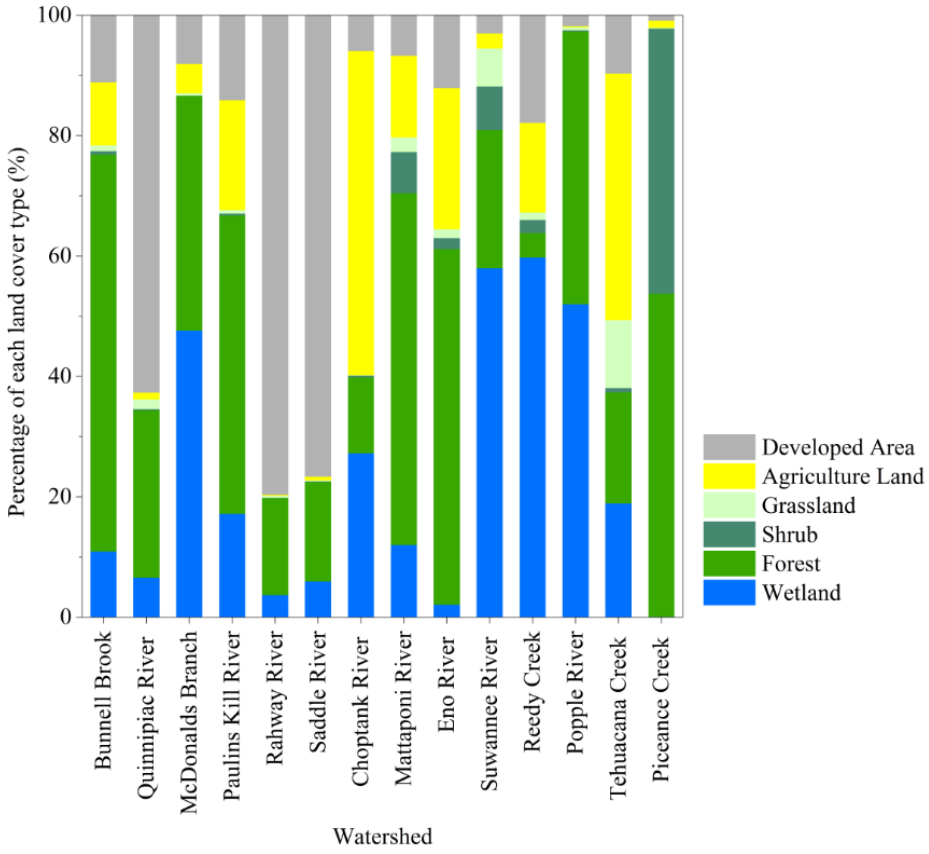

Figure 3.2. The percentage of the six land cover types in each of the 14 watersheds used in this study.

3.2.3 DOC Export Estimation

Because of the methodological weakness of lab measurement of DOC concentration, sample bias, and the limited samples that directly measured DOC concentration, the Weighted Regressions on Times, Discharges, and Season model (WRTDS, equation 3.1) proposed by Hirsch et al. (2010) was used to calculate DOC export from each watershed. This model allows for maximum flexibility in representations of the long-term trend, seasonal components, and discharge-related components of the behavior of the DOC export (Hirsch et al., 2010).

$$\ln(C) = \alpha \ln(Q) + \beta t_y + \gamma \sin(2\pi t_m) + \delta \cos(2\pi t_d) + \varepsilon$$

Equation 3.1.

where C is the daily DOC concentration, Q is the daily discharge, t_y is the order of the year, t_m is the order of month (i.e. 1, 2, 3 … 12), and t_d is the order of the day (i.e. 1, 2, 3 … 365 or 366).Parameters α, β, γ, and δ are fitted coefficients, and ε is the unexplained variation.

The monthly DOC export from a watershed was calculated with the daily discharge and estimated daily DOC concentration (equation 3.2).

$$M_{DOC} = \sum_{d=1}^{N} D_{DOC} * D_{Discharge}$$

Equation 3.2

where M_{DOC} is the monthly DOC export, D_{DOC} is the estimated daily DOC concentration, $D_{Discharge}$ is the daily discharge, and N is the total days in that month.

3.2.4 Relative Importance Analysis

Since these environmental factors were measured in different units, it was impossible to examine the relative magnitude of each factor by directly comparing coefficients of a multiple regression model. To overcome this problem, the standardized coefficient was used, which is an index that can estimate the relative importance of multiple independent variables on a dependent variable (Bring, 1994). To examine and compare the magnitudes of impacts of annual air temperature, precipitation, sulfur and nitrogen deposition on DOC export, all these variables were first standardized (equation 3.3 and 3.4).

$$\hat{y}_j = \frac{y_j - \bar{y}}{STD_y}$$

Equation 3.3

$$\hat{x}_{ij} = \frac{x_{ij} - \bar{x_i}}{STD_{x_i}}$$

Equation 3.4

where $\hat{y}$ is the normalized annual DOC export, j is the year, $\bar{y}$ is the mean of annual total DOC export, STD_y is the standard deviation of annual DOC exports, $\hat{x}_i$ is the normalized environmental factor i (i.e. air temperature, precipitation, sulfur and nitrogen), $\overline{x_i}$ is the mean value of factor i, STD_{x_i} is the standard deviation of environmental factor i. Then these standardized variables were used to create the multiple regression model (equation 3.5).

$$\hat{y} = \beta_T \hat{x}_T + \beta_P \hat{x}_P + \beta_S \hat{x}_S + \beta_N \hat{x}_N + \varphi$$

Equation 3.5

where β_i is the standardized coefficient representing the average change in y when x_i is changed by one unit, φ is the intercept. T is the mean annual air temperature, P is the total annual precipitation, S is the total annual sulfur deposition, and N is the total annual nitrogen deposition.

The multiple regression model was created for each of the 14 watersheds. A higher absolute value of standardized coefficient means that the changes of this environmental factor had a greater magnitude impact on DOC export. A negative value of the standardized coefficient indicates that the increasing absolute value of the factor was coincident with declining DOC export, but a positive value indicates that the increasing standardized coefficient for that factor was coincident with increasing DOC export.

3.2.5 Time-series Patterns Analysis

To characterize the time-series patterns, an additive model was used to decompose the monthly DOC export data (equation 3.6). The monthly DOC export from a watershed was decomposed to four temporal patterns including major level (DOC_{Level}), long-term trend (DOC_{Trend}), seasonal dynamics (DOC_{Season}), and random residual ($DOC_{Residual}$), through using the moving average decomposition method (frequency=12, Figure 3.3). Note that with this time series decomposition method, the major level was a constant value. Then, linear relationships

between environmental factors and total DOC export or these temporal patterns were assessed at different temporal scales, and strongly correlated environmental factors and total DOC export or temporal patterns were reported in this study (i.e., air temperature and seasonal dynamics at monthly temporal scale, total precipitation and DOC export at annual temporal scale, sulfur deposition and long-term trend at annual temporal scale).

$$DOC = DOC_{Level} + DOC_{Season} + DOC_{Trend} + DOC_{Residual}$$

Equation 3.6

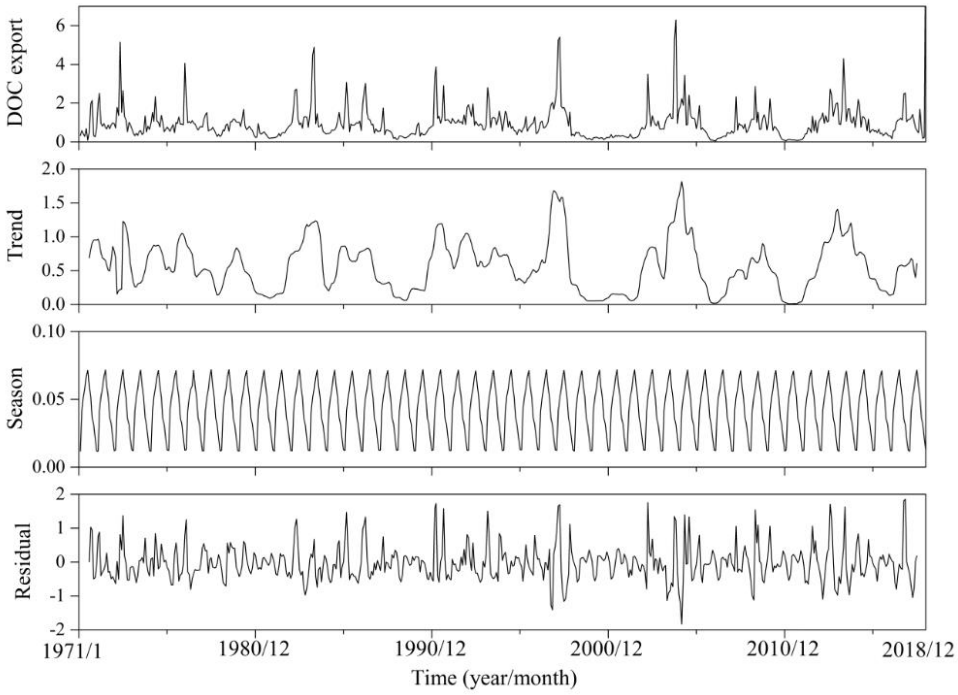

Figure 3.3. An example of the decomposed DOC export from Suwannee River watershed including long-term trend, seasonal dynamics, and random residual (The unit is gC/m^2 per month. Note that the major level is a constant value, it is not presented.).

Temporal autocorrelation of DOC export was examined using the Durbin-Watson (DW) test (equation 3.7). The hypotheses for the DW test was no first order autocorrelation with the

monthly random residual. When the DW value equals 2, it indicates no autocorrelation; when the DW value is larger than 0 but less than 2, it indicates a positive autocorrelation; when the DW value is larger than 2 but less than 4, it indicates a negative autocorrelation. A rule of thumb suggested by Field (2009) is that DW values under 1 or more than 3 are a definite cause for concern.

$$DW = \frac{\sum_{i=2}^{T}(E_t - E_{t-1})^2}{\sum_{i=1}^{T} E_i^2}$$

Equation 3.7

where E_t is the random residual at time t, T is the total number of the time-series data.

3.2.6 Land Cover Analysis

Annual land cover information for each watershed was not available, and the comparisons of land cover maps in 2006 (NLCD2006) and 2016 (NLCD2016) suggested that land cover changed less than 7.6% (ranged from 0.2 to 7.6%) in these 14 watersheds for that time period. Thus, the 14 watersheds were combined, and the linear relationship for each land cover type and the average annual DOC export was examined to assess the relationship between each land cover type and annual DOC export.

3.3 Results

3.3.1 Watershed DOC Export

The average annual DOC export from these 14 watersheds was 2.97±1.56 gC/m^2 per year (Table 3.1). Piceance Creek watershed had the lowest export of 0.08±0.07 gC/m^2 per year, and the Reedy Creek watershed had the highest export of 8.81±5.78 gC/m^2 per year. The magnitudes of interannual changes of these 14 watersheds varied greatly. Quinnipiac River watershed had the lowest significance of interannual changes (coefficient of variation=26%), and Piceance

Creek watershed had the highest significance of interannual changes (coefficient of variation=88%).

Table 3.1. The annual DOC export and coefficient of variation of these 14 watersheds (CV= coefficient of variation).

Watershed	Size (km^2)	DOC ($gC/m^2\ yr^{-1}$)		CV (%)
		Mean	Std	
Bunnell Brook	11	2.12	0.79	37
Quinnipiac River	298	2.42	0.63	26
McDonalds Branch	6	2.41	1.41	59
Paulins Kill River	326	2.16	0.81	38
Rahway River	106	1.85	0.63	34
Saddle River	141	2.68	0.77	29
Choptank River	293	2.53	1.57	62
Mattaponi River	1526	1.82	0.97	53
Eno River	171	1.33	0.69	52
Suwannee River	2927	7.80	4.83	62
Reedy Creek	219	8.81	5.78	66
Popple River	360	3.79	1.56	41
Tehuacana Creek	368	1.71	1.31	77
Piceance Creek	1311	0.08	0.07	88
Mean	576	2.97	1.56	52

The coefficient of determination (R^2) between sizes of watersheds and their annual DOC exports was 0.06 (Figure 4a), which indicated that there was no obvious relationship between sizes of watersheds and DOC exports (Note that the relationship between sizes of watersheds and their annual DOC exports was created with a bootstrapping method, which used ten estimated DOC exports from a watershed that randomly generated from its range.). The R^2 between sizes of watersheds and their magnitudes of interannual changes of DOC exports was 0.07 (Figure 3.4b), which indicated that there was no obvious relationship between sizes of watersheds and magnitudes of interannual changes of DOC exports.

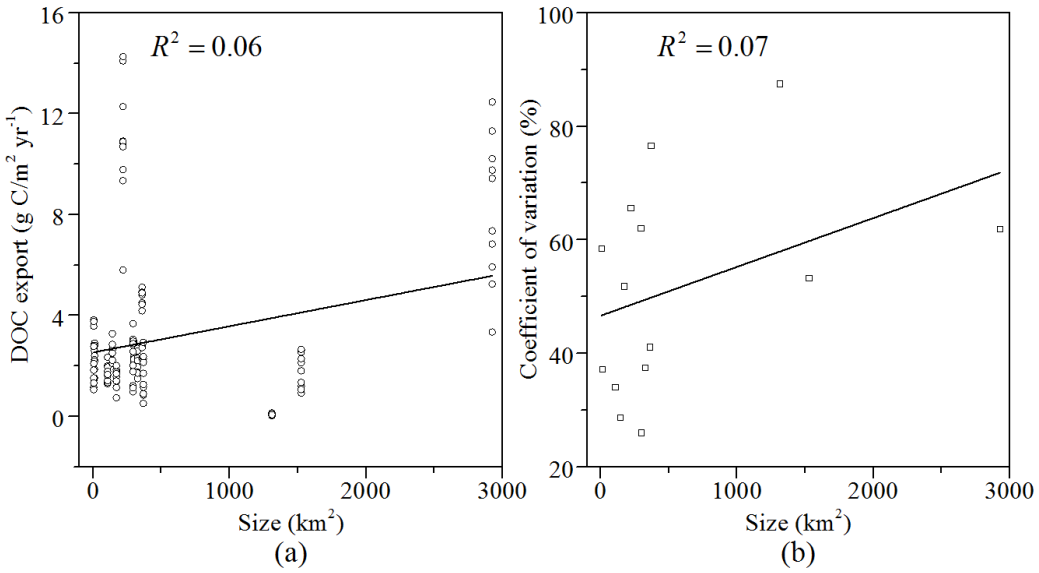

Figure 3.4. The coefficient of determination (R^2) between sizes of watersheds and their annual DOC exports (a), and the R^2 between sizes of watersheds and their magnitudes of interannual changes of DOC exports (b).

3.3.2 Relative Magnitudes of Environmental Factors

Standardized regression models for the 14 watersheds indicated that these models could adequately represent the relationship between these environmental variables and annual DOC export (Table 2, R^2=0.72±0.06). The standardized regression model created for the Saddle River watershed had the highest R^2 of 0.85, while Popple River watershed had the lowest R^2 of 0.65. Precipitation had the strongest impact on DOC export, with an average standardized coefficient of 0.81±0.07, but temperature had the weakest impact on DOC export with an average absolute standardized coefficient of 0.01±0.11. Precipitation had the strongest positive relationship with DOC export (0.81±0.07), while sulfur deposition had the strongest negative relationship (-0.22±0.20). Within all watersheds, precipitation showed a positive relationship with DOC export. Overall, nitrogen deposition showed a positive relationship with DOC export, and was negatively

related to sulfur deposition. However, the responses of DOC export to temperature were substantially different from watershed to watershed.

Table 3.2. The standardized coefficients of mean annual air temperature (Temp), total annual precipitation (Precip), total annual atmospheric sulfur (S) deposition, total annual nitrogen (N) deposition, R^2 for each standardized regression model, and their mean and mean of absolute values.

Watershed	Temp	Precip	S	N	R^2
Bunnell Brook	-0.08	0.84	-0.28	0.26	0.70
Quinnipiac River	-0.16	0.91	-0.13	-0.09	0.69
McDonalds Branch	-0.03	0.79	-0.09	0.23	0.75
Paulins Kill River	-0.09	0.80	-0.45	0.43	0.80
Rahway River	0.11	0.89	-0.78	0.02	0.76
Saddle River	-0.07	0.88	-0.11	0.15	0.85
Choptank River	-0.07	0.79	-0.44	0.27	0.78
Mattaponi River	0.00	0.78	0.00	0.13	0.68
Eno River	-0.07	0.65	-0.07	-0.09	0.66
Suwannee River	0.18	0.77	-0.13	-0.02	0.66
Reedy Creek	-0.07	0.83	-0.09	0.18	0.74
Popple River	0.00	0.79	-0.04	0.00	0.65
Tehuacana Creek	0.22	0.88	-0.24	0.09	0.73
Piceance Creek	-0.06	0.72	-0.24	0.29	0.68
Mean±Std	-0.01±0.11	0.81±0.07	-0.22±0.20	0.13±0.15	0.72±0.06
Mean±Std (abs)	0.09±0.06	0.81±0.07	0.22±0.20	0.16±0.12	0.72±0.06

3.3.3 Temporal Patterns of DOC Export

The coefficient of determination (R^2) between air temperature and seasonal dynamics at monthly temporal scale ranged from 0.59 in Reedy Creek watershed to 0.91 in Rahway River watershed with a mean of 0.74 (Table 3.3). The R^2 between total precipitation and DOC export at annual temporal scale ranged from 0.63 in Bunnell Brook watershed to 0.85 in Saddle River watershed with a mean of 0.70. The R^2 between sulfur deposition and long-term trend at annual

temporal scale ranged from -0.89 in Choptank River watershed to -0.59 in Piceance Creek Watershed with a mean of -0.72. The DW values ranged from 1.44 in McDonalds Branch watershed to 1.87 in Saddle River watershed with a mean of 1.68.

Table 3.3. Summary of the coefficient of determination (R^2) between environmental factors and temporal patterns or total DOC export, including air temperature and seasonal dynamics at monthly temporal scale (T - Season), total precipitation and DOC export at annual temporal scale (P - DOC), sulfur deposition and long trend at annual temporal scale (S - Trend), as well as autocorrelation of random residual (DW= Durbin-Watson Value).

Watershed	T - Season	P - DOC	S - Trend	DW
Bunnell Brook	0.69	0.63	-0.69	1.85
Quinnipiac River	0.75	0.65	-0.86	1.50
McDonalds Branch	0.85	0.70	-0.61	1.44
Paulins Kill River	0.85	0.76	-0.63	1.68
Rahway River	0.91	0.72	-0.74	1.47
Saddle River	0.75	0.85	-0.85	1.92
Choptank River	0.69	0.71	-0.89	1.91
Mattaponi River	0.62	0.73	-0.69	1.64
Eno River	0.67	0.66	-0.73	1.55
Suwannee River	0.66	0.64	-0.74	1.52
Reedy Creek	0.59	0.72	-0.76	1.73
Popple River	0.86	0.65	-0.73	1.76
Tehuacana Creek	0.71	0.67	-0.61	1.75
Piceance Creek	0.78	0.64	-0.59	1.84
Mean±Std	0.74±0.09	0.70±0.06	-0.72±0.09	1.68±0.16

3.3.4 Land Cover Influence

The percentage of wetlands within a watershed had a strong positive correlation with annual DOC export (R^2=0.81, Figure 3.5); however, all other land cover types studied did not show strong correlations with DOC export (R^2 ranges from 0.05 to 0.20).

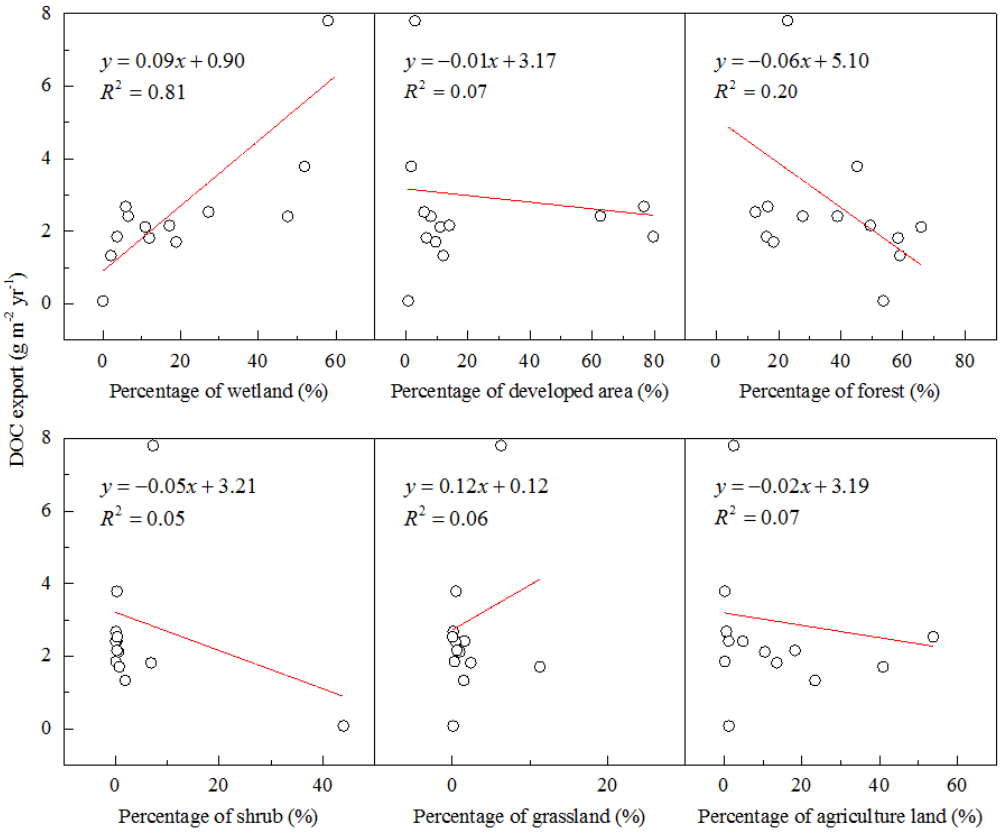

Figure 3.5. The relationship between annual DOC export and the percentage of each land cover type within a watershed.

3.4 Discussion

Our results indicate that annual DOC export from all 14 watersheds was only weakly influenced by mean annual air temperature, with high variability in the influence of annual temperature on DOC export across watersheds. The seasonal pattern is strongly positive-correlated with monthly temperature. Given the numerous other factors that can regulate DOC export, it is not surprising that air temperature and DOC export are not strongly related within all watersheds using annual data, and that the contribution of seasonality to DOC export only accounts for a small portion of the total annual DOC export. In fact, higher temperatures may accelerate the biological processes that are involved in the production of DOC (Schulze et al.,

2011; Solomon et al., 2015); however, higher temperatures may at the same time accelerate DOC decomposition in the water column, which increases outgassing from inland water bodies and thus reduces the amount that is ultimately exported from the watershed (Catalán et al., 2016; Søndergaard et al., 2000).

Our results suggest that precipitation has a dominant control on DOC export from watersheds for the variables studied at an annual scale, with increasing precipitation coincident with increasing DOC export in all 14 watersheds. In addition, the total DOC export is strongly correlated to precipitation at annual scale. This can be interpreted as reflecting the role of increasing precipitation in accelerating lateral flow through shallow soil layers, where DOC is rich, thereby increasing the DOC loading from soils to water bodies (Raymond et al., 2016). In addition, increasing discharge can accelerate flow speeds and make the residence times of DOC in waters shorter (Weyhenmeyer et al., 2012), which can reduce the sedimentation and decomposition of DOC in aquatic ecosystems. Especially in dry regions, precipitation is a strong and positive driver of DOC export (de Wit et al., 2016), which is the reason why precipitation has less impact on watersheds with a larger proportion of wetland area. The four watersheds including McDonalds Branch, Suwannee River, Reedy Creek and Popple River have more wetlands (> 47%) than others (Figure 2); their average standardized coefficient of precipitation is 0.75, which is less than the average of the other ten (0.83). Because temperature can increase the discharge from melting ice and snow (Winterdahl et al., 2016), and many of the study watersheds were within zones impacted by frozen winter precipitation, DOC export was more strongly correlated with precipitation at the annual temporal scale (R^2=0.74±0.09) than at a monthly scale (R^2=0.13±0.07)).

Decreasing sulfur deposition is coincident with increasing watershed DOC export. This is a result of declining soil acidity caused by declining sulfur deposition accelerating DOC production from organic matter decomposition and root exudates (Creed et al., 2018; Porcal et al., 2009). Decreasing atmospheric sulfur deposition results in recovery from acidification in watershed soils (Lawrence et al. 2015), and the resulting decrease in acidity and ionic strength of the soil solution can increase the solubility of soil organic matter and consequently increase DOC loading to drainage waters (Rosén et al., 2009). In contrast, in regions that previously experienced low loads of atmospheric sulfur deposition, the impact of sulfur deposition on DOC export is not obvious (Clark et al., 2010). In addition, the long-term trend of DOC export is strongly negative-correlated with sulfur deposition at annual scale. Deindustrialization in the conterminous United States in recent decades has reduced atmospheric sulfur deposition and is contributing to long-term increasing of DOC export (Meyer-Jacob et al., 2015).

Overall, increased DOC export is associated with higher rates of atmospheric nitrogen deposition, however, the magnitudes are varied greatly. This underlying mechanism remains debatable (Balestrini et al., 2019; Findlay, 2005; Rowe et al., 2014). More nitrogen deposition accelerates net primary production leading to increased litter generation, which is a substrate for DOC production (Sawicka et al., 2016). However, three watersheds including Quinnipiac River, Eno River, and Suwannee River showed that decreasing DOC export was associated with higher rates of atmospheric nitrogen deposition. One plausible mechanism is the reduction of DOC production due to more nitrogen deposition causing a decrease in soil pH, and further reducing the activity of microbes in soils (Findlay, 2005; Sinsabaugh et al., 2004). In addition, the standardized coefficients of the three watershed range from -0.02 to -0.09, with an average of -0.07, suggesting that other environmental factors have more significant impacts.

Our results suggest that there is a positive autocorrelation with DOC export (DW=1.68±0.16<2), which means that the DOC export increases in one month, it is also likely that the DOC export in the next month increases. But this positive autocorrelation is not obvious and does not need to be considered in modelling estimates (Field, 2009).

Some studies have linked the dynamics of DOC export to recent changes in land-use practices or to changes in land cover, which can greatly influence DOC production (Kothawala et al., 2015; Neff and Asner, 2001). Our results suggest that wetlands are the most important land cover type influencing DOC export and an increasing extent of wetland within a watershed enhances DOC export. This reflects the high rate of DOC production in wetlands that serve as a major contributor of DOC export (Dosskey and Bertsch, 1994). In addition, more wetland area increases the likelihood that DOC in soil will be moved via surface or near-surface hydrologic pathways provided by the wetland and then transferred to the water bodies (Creed et al., 2003). However, for other land cover types, our results suggest no clear relationship between cover type and DOC export. Our results indicate that there is no obvious relationship between DOC export and the proportional area of forested land cover in a watershed. This could be attributed to differences in forest composition, because the type of tree species has a significant impact on DOC production (Borken et al., 2011; Cuss and Guéguen, 2015). Precipitation plays a dominant role in regulating DOC flux from soil to surface waters in both grasslands and agriculture lands, therefore the relative proportion of these two land types does not explain variations in rates of DOC export from a watershed (Royer and David, 2005; Rüegg et al., 2015).

Given that vegetation species composition, nutrient availability, topography, and soil type also potentially influence the export of DOC from watersheds at the subcontinental scale, a more comprehensive examination of their relative influence would also contribute to the improvement

of DOC estimation and modelling. Because there were no large proportions of open water in these 14 watersheds (ranged from 0.01% to 5.03% with an average of 1.3%, *Table S2*), the processes of photosynthesis, decomposition, sedimentation, and movement of DOC in aquatic systems are not examined in this analysis. Available data sets for watersheds having large proportions of water bodies would give us a more comprehensive understanding of DOC export. The 14 watersheds varied significantly in size, but our results suggest that there is no obvious relationship between watershed size and DOC export.

3.5 Conclusion

Including the lateral flux of DOC in carbon estimation methods is necessary to improve our understanding of regional and global carbon cycles, but the relative magnitudes of different environmental factors and their effects on temporal patterns of DOC export are not well understood. Our results suggest that various environmental factors affect the DOC export, with precipitation emerging as the dominant factor for this process at annual time scale. Among all the land cover types evaluated, the proportion of wetlands within a watershed exerts the strongest control on annual DOC export. Through decomposing the time-series data of monthly DOC export, we found that the seasonal dynamics of DOC export is strongly positive-correlated with air temperature at monthly temporal scale; the long-term trend of DOC export is strongly negative-correlated with the sulfur disposition at annual temporal scale. In addition, there is no obvious autocorrelation with the DOC export. Our conclusions have important implications for deciding and selecting environment factors that should be included in estimating the lateral DOC export from watershed so as to characterize its temporal patterns.

CHAPTER 4

4. EXCLUDING IMPACTS OF CLIMATE AND ANTHROPOGENIC CHANGES ON DISSOLVED ORGANIC CARBON FLUX COULD NOT MODEL ITS SPATIO-TEMPORAL PATTERNS

4.1 Introduction

Inland waters receive large quantities of carbon from soils including dissolved organic carbon (DOC) and dissolved inorganic carbon (DIC), with recent studies suggesting that this lateral flux serves as an important component in global carbon budget (Drake et al., 2018; Tranvik et al., 2018). In inland waters, terrestrially-derived carbon can be released to the atmosphere through outgassing or buried in sediments, with the remainder transported to the ocean (Butman and Raymond, 2011; Cole et al., 2007). Existing estimates summarized by Drake et al. (2018) suggest that the contemporary global carbon flux from terrestrial to aquatic ecosystems ranges from 1.1 to 5.1 PgC per year with a mean of 3.2 PgC per year, 57% of which is emitted to the atmosphere via outgassing, 16% buried as sediment, and 27% exported to oceans. Compared with the global terrestrial biosphere carbon sink (0.7~2.2 PgC per year) (Huntzinger et al., 2014), the lateral flux of carbon through the aquatic system is a significant quantity, including this flux is required to improve the assessment of the global carbon budget, predict climate change, and reconcile the discrepancy between bottom-up estimates of carbon stock change (i.e., from field inventories and process-based models) with top-down estimates of terrestrial-atmosphere carbon exchange from inversion modeling frameworks (Hayes et al., 2018). In order to estimate carbon budgets of terrestrial and aquatic ecosystems, a better characterization of these biogeochemical processes and potential fates of carbon flux from

terrestrial ecosystems to the ocean through aquatic ecosystems is necessary (Battin et al., 2009; Regnier et al., 2013).

As a significant part of the total inland water carbon flux, DOC is primarily produced by the incomplete decomposition of soil organic carbon, exuded by plants, or moved along with the washout of organic compounds in vegetation throughfall (Aitkenhead-Peterson et al., 2003; Michalzik et al., 2003), with some proportion of this production then loaded into the aquatic system via surface runoff (Futter et al., 2011). In aquatic ecosystems, DOC can be decomposed as CO_2 and released to the atmosphere through outgassing or buried in the sediments of inland water bodies, with the remaining DOC transported to the ocean through riverine export (Cole et al., 2007). Climate changes and anthropogenic activities substantially regulate DOC production, movement in soils, flux from terrestrial to aquatic ecosystems, settlement and decomposition in inland waters, and transportation in rivers (Aitkenhead-Peterson et al., 2005; Lajtha and Jones, 2018). Recent studies suggest that these biogeochemical processes are related to air temperature (Raymond and Saiers, 2010), precipitation (Raymond et al., 2016), sulfur deposition (SanClements et al., 2012), nitrogen deposition (Chen et al., 2015), and land cover types (Webster and McLaughlin, 2010). Higher temperatures accelerate biological processes that are involved in the production of DOC in soils as well as the decomposition rate in waters (Solomon et al., 2015; Søndergaard et al., 2000). More precipitation accelerates lateral flow through shallow soil layers, thereby increasing the DOC loading from soils to inland waters (Raymond et al., 2016). Less sulfur deposition reduces the soil acidity and thus accelerates DOC production from root exudates and organic matter decomposition (Creed et al., 2018). More nitrogen deposition accelerates net primary production leading to increased soil organic carbon generation, which is a substrate for DOC production (Sawicka et al., 2016); however, it also

increases soil acidity, and constrains the activity of microbes in soils (Findlay, 2005). In addition, wetlands serve as a major contributor of DOC export (Dosskey and Bertsch, 1994) and more wetland area increases the likelihood that DOC in soil will be moved via surface or near-surface hydrologic pathways provided by the wetland and then transferred to the water bodies (Creed et al., 2003).

Numerous methods including field inventory, empirical modeling, and process-based simulation have been applied to estimate the terrestrial-aquatic DOC flux at various spatial and temporal scales. Stets and Striegl (2012), based on field measurements of discharge and water quality data from the network of the United States Geological Survey (USGS) gauging stations, estimated that the carbon export from the conterminous United States to the ocean is 41-49 TgC per year. Butman et al. (2016) used the field measurements together with empirical models to estimate the terrestrial-aquatic carbon fluxes (DOC and DIC) as well as their potential fates in the conterminous United States. They estimated a 106 TgC per year flux from soils to inland waters, 65% of which is released to the atmosphere, 20% is stored in the sediment, and the rest is delivered to oceans. Ludwig et al. (1996) used an empirical model together with various environmental factors to estimate a 710 TgC per year total flux of carbon from terrestrial to aquatic ecosystems globally, 205 TgC of which contains DOC. Aitkenhead and McDowell (2000) developed a linear empirical model based on soil carbon to nitrogen ratios and estimated the global DOC export from land to oceans as 360 TgC per year. Harrison et al. (2005) proposed an empirical modelling method using the runoff, wetland area, and consumptive water use to assess the global DOC export. They estimated that a 170 TgC per year of DOC is exported from land to oceans.

Process-based terrestrial biosphere models (TBMs) offer another approach to estimating the terrestrial-aquatic DOC flux. Kicklighter et al. (2013) applied the Terrestrial Ecosystem Model (TEM) across the pan-Arctic region and estimated a 32 TgC per year DOC loading from terrestrial ecosystems to the river networks. By this model, DOC production is a proportional of total soil organic matter decomposition, and the flux from soils to inland waters (i.e., "DOC loading") is determined by the runoff of rainwater and snowmelt. Ren et al. (2016) updated the Dynamic Land Ecosystem Model (DLEM) to simulate DOC export from the Mississippi River to the coastal ocean during 1901-2010. This model formulation integrated the processes of production, consumption, and transport of DOC in soils and surface waters. Lauerwald et al. (2017) added a DOC flux estimation module to the Organising Carbon and Hydrology in Dynamic Ecosystems (ORCHIDEE) model and named it as ORCHILEAK, which includes DOC production, leaching from soils to inland waters, and decomposition and releasing to the atmosphere in the water column. They applied it to assess the terrestrial-aquatic carbon flux (DOC and DIC) in the Amazon basin and estimated that total CO_2 evasion from the water surface equals about 5% of terrestrial net primary production. Nakhavali et al. (2018) developed the Joint UK Land Environment Simulator (JULES-DOCM) model, which integrates biogeochemical processes of DOC production in terrestrial ecosystems, decomposition within the soil column, and DOC loading to inland waters. Li et al. (2019) developed a process-based model, TRIPLEX-hydrological routing algorithm (TRIPLEX-HYDRA), which has the ability to simulate the fate of DOC in terrestrial and aquatic ecosystems. They applied the model to estimate a global flux of 235 TgC per year to oceans.

While these previous studies have provided broad constraints on global- and continental-scale DOC flux estimates, the key driving factors and sensitivities of the underlying

biogeochemical processes have not been well-studied and thus not well-represented in existing empirical models and TBMs. In this study, we developed a process-based model of terrestrial-aquatic DOC fluxes (TAF-DOC), which has the ability to estimate the spatial and temporal dynamics of DOC flux through incorporating various environmental factors (e.g., meteorology, atmospheric deposition, land cover and landscape attributes). We then applied TAF-DOC to assess the DOC flux and potential fates across the conterminous United States from 1985 to 2018.

4.2 Methodology and Data

4.2.1 Model Structure and Workflow

The process-based terrestrial-aquatic DOC fluxes model (TAF-DOC) developed for this study consists of three modules (Figure 1) and operates at annual temporal. TAF-DOC is operated at the fourth level of the United States Geological Survey (USGS) hydrologic watershed spatial scale. This hydrologic watershed is the smallest element in the hierarchy of hydrologic units, which is a geographic area representing part of all of a surface drainage basin, a combination of drainage basins, or a distinct hydrologic feature (Seaber et al., 1987). The Watershed Soil DOC Module ($WS_{DOC}M$) is used to estimate the DOC quantities available to be moved from soils to inland waters (DOC_M) of a given watershed by using the input soil organic carbon (SOC) data. The Watershed DOC Fluxes Module ($WF_{DOC}M$) is then used to estimate the fluxes and fates of DOC within a watershed (i.e., loading from soils, outgassing, sedimentation, and export). To drive this module, environmental factors including air temperature, precipitation, wet sulfur and nitrogen deposition, as well as information on various important landscape attributes of each watershed are required. In a watershed, the total DOC loading from terrestrial to aquatic ecosystems (DOC_F) is calculated as the total decomposed DOC, settled DOC, and

exported DOC from this watershed (equation 4.1). Flux to the Ocean Module ($FO_{DOC}M$) is used to estimate the fluxes and fates of exported DOC from a watershed outlet to the ocean. In a study area, the total DOC flux from terrestrial to aquatic ecosystems is calculated as the summary of DOC fluxes in all watersheds within the study area (equation 4.2).

$$DOC_F = DOC_S + DOC_G + DOC_E$$

Equation 4.1

$$Total\_DOC_F = \sum_{i=1}^{n} (DOC_S + DOC_S + DOC_E)_i$$

Equation 4.2

where DOC_F is the total DOC loading from terrestrial to aquatic ecosystems, DOC_S is the settled DOC as sediment and DOC_G is the decomposed DOC as outgassing within an individual watershed. DOC_E is the DOC exported from the watershed. $Total\_DOC_F$ is the total DOC flux from terrestrial to aquatic ecosystems in the study area, and *n* is total number of watersheds within the study area.

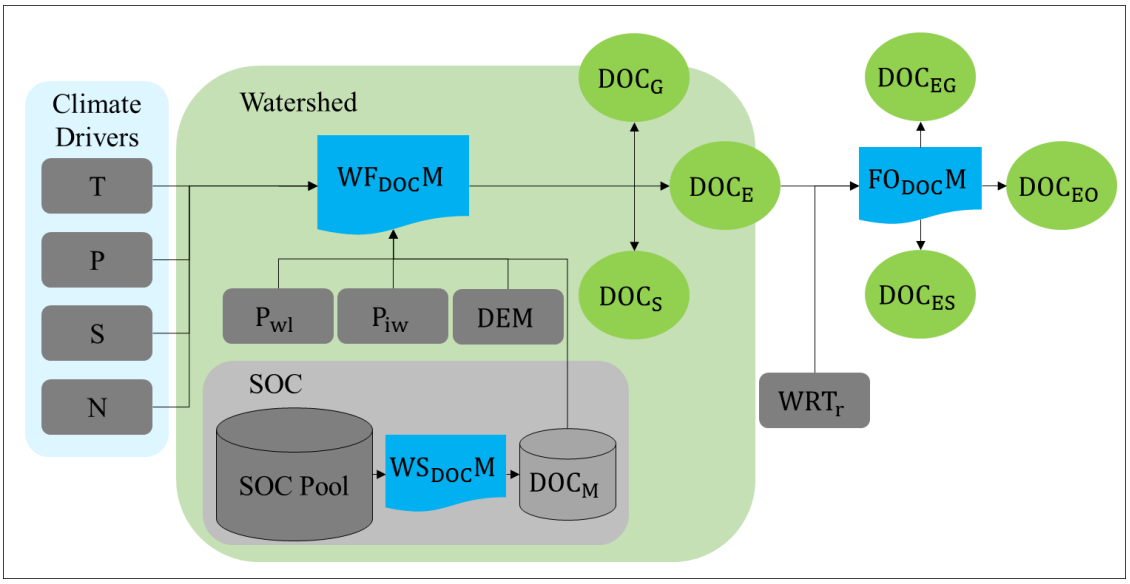

Figure 4.1. Structure and workflow of the process-based terrestrial-aquatic DOC fluxes model (TAF-DOC). Dark gray highlighted variables are input data sets.

In Figure 4.1, blue highlighted processes are simulation modules, and light green highlighted variables are output variables. T is air temperature, P is precipitation, N is wet sulfur deposition, N is wet nitrogen deposition, and P_{wl} and P_{iw} are the proportions of wetland land cover and inland water surface area within the watershed, respectively. DEM is the raster Digital Elevation Model. SOC is the soil organic carbon, and DOC_M is the DOC can be moved from soils to inland waters. DOC_S is the settled DOC as sediment, and DOC_G is the decomposed DOC as outgassing within the watershed. DOC_E is the DOC exported from the watershed. WRT_r is the water retention time in the river. DOC_{EG} is the decomposed DOC_E as outgassing, and DOC_{ES} is the settled DOC_E as sediment during the delivery process from the watershed outlet to the ocean. DOC_{EO} is the DOC ultimately exported to the ocean.

4.2.2 Watershed Soil DOC Module ($WS_{DOC}M$)

The $WS_{DOC}M$ estimates the soil DOC pool and the DOC available to be moved from soils to inland waters (DOC_M). The soil DOC (S_{DOC}) is formed by the incomplete decomposition of

SOC, the production of root exudates by vegetation, and the washout of organic compounds in throughfall (Guggenberger and Kaiser, 2003; Sokol and Bradford, 2019). Because of the relatively high biodegradability of the organic components of throughfall (Qualls and Haines, 1992), the model does not regard throughfall DOC as a direct contributor to S_{DOC}, but simply as a part of the carbon input to the soil. Because the contributions of different soil layers to the DOC loading from soils to inland waters are greatly different (Neff and Asner, 2001), the S_{DOC} pool consists of top- (0-30cm) and sub- layer S_{DOC} pools (30-100cm) (equation 4.3). The DOC_M is estimated with the a desorption model (equation 4.4) (Jones and Willett, 2006).

$$S_{DOC} = K_T * TS_{SOC} + K_S * SS_{SOC}$$

Equation 4.3

$$DOC_M = K_{DT} \times TS_{SOC} + K_{DS} \times SS_{SOC}$$

Equation 4.4

where S_{DOC} (gC/m^2) is the soil DOC concentration, TS_{SOC} (gC/m^2) is the top soil layer (0-30cm) SOC concentration, SS_{SOC} (gC/m^2) is the sub soil layer SOC concentration (30-100cm), and K_T and K_S (%) are the ratios of DOC in top and sub soil layers, respectively (Table 4.1). TS_{DOC} (gC/m^2) is the top soil layer DOC concentration and SS_{DOC} (gC/m^2) is the sub soil layer DOC concentration. K_{DT} and K_{DS} (%) are the desorption coefficients of DOC in the top and sub soil layers, respectively (Table 4.1). DOC_M (gC/m^2) is the total S_{DOC} available to be moved from soils to inland waters.

Table 4.1. Summary of the symbols used in TAF-DOC.

Symbol	Value	Reference
K_T	0.1181	Michalzik et al. (2001)
K_S	0.0680	Guggenberger and Kaiser (2003)
K_{DT}	0.9891	Neff and Asner (2001)
K_{DS}	0.7770	Neff and Asner (2001)
ε_{dw}	0.3745	Hanson et al. (2011)
μ_{dw}	0.5250	Hanson et al. (2011)
φ	0.5250	Cole et al. (2007)
ω	0.0016	Cole et al. (2007)
ε_{RS}	1.0891	McGuire et al. (2005)
μ_{RS}	-0.3052	McGuire et al. (2005)
α	0.0050	Coynel et al. (2005)
β	148.6111	Coynel et al. (2005)
γ	-0.0013	Coynel et al. (2005)

4.2.3 Watershed DOC Fluxes Module ($WF_{DOC}M$)

The $WF_{DOC}M$ estimates the DOC flux within a watershed including the flux from soils to inland waters and the delivery process to the outlet of the watershed. Because it is impossible to directly measure the amount of DOC flux from soils to inland waters in a watershed, but the DOC export from a watershed through the watershed outlet can be directly measured, the DOC export from a watershed is firstly estimated in the $WF_{DOC}M$. Observational data sets from 14 watersheds in the conterminous United States analyzed in the study by Chapter 3 were used to build multiple regression models, which together represent the relationships among DOC export from a watershed with the impacts of environmental factors (i.e., air temperature, precipitation, sulfur and nitrogen deposition). Since the extent of wetlands within a watershed greatly influences the DOC export, the data sets of these 14 watersheds were classified to five groups based on the criteria that the changes of the percentage of wetland (P_{wl}) could result in a more than 50% change of average annual DOC export from a watershed (Table 4.2). A multiple linear

regression model of annual DOC export (y_{DOC} as gC/m^2 of watershed area per year) was parameterized for each of these five classes (equation 4.5, Table 4.2).

$$y_{DOC} = a_i * T + b_i * P + c_i * S + d_i * N + e_i$$

Equation 4.5

where *T* is the mean annual air temperature (°C), *P* is the total annual precipitation (cm), *S* is the total annual sulfur deposition (g/m^2 per year as sulfur), and *N* is the total annual nitrogen deposition (g/m^2 per year as nitrogen). These coefficients and interceptions are summarized in Table 4.2.

Table 4.2. Coefficients and interceptions of these 5 multiple regression models (P_{wl} is the percentage of wetland with a watershed.).

i	P_{wl} (%)	a_i	b_i	c_i	d_i	e_i
1	<1	-0.0072	0.0061	-0.4039	0.3055	-0.1207
2	1~5	-0.0507	0.0333	-0.2503	-0.1859	-0.6080
3	5~50	0.0906	0.0514	-0.3544	1.724	-4.0303
4	50~55	0.0103	0.1775	-2.389	-0.3321	-5.2635
5	>55	-0.9553	0.3371	-0.3368	1.3467	-5.2082

Because the extent of wetland in a watershed and annual precipitation are the most important environmental factors that regulate the annual DOC export (Chapter 3), in cases where not all of the climate drivers are available the estimation method is replaced by a simple linear regression model that only used the P_{wl} and precipitation drivers. A linear regression model was created for each P_{wl} level (equation 4.6, Table 4.3).

$$y_{DOC} = \delta_i * P + \sigma_i$$

Equation 4.6

Table 4.3. Coefficients and interceptions of the five linear regression models (P_{wl} is the percentage of wetland within a watershed.).

i	P_{wl} (%)	δ	σ
1	<1	0.0053	-0.1976
2	1~5	0.0257	-1.4293
3	5~50	0.0369	-2.0598
4	50~55	0.1486	-7.7067
5	>55	0.2238	-20.4120

The decomposition ratio of DOC in aquatic ecosystems is related to the water retention time (Catalán et al., 2016; Weyhenmeyer et al., 2012) (equation 4.7). The annual decomposition rate is calculated with an exponential model by using the proportion of open water in the watershed (equation 8), and the water retention time of this watershed is estimated by using the Digital Elevation Model (DEM) together with an exponential model proposed by McGuire et al. (2005) (equation 4.9). The sedimentation ratio of DOC in the aquatic ecosystems within a watershed is calculated with an exponential model, which also uses the water retention time (equation 4.10) (Cole et al., 2007).

$$R_G = d_w \times \tau$$

Equation 4.7

$$d_w = P_{iw} \times \varepsilon_{dw} + \mu_{dw}$$

Equation 4.8

$$\tau = \varphi \times e^{\left(\frac{\sum_j^m E_j}{m} \times \omega\right)}$$

Equation 4.9

$$R_S = \tau \times \varepsilon_{RS} + \mu_{RS}$$

Equation 4.10

where R_G is the DOC decomposition ratio, d_w is the annual DOC decomposition rate, and τ is the water retention time (years, e.g., 0.5 year, 3.5 years). P_{iw} is the proportion of inland water surface area within a watershed. m is the total number of grids of the DEM within a watershed and E is the elevation of grid cell j. R_S is the DOC settlement ratio in the watershed. All the parameters are summarized in Table 4.1.

4.2.4 DOC Fluxes to Ocean Module ($FO_{DOC}M$)

The DOC Fluxes to Ocean Module ($FO_{DOC}M$) estimates the flux processes of exported DOC from a watershed (DOC_E) to the ocean. During the riverine transportation process, DOC_E is moved from the outlet of a watershed to the ocean, the decomposition ratio is estimated with the decomposition empirical model (equation 4.7), and the settlement ratio is estimated with an exponential model (equation 11) (Coynel et al., 2005). The water retention time was obtained by using the DEM data and Hydrology Analysis Module in ArcGIS Pro.

$$R_{ES} = \alpha \times e^{\beta \times \tau} + \gamma$$

Equation 4.11

where R_{ES} is the settlement ratio of DOC export from the watershed outlet, and τ is the water retention time (years, e.g. 0.5 year, 3.5 years). All the parameters were summarized in Table 4.1.

4.2.5 Model Input Data

The study area was the conterminous United States, and there were 2110 fourth level of USGS hydrologic watersheds. The watershed boundary data was obtained from the USGS Watershed Boundary Dataset (WBD) of the National Geospatial Program (NGP; usgs.gov/core-science-systems/ngp/national-hydrography). The size of these watersheds ranges from 184 to

22963 km^2 with a mean of 3688 km^2 (*Figure S1*). The elevation data (DEM) was obtained from Global 30 Arc-Second Elevation (GTOPO30) provided by the USGS Earth Resources Observation and Science (EROS) Center (https://www.usgs.gov/centers/eros/science/), and the spatial resolution is 1×1 km. The mean annual air temperature (°C) was provided by the Global Historical Climatology Network Monthly - Version 4 (GHCN) data set from the National Oceanic and Atmospheric Administration (NOAA; https://ncdc.noaa.gov/), and this is climate divisional data (NOAA 2020). The annual total precipitation (cm) was provided by the Daily Surface Weather and Climatological Summaries (DAYMET) from Oak Ridge National Laboratory Distributed Active Archive Center (ORNL DAAC; https://daac.ornl.gov/) (Thornton et al., 2017), and the spatial resolution is 1×1 km. The wet sulfur (SO_4^{2-} deposition, g/m^2/year as sulfur) and nitrogen (NH_4^+ and NO_3^- deposition, g/m^2/year as nitrogen) deposition gridded data sets were obtained from the National Trends Network (NTN) of National Atmospheric Deposition Program (NADP; http://nadp.slh.wisc.edu/data/) (NADP, 2019), and the spatial resolution is 2.3×2.3 km. The most recent National Land Cover Database 2016 (NLCD2016) (Yang et al., 2018), provided by the Multi-Resolution Land Characteristics (MRLC) Consortium (https://www.mrlc.gov/), was used to characterize each watershed by its proportional wetland and open water. The spatial resolution of the NLCD2016 data is 30×30 m. The most recent Gridded Soil Survey Geographic (gSSURGO) Database (https://gdg.sc.egov.usda.gov/) provided the soil organic carbon data (gSSURGO, 2019), and the spatial resolution is 90×90 m.

4.2.6 Benchmarks

To validate the estimation results, the USGS measured daily DOC concentration and discharge data together with DOC export estimation method proposed by Hirsch et al. (2010) were used to estimate the annual DOC exports to oceans from three continental-scale watersheds,

including the Mississippi, Colorado and Rio Grande basins, and then were compared with the TAF-DOC estimates. Differences between the two estimates of DOC export were assessed using a two-sample t-test. In addition, the DOC flux from terrestrial ecosystems to oceans can be estimated with the soil carbon and nitrogen ratio (C:N) method (Aitkenhead and McDowell, 2000) (equation 4.12). This model was applied together with the C:N data provided by International Soil Reference and Information Centre-World Inventory of Soil Emission Potentials (ISRIC-WISE, https://www.isric.org/) (Batjes, 2005) to estimate the DOC flux to oceans in the conterminous United States and thus compared with TAF-DOC estimates.

$$DOC_{EO} = 4.863 \times (\mathrm{C{:}\,N}) - 60.873$$

Equation 4.12

4.2.7 Model Sensitivity Test

To assess the model's global sensitivity to four input environmental drivers (i.e., annual air temperature, precipitation, sulfur and nitrogen deposition), we used the Monte Carlo simulation approach together with the Pearson correlation coefficient (Pearson's r) global sensitivity test (Gardner et al., 1981; Hamby, 1994). A higher value of Pearson's r indicates a more sensitive relationship. This test was operated as the following steps: firstly, in a watershed, one year driver was randomly selected from its 34-year driver dataset. This process was repeated for these 2110 watersheds and thus to organize one year driver dataset; Secondly, this process was repeated 500 times, and thus generated a 500-year driver dataset; Thirdly, a 500-year simulation with TAF-DOC model was conducted by this driver dataset; Fourthly, the Pearson's r of annual total terrestrial-aquatic DOC flux with each driver was calculated to assess the sensitivity.

4.3 Results

4.3.1 The Spatio-temporal Patterns of DOC Flux

Over the 1985-2018 time period, the total annual DOC loading from terrestrial to aquatic ecosystems in conterminous United States watersheds ranged from 30.5 (1988) to 40.8 TgC (2018) with a mean of 33.5 TgC per year. The estimated DOC flux from soils to inland waters of these 2110 watersheds ranged from 0.1 to 25.7 gC/m^2 per year with a mean of 4.4 gC/m^2 per year (Figure 2). Regions having higher DOC loading were mostly located in seaboard areas (Atlantic Ocean Seaboard and Gulf of Mexico Seaboard) (Figure 4.2). The low DOC flux regions were located in the southwestern and mid-southern conterminous United States (Figure 4.2).

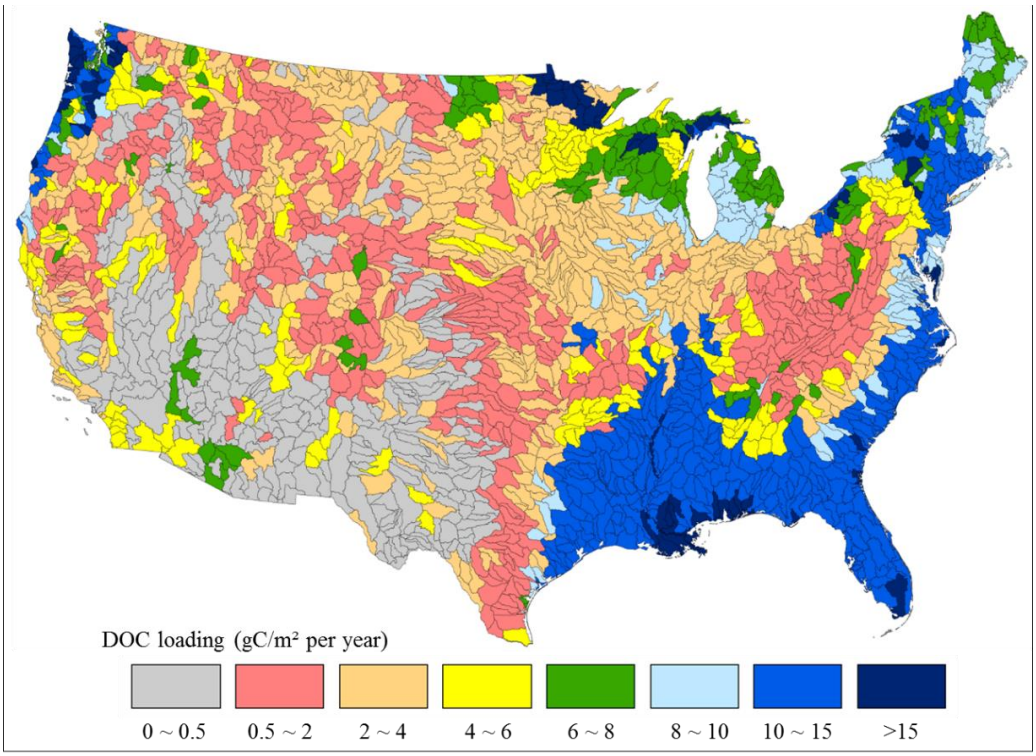

Figure 4.2. The spatial pattern of mean annual DOC loading from terrestrial to aquatic ecosystems in each conterminous United States watershed during 1985-2018.

The estimated annual DOC loading from terrestrial to aquatic ecosystems in the conterminous United States was 33.5±2.2 TgC per year over the of 1985-2018 time period. In the aquatic ecosystems of these 2110 watersheds, 10.8±0.3 TgC per year of DOC was estimated to be decomposed and released to the atmosphere, and 5.4±0.2 TgC per year DOC was buried in sediment (Figure 4.3). The remaining 17.3±0.5 TgC per year of the total DOC budget was ultimately exported from these individual watershed areas. In the transportation process of DOC from watershed outlets to the ocean, 2.1±0.1 TgC per year of DOC was estimated to be decomposed and released to the atmosphere, 1.7±0.1 TgC per year DOC buried in sediment, and 13.5±0.9 TgC per year DOC was ultimately exported to oceans. Note that in Figure 4.3, DOC_S is buried as sediment, and DOC_G is decomposed and outgassed from individual watershed. DOC_E is the DOC exported from a watershed. DOC_{EG} is the decomposed DOC_E as outgassing, and DOC_{ES} is the DOC_E buried in sediment during the transportation process from the watershed outlet to the ocean. DOC_{EO} is the DOC exported to the ocean.

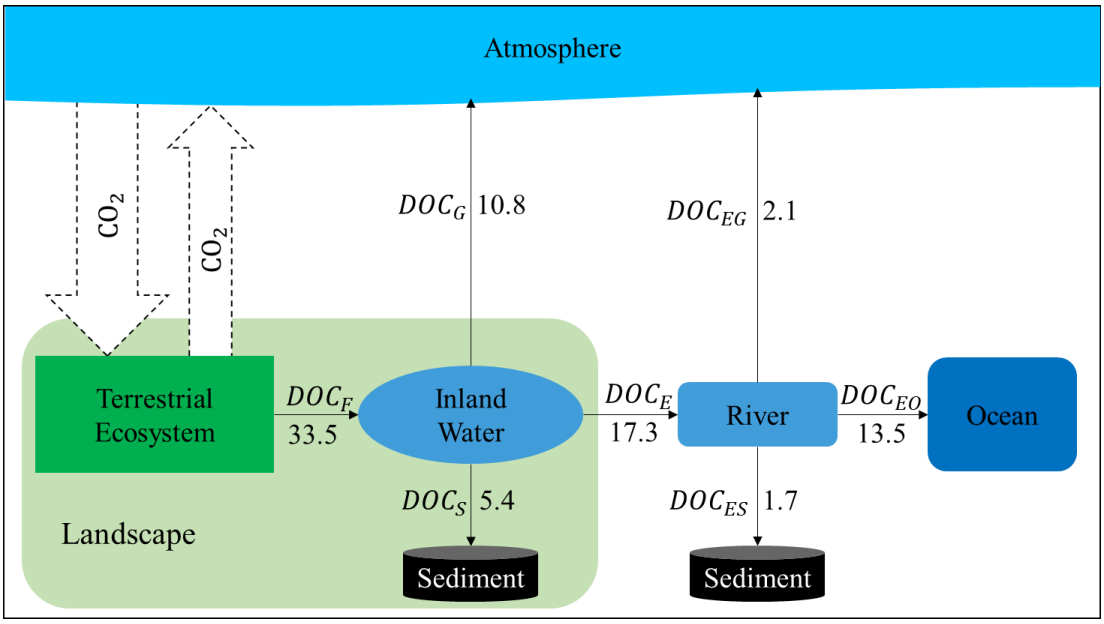

Figure 4.3. The DOC budget of the conterminous United States in the period of 1985-2018, in units of Tg C per year.

4.3.2 Benchmarks and Model Performance

The annual DOC export from the Colorado River watershed to the ocean provided by USGS measurements ranged from 0.6 TgC (2007) to 1.9 TgC (1998) with a mean of 0.9 TgC per year in the period of 1996-2018 (Figure 4.4). In the same time period, the simulated DOC export with TAF-DOC from this watershed ranged from 0.3 TgC (2009) to 1.6 TgC per year (1998) with a mean of 0.8 TgC per year, which was 10% lower than USGS measurements. The two estimates were not significant difference (p=0.07) The DOC export from the Mississippi River watershed to the ocean provided by USGS measurements ranged from 1.7 TgC (2012) to 3.5 TgC (2009) with a mean of 2.7 TgC per year. In the same time period, the simulated DOC export with TAF-DOC ranged from 1.9 TgC (2006) to 3.7 TgC (2009) with a mean of 2.8 TgC per year, which is 4% higher than USGS measurements. The two estimates were not significant difference (p=0.09). The DOC export from Rio Grande Watershed provided by USGS measurements

ranged from 0.03 TgC (2011) to 0.7 TgC (2009) with a mean of 0.3 TgC per year in the period of 2008-2018. In the same time period, the simulated DOC export with TAF-DOC from Rio Grande Watershed ranged from 0.02 TgC (2012) to 0.8 TgC (2009) with a mean of 0.3 TgC per year, which is 10% lower than USGS measurements. The two estimates were not significant difference (p=0.39).

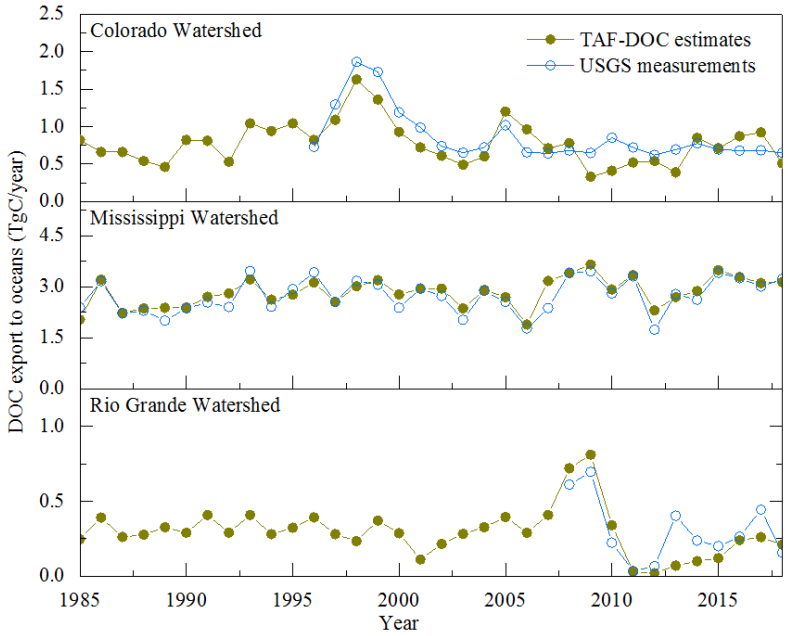

Figure 4.4. The annual DOC export from the three continental-scale watersheds (i.e., Colorado, Mississippi, and Rio Grande watersheds) to oceans as estimated by the TAF-DOC model and compared against benchmark data from USGS measurements over the 1985-2018 time period.

Using the soil organic carbon to nitrogen ratio method, the estimated annual DOC export from the conterminous United States was 18.2 TgC per year, which is 18% higher than the estimate by TAF-DOC (13.6 TgC per year). The spatial patterns of the two estimates were similar (Figure 4.5). Both methods identified that the regions having higher DOC flux were mostly located in seaboard areas (Atlantic Ocean Seaboard and Gulf of Mexico Seaboard), and the contributions of the southwestern and mid-southern conterminous United States were lower.

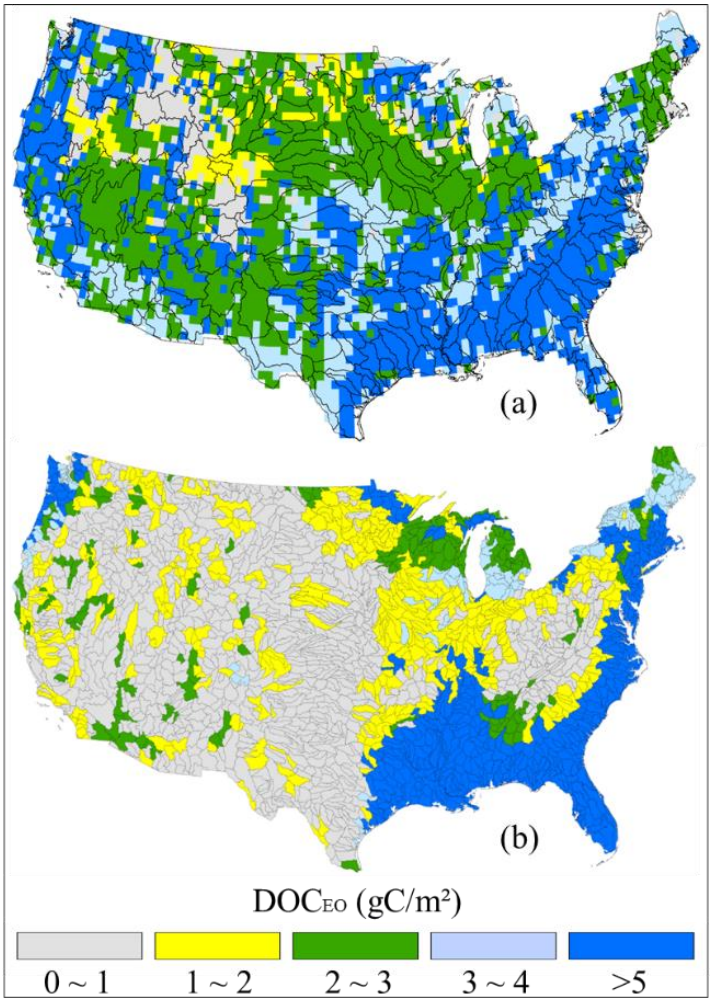

Figure 4.5. The DOC export from the conterminous United States to oceans estimated by the soil organic carbon and nitrogen ratio method (a) and terrestrial-aquatic DOC fluxes (TAF-DOC) model (b).

4.3.4 Global Sensitivity

The linear relationship between each input driver and DOC flux from terrestrial to aquatic ecosystems suggested that annual DOC flux was the most sensitive to annual precipitation (R^2 = 0.48) (Figure 4.6), and also sensitive to sulfur deposition (R^2 = 0.46). However, the DOC flux was no sensitive to air temperature and nitrogen deposition (R^2 = 0.00 and 0.01 respectively). In addition, the precipitation had a positive sensitivity (correlation

coefficient = 0.89), while the sulfur deposition had a negative sensitivity (correlation coefficient = -21.35).

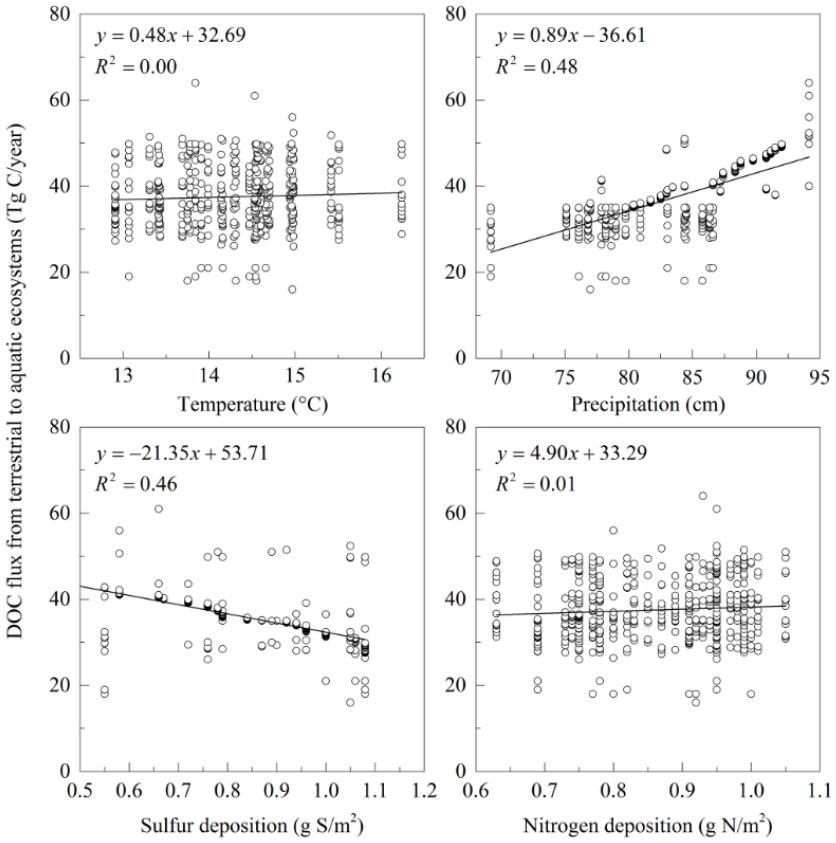

Figure 4.6. The linear relationship between each input driver (i.e., air temperature, precipitation, sulfur and nitrogen deposition) and DOC flux from terrestrial to aquatic ecosystems.

4.4 Discussion

Our results estimate that a total of 33.5±2.2 TgC per year was transferred from the terrestrial to aquatic ecosystems (DOC loading) in the conterminous United States during 1985-2018, which represents about 0.39-0.49% of the total soil organic carbon (gSSURGO, 2019). The dominant fate of the DOC is export to the ocean (41%), while 38% is decomposed in the aquatic ecosystems and released to the atmosphere, and the remaining 21% is buried in sediment. The mean of net carbon exchange (NEE) estimates for the conterminous United States as

estimated by an ensemble 22 terrestrial biosphere models (TBMs) that participated in the North American Carbon Program (NACP) Multi-scale Synthesis and Terrestrial Model Intercomparison Project (MsTMIP) is -371 TgC per year (carbon sinks). Hayes et al. (2012) calculated the NEE as -357 TgC per year with forward models and -302 TgC per year with the inventory-based method. The fates of DOC as sediment and export to the ocean can be assumed as annual terrestrial carbon sequestration (Hayes et al., 2018). But these methods ignore the lateral DOC flux and thus underestimate the annual carbon uptake as much as 5.5-6.4%.

The DOC loading from soil to inland waters estimated with TAF-DOC ranges from 0.1 to 25.7 gC/m^2 per year among these 2110 watersheds with a mean of 4.4 gC/m^2 per year, which is similar with the results provided by Hope et al. (1994) (1 to 10 gC/m^2 per year). Butman et al. (2016) estimated that the total DOC and DIC fluxes from land to inland waters is 106 (ranged from 71 to 149) TgC per year in the conterminous United States, and ~30% of this flux is DOC. Therefore, the total DOC flux from terrestrial to aquatic ecosystems is about 31.8 (ranging from 21.3 to 44.7) TgC per year, which is similar with our estimated 33.5 (30.46 to 40.8) TgC per year.

TAF-DOC estimates DOC flux based on the watershed level, however these 2110 watersheds greatly differ in their size ranging from 184 to 22963 km^2 with a mean of 3689 km^2 (Figure S1). Our results suggest that there is no obvious relationship between the size of watershed and terrestrial-aquatic DOC flux density ($y=-3.91x+18.63$, $R^2=0.05$) (Figure S2). Chapter 3 suggested that precipitation is the major driver for the interannual variability in DOC loading from terrestrial to aquatic ecosystems and Futter et al. (2011) concluded that sulfur deposition can explain the long-term trend in DOC loading. TAF-DOC includes these environmental factors and successfully estimates the DOC loading as compared to independent

benchmark datasets, and characterizes the spatial and temporal patterns of DOC loading at the watershed-scale (Figure 7a). Our results suggest that precipitation is the major driver for the interannual dynamics of DOC loading (Figure 4.7a and b), which agrees with the conclusion of the study by (Futter et al., 2007). Overall, in the period of 1985-2018, the DOC loading from terrestrial to aquatic ecosystems is continually increasing; however, the sulfur deposition is continually decreasing (Figure 7a), with an obvious negative relationship between them (Figure 7c). Note that in figure 4.7, the time-series plots include DOC flux anomaly (N [DOC Anomaly]), temperature anomaly (N [T Anomaly]), precipitation anomaly (N [P Anomaly]), sulfur deposition anomaly (N [S Anomaly]), and nitrogen deposition (N [N Anomaly]) anomaly in the period of 1985-2018 (a). The linear relationship between N [DOC Anomaly] and N [P Anomaly] (b). The linear relationship between N [DOC Anomaly] and N [S Anomaly] (c).

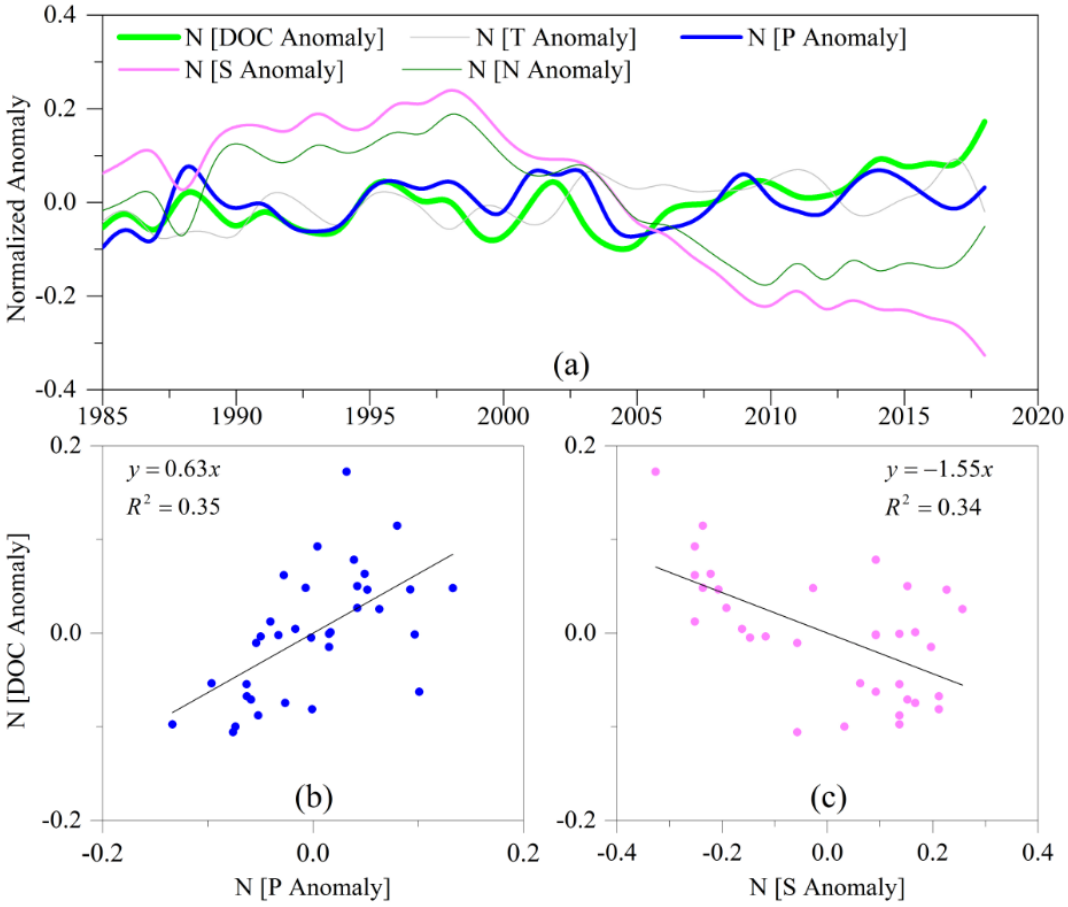

Figure 4.7. The time series of normalized DOC flux anomaly from terrestrial to aquatic ecosystems.

The atmosphere inverse model approach was used to estimate a 689 TgC per year carbon uptake in the conterminous United States (Hayes et al., 2012), and the carbon uptake estimated with inventory measurements and bottom-up models is 323-392 TgC per year when including the DOC flux component in the overall calculation. There is still a discrepancy between the two estimation frameworks. This is because that DIC, particulate inorganic carbon (PIC) and particulate organic carbon (POC) are not included in these bottom-up estimates. In the future, including these fluxes in bottom-up frameworks could better explain this difference. In addition,

the carbon flux of inland water photosynthesis and other biogeochemical processes are not counted, which could be another reason for this difference.

4.5. Conclusion

Our results suggest that this proposed process-based terrestrial-aquatic DOC fluxes model (TAF-DOC) can successfully estimate the total flux DOC fluxes and capture the watershed-scale spatial and annual temporal dynamics of DOC loading, burial, outgassing and export. Precipitation is the dominant driver for the interannual DOC dynamics, while the longer-term trend of DOC flux is greatly controlled by the rate of sulfur deposition. Our results estimate total DOC loading from terrestrial to aquatic ecosystems across the watersheds of the conterminous United States to be 33.5±2.1 TgC per year on average, which is about 0.39-0.49% of the total soil organic carbon pool. In aquatic ecosystems, 38% of the total DOC is decomposed and emitted as outgassing, 21% DOC settles into sediment, and the remaining 41% is ultimately delivered to the ocean. Considering the sedimentation and export of DOC to the ocean as a relatively long-term sink of sequestered carbon, the annual terrestrial net carbon uptake will be underestimated by as much as 5.5-6.4% using carbon budget estimation and modeling approaches that do not include DOC fluxes.

BIBLIOGRAPHY

Adams, H.D. et al., 2017. A multi-species synthesis of physiological mechanisms in drought-induced tree mortality. Nature Ecology & Evolution, 1(9): 1285-1291.

Aitkenhead-Peterson, J.A., McDowell, W.H. and Neff, J.C., 2003. Sources, production, and regulation of allochthonous dissolved organic matter inputs to surface waters, Aquatic Ecosystems. Elsevier, pp. 25-70.

Aitkenhead-Peterson, J., Alexander, J. and Clair, T., 2005. Dissolved organic carbon and dissolved organic nitrogen export from forested watersheds in Nova Scotia: Identifying controlling factors. Global Biogeochemical Cycles, 19(4).

Aitkenhead, J. and McDowell, W.H., 2000. Soil C: N ratio as a predictor of annual riverine DOC flux at local and global scales. Global Biogeochemical Cycles, 14(1): 127-138.

Alencar, A., Nepstad, D. and Diaz, M.C.V., 2006. Forest understory fire in the Brazilian Amazon in ENSO and non-ENSO years: area burned and committed carbon emissions. Earth Interactions, 10(6): 1-17.

Atkin, O.K. and Macherel, D., 2008. The crucial role of plant mitochondria in orchestrating drought tolerance. Annals of Botany, 103(4): 581-597.

Bachmair, S., Kohn, I. and Stahl, K., 2015. Exploring the link between drought indicators and impacts. Natural Hazards and Earth System Sciences, 15(6): 1381-1397.

Balestrini, R. et al., 2019. Dynamic of nitrogen and dissolved organic carbon in an alpine forested catchment: atmospheric deposition and soil solution trends. Nature Conservation, 34: 41.

Balshi, M. et al., 2007. The role of historical fire disturbance in the carbon dynamics of the pan-boreal region: A process-based analysis. Journal of Geophysical Research: Biogeosciences, 112(G2).

Bartlett, M.K., Scoffoni, C. and Sack, L., 2012. The determinants of leaf turgor loss point and prediction of drought tolerance of species and biomes: a global meta-analysis. Ecology Letters, 15(5): 393-405.

Batjes, N., 2005. ISRIC-WISE global data set of derived soil properties on a 0.5 by 0.5 degree grid (Version 3.0). ISRIC-World Soil Information, Wageningen.

Battin, T.J. et al., 2009. The boundless carbon cycle. Nature Geoscience, 2(9): 598.

Beguería, S., Vicente-Serrano, S.M., Reig, F. and Latorre, B., 2014. Standardized precipitation evapotranspiration index (SPEI) revisited: parameter fitting, evapotranspiration models, tools, datasets and drought monitoring. International Journal of Climatology, 34(10): 3001-3023.

Bird, M.I. et al., 2017. Loss and gain of carbon during char degradation. Soil Biology and Biochemistry, 106: 80-89.

Bird, M.I., Wynn, J.G., Saiz, G., Wurster, C.M. and McBeath, A., 2015. The pyrogenic carbon cycle. Annual Review of Earth and Planetary Sciences, 43: 273-298.

Black, T. et al., 2000. Increased carbon sequestration by a boreal deciduous forest in years with a warm spring. Geophysical Research Letters, 27(9): 1271-1274.

Blauhut, V. et al., 2016. Estimating drought risk across Europe from reported drought impacts, drought indices, and vulnerability factors. Hydrology and Earth System Sciences, 20(7): 2779-2800.

Boese, S., Jung, M., Carvalhais, N., Teuling, A.J. and Reichstein, M., 2019. Carbon–water flux coupling under progressive drought. Biogeosciences, 16(13): 2557-2572.

Borken, W., Ahrens, B., Schulz, C. and Zimmermann, L., 2011. Site-to-site variability and temporal trends of DOC concentrations and fluxes in temperate forest soils. Global Change Biology, 17(7): 2428-2443.

Brewer, N.W. et al., 2013. Fuel moisture influences on fire-altered carbon in masticated fuels: An experimental study. Journal of Geophysical Research: Biogeosciences, 118(1): 30-40.

Bring, J., 1994. How to standardize regression coefficients. The American Statistician, 48(3): 209-213.

Butman, D. and Raymond, P.A., 2011. Significant efflux of carbon dioxide from streams and rivers in the United States. Nature Geoscience, 4(12): 839.

Butman, D. et al., 2016. Aquatic carbon cycling in the conterminous United States and implications for terrestrial carbon accounting. Proceedings of the National Academy of Sciences, 113(1): 58-63.

Catalán, N., Marcé, R., Kothawala, D.N. and Tranvik, L.J., 2016. Organic carbon decomposition rates controlled by water retention time across inland waters. Nature Geoscience, 9(7): 501.

Chapin, F.S. et al., 2006. Reconciling carbon-cycle concepts, terminology, and methods. Ecosystems, 9(7): 1041-1050.

Chen, C., Wei, X., Weiskittel, A. and Hayes, D.J., 2019. Above-ground carbon stock in merchantable trees not reduced between cycles of spruce budworm outbreaks due to changing species composition in spruce-fir forests of Maine, USA. Forest Ecology and Management, 453: 117590.

Chen, G., Hayes, D.J. and McGuire, A.D., 2017. Contributions of wildland fire to terrestrial ecosystem carbon dynamics in North America from 1990-2012. Global Biogeochemical Cycles.

Chen, H. et al., 2015. Effects of nitrogen deposition on carbon cycle in terrestrial ecosystems of China: A meta-analysis. Environmental Pollution, 206: 352-360. https://doi.org/10.1016/j.foreco.2019.117590

Ciais, Reichstein, M., Viovy, N. and Granier, A., 2005. Europe-wide reduction in primary productivity caused by the heat and drought in 2003. Nature, 437(7058): 529.

Clark, J. et al., 2010. The importance of the relationship between scale and process in understanding long-term DOC dynamics. Science of the Total Environment, 408(13): 2768-2775.

Clay, G.D. and Worrall, F., 2011. Charcoal production in a UK moorland wildfire–How important is it? Journal of Environmental Management, 92(3): 676-682.

Cole, J.J. et al., 2007. Plumbing the global carbon cycle: integrating inland waters into the terrestrial carbon budget. Ecosystems, 10(1): 172-185.

Comery, J. A. (1981). Elemental carbon deposition and flux from prescribed burning on a longleaf pine site in Florida (Doctoral dissertation, University of Washington).

Cooke, W.F. and Wilson, J.J., 1996. A global black carbon aerosol model. Journal of Geophysical Research: Atmospheres, 101(D14): 19395-19409.

Cotrufo, M.F. et al., 2016. Quantification of pyrogenic carbon in the environment: An integration of analytical approaches. Organic Geochemistry, 100: 42-50.

Cox, P.M., Betts, R.A., Jones, C.D., Spall, S.A. and Totterdell, I.J., 2000. Acceleration of global warming due to carbon-cycle feedbacks in a coupled climate model. Nature, 408(6809): 184.

Coynel, A., Seyler, P., Etcheber, H., Meybeck, M. and Orange, D., 2005. Spatial and seasonal dynamics of total suspended sediment and organic carbon species in the Congo River. Global Biogeochemical Cycles, 19(4).

Creed, I., Sanford, S., Beall, F., Molot, L. and Dillon, P., 2003. Cryptic wetlands: integrating hidden wetlands in regression models of the export of dissolved organic carbon from forested landscapes. Hydrological Processes, 17(18): 3629-3648.

Creed, I.F. et al., 2018. Global change-driven effects on dissolved organic matter composition: Implications for food webs of northern lakes. Global Change Biology, 24(8): 3692-3714.

Crutzen, P.J. and Andreae, M.O., 1990. Biomass burning in the tropics: Impact on atmospheric chemistry and biogeochemical cycles. Science, 250(4988): 1669-1679.

Cuss, C. and Guéguen, C., 2015. Relationships between molecular weight and fluorescence properties for size-fractionated dissolved organic matter from fresh and aged sources. Water Research, 68: 487-497.

Czimczik, C., Schmidt, M. and Schulze, E.D., 2005. Effects of increasing fire frequency on black carbon and organic matter in Podzols of Siberian Scots pine forests. European Journal of Soil Science, 56(3): 417-428.

Czimczik, C.I., Preston, C.M., Schmidt, M.W.I. and Schulze, E.D., 2003. How surface fire in Siberian Scots pine forests affects soil organic carbon in the forest floor: Stocks, molecular structure, and conversion to black carbon (charcoal). Global Biogeochemical Cycles, 17(1).

Dai, A., Trenberth, K.E. and Qian, T., 2004. A global dataset of Palmer Drought Severity Index for 1870–2002: Relationship with soil moisture and effects of surface warming. Journal of Hydrometeorology, 5(6): 1117-1130.

de Wit, H.A. et al., 2016. Current browning of surface waters will be further promoted by wetter climate. Environmental Science & Technology Letters, 3(12): 430-435.

Delmas, R.A., Loudjani, P., Podaire, A. and Menaut, J.-C., 1991. Biomass burning in Africa: As assessment of annually burned biomass, *In* Global biomass burning. Atmospheric, climatic, and biospheric implications.

Dixon, R.K. et al., 1994. Carbon pools and flux of global forest ecosystems. Science, 263(5144): 185-190.

Dosskey, M.G. and Bertsch, P.M., 1994. Forest sources and pathways of organic matter transport to a blackwater stream: a hydrologic approach. Biogeochemistry, 24(1): 1-19.

Doughty, C.E. et al., 2015. Drought impact on forest carbon dynamics and fluxes in Amazonia. Nature, 519(7541): 78.

Drake, T.W., Raymond, P.A. and Spencer, R.G., 2018. Terrestrial carbon inputs to inland waters: A current synthesis of estimates and uncertainty. Limnology and Oceanography Letters, 3(3): 132-142.

Eckmeier, E., Gerlach, R., Skjemstad, J., Ehrmann, O. and Schmidt, M., 2007. Minor changes in soil organic carbon and charcoal concentrations detected in a temperate deciduous forest a year after an experimental slash-and-burn. Biogeosciences, 4(3): 377-383.

Fearnside, P.M. and Barbosa, R.I., 1996. Political benefits as barriers to assessment of environmental costs in Brazil's Amazonian development planning: The example of the Jatapu Dam in Roraima. Environmental Management, 20(5): 615.

Fearnside, P.M., Barbosa, R.I. and de Alencastro Graça, P.M.L., 2007. Burning of secondary forest in Amazonia: Biomass, burning efficiency and charcoal formation during land preparation for agriculture in Apiaú, Roraima, Brazil. Forest Ecology and Management, 242(2-3): 678-687.

Fearnside, P.M., de Alencastro Graça, P.M.c.L. and Rodrigues, F.J.A., 2001. Burning of Amazonian rainforests: burning efficiency and charcoal formation in forest cleared for cattle pasture near Manaus, Brazil. Forest Ecology and Management, 146(1): 115-128.

Fearnside, P.M., Leal, N. and Fernandes, F.M., 1993. Rainforest burning and the global carbon budget: biomass, combustion efficiency, and charcoal formation in the Brazilian Amazon. Journal of Geophysical Research: Atmospheres, 98(D9): 16733-16743.

Field, A., 2009. Discovering Statistics through SPSS:(and sex and drugs and rock'n'roll). Thousand Oaks, CA, USA: Sage Publications.

Findlay, S.E., 2005. Increased carbon transport in the Hudson River: unexpected consequence of nitrogen deposition? Frontiers in Ecology and the Environment, 3(3): 133-137.

Finkral, A.J., Evans, A.M., Sorensen, C.D. and Affleck, D.L., 2012. Estimating consumption and remaining carbon in burned slash piles. Canadian Journal of Forest Research, 42(9): 1744-1749.

Fisher, J.B., Huntzinger, D.N., Schwalm, C.R. and Sitch, S., 2014. Modeling the terrestrial biosphere. Annual Review of Environment and Resources, 39: 91-123.

Foken, T., Aubinet, M. and Leuning, R., 2012. The eddy covariance method, Eddy covariance. Springer, pp. 1-19. Dordrecht.

Forbes, M.S., Raison, R.J. and Skjemstad, J.O., 2006. Formation, transformation and transport of black carbon (charcoal) in terrestrial and aquatic ecosystems. Science of the Total Environment, 370(1): 190-206.

Frank, D. et al., 2015. Effects of climate extremes on the terrestrial carbon cycle: concepts, processes and potential future impacts. Global change biology, 21(8): 2861-2880.

French, N.H. et al., 2011. Model comparisons for estimating carbon emissions from North American wildland fire. Journal of Geophysical Research: Biogeosciences, 116(G4).

Futter, M. et al., 2007. Modeling the mechanisms that control in-stream dissolved organic carbon dynamics in upland and forested catchments. Water Resources Research, 43(2).

Futter, M. et al., 2011. Simulating dissolved organic carbon dynamics at the Swedish integrated monitoring sites with the integrated catchments model for carbon, INCA-C. Ambio, 40(8): 906-919.

Gardner, R., O'neill, R., Mankin, J. and Carney, J., 1981. A comparison of sensitivity analysis and error analysis based on a stream ecosystem model. Ecological Modelling, 12(3): 173-190.

Giglio, L., Randerson, J.T. and Werf, G.R., 2013. Analysis of daily, monthly, and annual burned area using the fourth-generation global fire emissions database (GFED4). Journal of Geophysical Research: Biogeosciences, 118(1): 317-328.

Gouveia, C., Trigo, R., Beguería, S. and Vicente-Serrano, S., 2017. Drought impacts on vegetation activity in the Mediterranean region: An assessment using remote sensing data and multi-scale drought indicators. Global and Planetary Change, 151: 15-27.

Graça, P.M.c.L., Fearnside, P.M. and Cerri, C.C., 1999. Burning of Amazonian forest in Ariquemes, Rondônia, Brazil: biomass, charcoal formation and burning efficiency. Forest Ecology and Management, 120(1): 179-191.

Graetz, R. D., & Skjemstad, J. O. (2003). The charcoal sink of biomass burning on the Australian continent (Vol. 64, pp. 1-61). CSIRO Atmospheric Research.

Granier, A. et al., 2007. Evidence for soil water control on carbon and water dynamics in European forests during the extremely dry year: 2003. Agricultural and Forest Meteorology, 143(1-2): 123-145.

Greenwood, S. et al., 2017. Tree mortality across biomes is promoted by drought intensity, lower wood density and higher specific leaf area. Ecology letters, 20(4): 539-553.

Guggenberger, G. and Kaiser, K., 2003. Dissolved organic matter in soil: challenging the paradigm of sorptive preservation. Geoderma, 113(3-4): 293-310.

Hamby, D., 1994. A review of techniques for parameter sensitivity analysis of environmental models. Environmental Monitoring and Sssessment, 32(2): 135-154.

Hanson, P. C., Hamilton, D. P., Stanley, E. H., Preston, N., Langman, O. C., & Kara, E. L. (2011). Fate of allochthonous dissolved organic carbon in lakes: a quantitative approach. PLoS One, 6(7).

Hao, W.M., Liu, M.-H. and Crutzen, P.J., 1990. Estimates of annual and regional releases of CO2 and other trace gases to the atmosphere from fires in the tropics, based on the FAO statistics for the period 1975–1980, Fire in the Tropical Biota. Springer, pp. 440-462.

Harrison, J.A., Caraco, N. and Seitzinger, S.P., 2005. Global patterns and sources of dissolved organic matter export to the coastal zone: Results from a spatially explicit, global model. Global Biogeochemical Cycles, 19(4).

Hayes, D. and Turner, D., 2012. The need for “apples-to-apples” comparisons of carbon dioxide source and sink estimates. Eos, Transactions American Geophysical Union, 93(41): 404-405.

Hayes, D.J. et al., 2011. Is the northern high-latitude land-based CO_2 sink weakening? Global Biogeochemical Cycles, 25(3).

Hayes, D.J. et al., 2012. Reconciling estimates of the contemporary North American carbon balance among terrestrial biosphere models, atmospheric inversions, and a new approach for estimating net ecosystem exchange from inventory-based data. Global Change Biology, 18(4): 1282-1299.

Hayes, D. J., R. Vargas, S. R. Alin, R. T. Conant, L. R. Hutyra, A. R. Jacobson, W. A. Kurz, S. Liu, A. D. McGuire, B. Poulter, and C. W. Woodall, 2018: Chapter 2: The North American carbon budget. In Second State of the Carbon Cycle Report (SOCCR2): A Sustained Assessment Report [Cavallaro, N., G. Shrestha, R. Birdsey, M. A. Mayes, R. G. Najjar, S. C. Reed, P. Romero-Lankao, and Z. Zhu (eds.)]. U.S. Global Change Research Program, Washington, DC, USA, pp. 71-108, https://doi.org/10.7930/SOCCR2.2018.Ch2.

He, B., Huang, L., Chen, Z. and Wang, H., 2018. Weakening sensitivity of global vegetation to long-term droughts. Science China Earth Sciences, 61(1): 60-70.

Heimann, M. and Reichstein, M., 2008. Terrestrial ecosystem carbon dynamics and climate feedbacks. Nature, 451(7176): 289.

Hirsch, R.M., Moyer, D.L. and Archfield, S.A., 2010. Weighted regressions on time, discharge, and season (WRTDS), with an application to Chesapeake Bay river inputs 1. JAWRA Journal of the American Water Resources Association, 46(5): 857-880.

Hope, D., Billett, M. and Cresser, M., 1994. A review of the export of carbon in river water: fluxes and processes. Environmental Pollution, 84(3): 301-324.

Huang, J., Yu, H., Dai, A., Wei, Y. and Kang, L., 2017. Drylands face potential threat under 2 C global warming target. Nature Climate Change, 7(6): 417.

Huang, S. et al., 2011. Analysis of nitrogen controls on carbon and water exchanges in a conifer forest using the CLASS-CTEM N+ model. Ecological Modelling, 222(20): 3743-3760.

Huete, A.R. et al., 2006. Amazon rainforests green-up with sunlight in dry season. Geophysical Research Letters, 33(6).

Huntzinger, D. et al., 2017. Uncertainty in the response of terrestrial carbon sink to environmental drivers undermines carbon-climate feedback predictions. Scientific Reports, 7(1), 1-8.

Huntzinger, D. et al., 2014. NACP MsTMIP summary of model structure and characteristics. ORNL DAAC.

Huntzinger, D.N. et al., 2013. The north american carbon program multi-scale synthesis and terrestrial model intercomparison project–part 1: Overview and experimental design. Geoscientific Model Development, 6(6): 2121-2133.

Hurst, D.F., Griffith, D.W.T. and Cook, G.D., 1994. Trace gas emissions from biomass burning in tropical Australian savannas. Journal of Geophysical Research: Atmospheres, 99(D8): 16441-16456.

Huston, M.A. and Wolverton, S., 2009. The global distribution of net primary production: resolving the paradox. Ecological Monographs, 79(3): 343-377.

Ito, A., 2010. Changing ecophysiological processes and carbon budget in East Asian ecosystems under near-future changes in climate: implications for long-term monitoring from a process-based model. Journal of Plant Research, 123(4): 577-588.

Jager, D.F., Wilmking, M. and Kukkonen, J.V., 2009. The influence of summer seasonal extremes on dissolved organic carbon export from a boreal peatland catchment: Evidence from one dry and one wet growing season. Science of the Total Environment, 407(4): 1373-1382.

Jenkins, M.E., Bell, T.L., Poon, L.F., Aponte, C. and Adams, M.A., 2016. Production of pyrogenic carbon during planned fires in forests of East Gippsland, Victoria. Forest Ecology and Management, 373: 9-16.

Jones, D. and Willett, V., 2006. Experimental evaluation of methods to quantify dissolved organic nitrogen (DON) and dissolved organic carbon (DOC) in soil. Soil Biology and Biochemistry, 38(5): 991-999.

Kasischke, E.S. et al., 2013. Impacts of disturbance on the terrestrial carbon budget of North America. Journal of Geophysical Research: Biogeosciences, 118(1): 303-316.

Kauffman, J.B., Cummings, D., Ward, D. and Babbitt, R., 1995. Fire in the Brazilian Amazon: 1. Biomass, nutrient pools, and losses in slashed primary forests. Oecologia, 104(4): 397-408.

Keenan, T., Sabate, S. and Gracia, C., 2010. The importance of mesophyll conductance in regulating forest ecosystem productivity during drought periods. Global Change Biology, 16(3): 1019-1034.

Kicklighter, D.W. et al., 2013. Insights and issues with simulating terrestrial DOC loading of Arctic river networks. Ecological Applications, 23(8): 1817-1836.

King, A.W. et al., 2015. North America's net terrestrial CO_2 exchange with the atmosphere 1990-2009. Biogeosciences, 12(2): 399.

Klesse, S., Etzold, S. and Frank, D., 2016. Integrating tree-ring and inventory-based measurements of aboveground biomass growth: research opportunities and carbon cycle consequences from a large snow breakage event in the Swiss Alps. European Journal of Forest Research, 135(2): 297-311.

Kolus, H.R. et al., 2019. Land carbon models underestimate the severity and duration of drought's impact on plant productivity. Scientific Reports, 9(1): 1-10.

Kothawala, D.N. et al., 2015. The relative influence of land cover, hydrology, and in-stream processing on the composition of dissolved organic matter in boreal streams. Journal of Geophysical Research: Biogeosciences, 120(8): 1491-1505.

Kuhlbusch, T.A.J. et al., 1996. Black carbon formation by savanna fires: Measurements and implications for the global carbon cycle. Journal of Geophysical Research: Atmospheres, 101(D19): 23651-23665.

Kuhlbusch, T.A.J. and Crutzen, P.J., 1995. Toward a global estimate of black carbon in residues of vegetation fires representing a sink of atmospheric CO_2 and a source of O_2. Global Biogeochemical Cycles, 9(4): 491-501.

Kuhlbusch, T.A.J. and Crutzen, P.J., 1996. Black carbon, the global carbon cycle, and atmospheric carbon dioxide. Biomass Burning and Global Change, 1: 160-169.

Kuzyakov, Y., Bogomolova, I. and Glaser, B., 2014. Biochar stability in soil: Decomposition during eight years and transformation as assessed by compound-specific ^{14}C analysis. Soil Biology and Biochemistry, 70: 229-236.

Lacaux, J.P., Cachier, H. and Delmas, R., 1993. Biomass burning in Africa: An overview of its impact on atmospheric chemistry. Fire in the Environment: The Ecological, Atmospheric, and Climatic Importance of Vegetation Fires: 159-191.

Lajtha, K. and Jones, J., 2018. Forest harvest legacies control dissolved organic carbon export in small watersheds, western Oregon. Biogeochemistry, 140(3): 299-315.

Landry, J.S. and Matthews, H.D., 2017. The global pyrogenic carbon cycle and its impact on the level of atmospheric CO2 over past and future centuries. Global Change Biology. 23(8), 3205-3218.

Lauerwald, R. et al., 2017. ORCHILEAK (revision 3875): a new model branch to simulate carbon transfers along the terrestrial–aquatic continuum of the Amazon basin. Geoscientific Model Development Discuss, 1-58.

Le Quéré, C. et al., 2009. Trends in the sources and sinks of carbon dioxide. Nature Geoscience, 2(12): 831.

Li, H. et al., 2011. Evaluating runoff simulations from the Community Land Model 4.0 using observations from flux towers and a mountainous watershed. Journal of Geophysical Research: Atmospheres, 116(D24).

Li, M. et al., 2019. Modeling Global Riverine DOC Flux Dynamics From 1951 to 2015. Journal of Advances in Modeling Earth Systems, 11(2): 514-530.

Liski, J. et al., 2006. Carbon accumulation in Finland's forests 1922–2004–an estimate obtained by combination of forest inventory data with modelling of biomass, litter and soil. Annals of Forest Science, 63(7): 687-697.

Lobert, J.M. et al., 1991. Experimental evaluation of biomass burning emissions: Nitrogen and carbon containing compounds, Global biomass burning. Atmospheric, climatic, and biospheric implications.

Ludwig, W., Amiotte Suchet, P. and Probst, J.-L., 1996. River discharges of carbon to the world's oceans: determining local inputs of alkalinity and of dissolved and particulate organic carbon. Sciences de la terre et des planètes (Comptes rendus de l'Académie des sciences), 323: 1007-1014.

Maherali, H., Pockman, W.T. and Jackson, R.B., 2004. Adaptive variation in the vulnerability of woody plants to xylem cavitation. Ecology, 85(8): 2184-2199.

Mao, J. et al., 2013. Global latitudinal-asymmetric vegetation growth trends and their driving mechanisms: 1982–2009. Remote Sensing, 5(3): 1484-1497.

Mao, J., Thornton, P.E., Shi, X., Zhao, M. and Post, W.M., 2012. Remote sensing evaluation of CLM4 GPP for the period 2000-2009. Journal of Climate, 25(15): 5327-5342.

Marle, M.J. et al., 2017. Fire and deforestation dynamics in Amazonia (1973–2014). Global Biogeochemical Cycles, 31(1): 24-38.

Maurcio, L. D. A. G. P., Fearnside, P. M., & Cerri, C. C. (1999). Burning of Amazonian forest in Ariquemes, Rondônia, Brazil: biomass, charcoal formation and burning efficiency. Forest ecology and Management, 120(1-3), 179-191.

McGuire, A.D. et al., 2000. Modelling carbon responses of tundra ecosystems to historical and projected climate: Sensitivity of pan-Arctic carbon storage to temporal and spatial variation in climate. Global Change Biology, 6(S1): 141-159.

McGuire, K. et al., 2005. The role of topography on catchment-scale water residence time. Water Resources Research, 41(5).

McKee, T.B., Doesken, N.J. and Kleist, J., 1993. The relationship of drought frequency and duration to time scales, Proceedings of the 8th Conference on Applied Climatology. American Meteorological Society Boston, MA, pp. 179-183.

Meir, P., Metcalfe, D.B., Costa, A. and Fisher, R.A., 2008. The fate of assimilated carbon during drought: impacts on respiration in Amazon rainforests. Philosophical Transactions of the Royal Society of London B: Biological Sciences, 363(1498): 1849-1855.

Mekonnen, Z.A., Grant, R.F. and Schwalm, C., 2017. Carbon sources and sinks of North America as affected by major drought events during the past 30 years. Agricultural and Forest Meteorology, 244: 42-56.

Menaut, J.-C., Abbadie, L., Lavenu, F., Loudjani, P. and Podaire, A., 1991. Biomass burning in West African savannas, Global biomass burning. Atmospheric, climatic, and biospheric implications.

Meyer-Jacob, C., Tolu, J., Bigler, C., Yang, H. and Bindler, R., 2015. Early land use and centennial scale changes in lake-water organic carbon prior to contemporary monitoring. Proceedings of the National Academy of Sciences: 112(21), 6579-6584.

Michalzik, B., Kalbitz, K., Park, J.-H., Solinger, S. and Matzner, E., 2001. Fluxes and concentrations of dissolved organic carbon and nitrogen–a synthesis for temperate forests. Biogeochemistry, 52(2): 173-205.

Michalzik, B. et al., 2003. Modelling the production and transport of dissolved organic carbon in forest soils. Biogeochemistry, 66(3): 241-264.

Miesel, J.R., Reiner, A., Ewell, C. and Maestrini, B., 2018. Quantifying changes in total and pyrogenic carbon stocks across fire severity gradients using active wildfire incidents. Frontiers in Earth Science, 6: 41.

Myers-Smith, I.H. et al., 2011. Shrub expansion in tundra ecosystems: dynamics, impacts and research priorities. Environmental Research Letters, 6(4): 045509.

Myneni, R.B., Keeling, C., Tucker, C.J., Asrar, G. and Nemani, R.R., 1997. Increased plant growth in the northern high latitudes from 1981 to 1991. Nature, 386(6626): 698.

Nakhavali, M. et al., 2018. Representation of dissolved organic carbon in the JULES land surface model (vn4. 4-JULES-DOCM). Geoscientific Model Development.11, 593–609, https://doi.org/10.5194/gmd-11-593-2018.

National Atmospheric Deposition Program (NRSP-3). (2019). NADP Program Office, Wisconsin State Laboratory of Hygiene, 465 Henry Mall, Madison, WI 53706.

Neff, J.C. and Asner, G.P., 2001. Dissolved organic carbon in terrestrial ecosystems: synthesis and a model. Ecosystems, 4(1): 29-48.

NOAA National Centers for Environmental information, Climate at a Glance: Global Time Series, published March 2020, retrieved on March 28, 2020 from https://www.ncdc.noaa.gov/cag/

Oechel, W.C. et al., 1993. Recent change of Arctic tundra ecosystems from a net carbon dioxide sink to a source. Nature, 361(6412): 520.

Olson, D.M. et al., 2001. Terrestrial Ecoregions of the World: A New Map of Life on Earth: A new global map of terrestrial ecoregions provides an innovative tool for conserving biodiversity. Bioscience, 51(11): 933-938.

Pan, Y. et al., 2011. A large and persistent carbon sink in the world's forests. Science, 333(6045): 988-993.

Peñuelas, J. et al., 2007. Response of plant species richness and primary productivity in shrublands along a north–south gradient in Europe to seven years of experimental warming and drought: reductions in primary productivity in the heat and drought year of 2003. Global Change Biology, 13(12): 2563-2581.

Peters, W. et al., 2007. An atmospheric perspective on North American carbon dioxide exchange: CarbonTracker. Proceedings of the National Academy of Sciences of the United States of America, 104(48): 18925-18930.

Phillips, O.L. et al., 2010. Drought–mortality relationships for tropical forests. New Phytologist, 187(3): 631-646.

Pilegaard, K., Ibrom, A., Courtney, M.S., Hummelshøj, P. and Jensen, N.O., 2011. Increasing net CO2 uptake by a Danish beech forest during the period from 1996 to 2009. Agricultural and Forest Meteorology, 151(7): 934-946.

Pingree, M.R., Homann, P.S., Morrissette, B. and Darbyshire, R., 2012. Long and short-term effects of fire on soil charcoal of a conifer forest in southwest Oregon. Forests, 3(2): 353-369.

Porcal, P., Koprivnjak, J.-F., Molot, L.A. and Dillon, P.J., 2009. Humic substances—part 7: the biogeochemistry of dissolved organic carbon and its interactions with climate change. Environmental Science and Pollution Research, 16(6): 714-726.

Post, W.M., King, A.W. and Wullschleger, S.D., 1997. Historical variations in terrestrial biospheric carbon storage. Global Biogeochemical Cycles, 11(1): 99-109.

Prentice, I.C. et al., 1992. Special paper: a global biome model based on plant physiology and dominance, soil properties and climate. Journal of Biogeography: 117-134.

Preston, C.M. and Schmidt, M.W.I., 2006. Black (pyrogenic) carbon in boreal forests: a synthesis of current knowledge and uncertainties. Biogeosciences Discussions, 3(1): 211-271.

Qi, L., Li, Q., Li, Y. and He, C., 2017. Factors controlling black carbon distribution in the Arctic. Atmospheric Chemistry and Physics, 17(2): 1037-1059.

Qualls, R.G. and Haines, B.L., 1992. Biodegradability of dissolved organic matter in forest throughfall, soil solution, and stream water. Soil Science Society of America Journal, 56(2): 578-586.

Raymond, P.A. and Saiers, J.E., 2010. Event controlled DOC export from forested watersheds. Biogeochemistry, 100(1-3): 197-209.

Raymond, P.A., Saiers, J.E. and Sobczak, W.V., 2016. Hydrological and biogeochemical controls on watershed dissolved organic matter transport: Pulse-shunt concept. Ecology, 97(1): 5-16.

Regnier, P. et al., 2013. Anthropogenic perturbation of the carbon fluxes from land to ocean. Nature Geoscience, 6(8): 597.

Ren, W. et al., 2016. Century-long increasing trend and variability of dissolved organic carbon export from the Mississippi River basin driven by natural and anthropogenic forcing. Global Biogeochemical Cycles, 30(9): 1288-1299.

Righi, C.A., de Alencastro Graça, P.M.L., Cerri, C.C., Feigl, B.J. and Fearnside, P.M., 2009. Biomass burning in Brazil's Amazonian “arc of deforestation”: Burning efficiency and charcoal formation in a fire after mechanized clearing at Feliz Natal, Mato Grosso. Forest Ecology and Management, 258(11): 2535-2546.

Rosén, P., Cunningham, L., Vonk, J. and Karlssona, J., 2009. Effects of climate on organic carbon and the ratio of planktonic to benthic primary producers in a subarctic lake during the past 45 years. Limnology and Oceanography, 54(5): 1723-1732.

Rowe, E. et al., 2014. Predicting nitrogen and acidity effects on long-term dynamics of dissolved organic matter. Environmental Pollution, 184: 271-282.

Royer, T.V. and David, M.B., 2005. Export of dissolved organic carbon from agricultural streams in Illinois, USA. Aquatic Sciences, 67(4): 465-471.

Rüegg, J., Eichmiller, J.J., Mladenov, N. and Dodds, W.K., 2015. Dissolved organic carbon concentration and flux in a grassland stream: spatial and temporal patterns and processes from long-term data. Biogeochemistry, 125(3): 393-408.

Saiz, G. et al., 2014. Pyrogenic carbon from tropical savanna burning: production and stable isotope composition. Biogeosciences Discussions, 11(10): 15149-15183.

SanClements, M.D., Oelsner, G.P., McKnight, D.M., Stoddard, J.L. and Nelson, S.J., 2012. New insights into the source of decadal increases of dissolved organic matter in acid-sensitive lakes of the Northeastern United States. Environmental Science & Technology, 46(6): 3212-3219.

Santín, C. et al., 2016. Towards a global assessment of pyrogenic carbon from vegetation fires. Global Change Biology, 22(1): 76-91.

Santín, C., Doerr, S.H., Preston, C.M. and González-Rodríguez, G., 2015. Pyrogenic organic matter production from wildfires: a missing sink in the global carbon cycle. Global Change Biology, 21(4): 1621-1633.

Sawicka, K., Monteith, D., Vanguelova, E., Wade, A.J. and Clark, J.M., 2016. Fine-scale temporal characterization of trends in soil water dissolved organic carbon and potential drivers. Ecological indicators, 68: 36-51.

Schaefer, K. et al., 2008. Combined simple biosphere/Carnegie-Ames-Stanford approach terrestrial carbon cycle model. Journal of Geophysical Research: Biogeosciences, 113(G3).

Schaefer, K. et al., 2009. Improving simulated soil temperatures and soil freeze/thaw at high-latitude regions in the Simple Biosphere/Carnegie-Ames-Stanford Approach model. Journal of Geophysical Research: Earth Surface, 114(F2).

Schmidt, M.W.I. and Noack, A.G., 2000. Black carbon in soils and sediments: analysis, distribution, implications, and current challenges. Global Biogeochemical Cycles, 14(3): 777-793.

Schuh, A.E. et al., 2019. Quantifying the impact of atmospheric transport uncertainty on CO2 surface flux estimates. Global Biogeochemical Cycles, 33(4): 484-500.

Schulze, K., Borken, W. and Matzner, E., 2011. Dynamics of dissolved organic ^{14}C in throughfall and soil solution of a Norway spruce forest. Biogeochemistry, 106(3): 461-473.

Schwalm et al., 2015. Toward "optimal" integration of terrestrial biosphere models. Geophysical Research Letters, 42(11): 4418-4428.

Schwalm, C.R. et al., 2017. Global patterns of drought recovery. Nature, 548(7666), 202-205.

Schwalm, C.R. et al., 2010. Assimilation exceeds respiration sensitivity to drought: A FLUXNET synthesis. Global Change Biology, 16(2): 657-670.

Scott, R.L., Jenerette, G.D., Potts, D.L. and Huxman, T.E., 2009. Effects of seasonal drought on net carbon dioxide exchange from a woody-plant-encroached semiarid grassland. Journal of Geophysical Research: Biogeosciences, 114(G4).

Seaber, P.R., Kapinos, F.P. and Knapp, G.L., 1987. Hydrologic unit maps.

Seiler, W. and Crutzen, P.J., 1980. Estimates of gross and net fluxes of carbon between the biosphere and the atmosphere from biomass burning. Climatic Change, 2(3): 207-247.

Singh, N. et al., 2014. Transformation and stabilization of pyrogenic organic matter in a temperate forest field experiment. Global Change Biology, 20(5): 1629-1642.

Sinsabaugh, R., Zak, D., Gallo, M., Lauber, C. and Amonette, R., 2004. Nitrogen deposition and dissolved organic carbon production in northern temperate forests. Soil Biology and Biochemistry, 36(9): 1509-1515.

Sitch, S. et al., 2003. Evaluation of ecosystem dynamics, plant geography and terrestrial carbon cycling in the LPJ dynamic global vegetation model. Global Change Biology, 9(2): 161-185.

Sloan, S., Locatelli, B., Wooster, M.J. and Gaveau, D.L., 2017. Fire activity in Borneo driven by industrial land conversion and drought during El Niño periods, 1982–2010. Global Environmental Change, 47: 95-109.

Sokol, N.W. and Bradford, M.A., 2019. Microbial formation of stable soil carbon is more efficient from belowground than aboveground input. Nature Geoscience, 12(1): 46.

Soil Survey Staff. Gridded Soil Survey Geographic (gSSURGO) Database for the Conterminous United States. United States Department of Agriculture, Natural Resources Conservation Service. Available online at https://gdg.sc.egov.usda.gov/. November 16, 2019 (FY2019 official release).

Solomon, C.T. et al., 2015. Ecosystem consequences of changing inputs of terrestrial dissolved organic matter to lakes: current knowledge and future challenges. Ecosystems, 18(3): 376-389.

Solomon, S. et al., 2007. Contribution of working group I to the fourth assessment report of the intergovernmental panel on climate change, 2007. Cambridge University Press, Cambridge.

Søndergaard, M., Borch, N.H. and Riemann, B., 2000. Dynamics of biodegradable DOC produced by freshwater plankton communities. Aquatic Microbial Ecology, 23(1): 73-83.

Stets, E.G. and Striegl, R.G., 2012. Carbon export by rivers draining the conterminous United States. Inland Waters, 2(4): 177-184.

Stocker, B.D. et al., 2019. Drought impacts on terrestrial primary production underestimated by satellite monitoring. Nature Geoscience, 12(4): 264.

Tank, S.E., Fellman, J.B., Hood, E. and Kritzberg, E.S., 2018. Beyond respiration: Controls on lateral carbon fluxes across the terrestrial-aquatic interface. Limnology and Oceanography Letters, 3(3): 76-88.

Teuling, A.J., Uijlenhoet, R., Hupet, F. and Troch, P.A., 2006. Impact of plant water uptake strategy on soil moisture and evapotranspiration dynamics during drydown. Geophysical Research Letters, 33(3).

Thompson, D., Schiks, T. and Wotton, B., 2016. Fuel size impacts on carbon residuals and combustion dynamics in masticated woody debris. Forest Ecology and Management, 369: 59-65.

Thornton, M.M., P.E. Thornton, Y. Wei, R.S. Vose, and A.G. Boyer. 2017. Daymet: Station-Level Inputs and Model Predicted Values for North America, Version 3. ORNL DAAC, Oak Ridge, Tennessee, USA. https://doi.org/10.3334/ORNLDAAC/1391

Tinker, D.B. and Knight, D.H., 2000. Coarse woody debris following fire and logging in Wyoming lodgepole pine forests. Ecosystems, 3(5): 472-483.

Tolk, J.A., 2003. Plant available soil water. Encyclopedia of water science. New York, NY, USA: Marcel-Dekker, Inc: 669-672.

Tranvik, L.J., Cole, J.J. and Prairie, Y.T., 2018. The study of carbon in inland waters—from isolated ecosystems to players in the global carbon cycle. Limnology and Oceanography letters, 3(3): 41-48.

van den Dool, H., Huang, J. and Fan, Y., 2003. Performance and analysis of the constructed analogue method applied to US soil moisture over 1981–2001. Journal of Geophysical Research: Atmospheres, 108(D16).

van der Molen, M.K. et al., 2011. Drought and ecosystem carbon cycling. Agricultural and Forest Meteorology, 151(7): 765-773.

van der Werf, G. R., Randerson, J. T., Giglio, L., van Leeuwen, T. T., Chen, Y., Rogers, B. M., ... & Yokelson, R. J. (2017). Global fire emissions estimates during 1997–2015, Earth System Science Data. 9, 697–720, https://doi.org/10.5194/essd-9-697-2017.

van der Werf, G. et al., 2017. Global fire emissions estimates during 1997–2015, Earth Syst. Sci. Data Discuss.

van der Werf, G.R. et al., 2010. Global fire emissions and the contribution of deforestation, savanna, forest, agricultural, and peat fires (1997–2009). Atmospheric Chemistry and Physics, 10(23): 11707-11735.

Vargas, R. et al., 2010. Ecosystem CO2 fluxes of arbuscular and ectomycorrhizal dominated vegetation types are differentially influenced by precipitation and temperature. New Phytologist, 185(1): 226-236.

Vicente-Serrano, S.M., Beguería, S. and López-Moreno, J.I., 2010. A multiscalar drought index sensitive to global warming: the standardized precipitation evapotranspiration index. Journal of Climate, 23(7): 1696-1718.

Vicente-Serrano, S.M. et al., 2013. Response of vegetation to drought time-scales across global land biomes. Proceedings of the National Academy of Sciences, 110(1): 52-57.

Wagner, S., Jaffé, R. and Stubbins, A., 2018. Dissolved black carbon in aquatic ecosystems. Limnology and Oceanography Letters, 3(3): 168-185.

Ward, A., Cansler, C. and Larson, A., 2017. Black carbon on coarse woody debris in once-and twice-burned mixed-conifer forest. Fire Ecology, 13(2): 143-147.

Webster, K.L. and McLaughlin, J.W., 2010. Importance of the water table in controlling dissolved carbon along a fen nutrient gradient. Soil Science Society of America Journal, 74(6): 2254-2266.

Wei, X., Hayes, D.J., Fraver, S. and Chen, G., 2018. Global Pyrogenic Carbon Production During Recent Decades Has Created the Potential for a Large, Long-Term Sink of Atmospheric CO_2. Journal of Geophysical Research: Biogeosciences, 123(12): 3682-3696.

Wei, X. and Larsen, C., 2018. Assessing the Minimum Number of Time Since Last Fire Sample-Points Required to Estimate the Fire Cycle: Influences of Fire Rotation Length and Study Area Scale. Forests, 9(11): 708.

Wei, X. and Larsen, C.P., 2019. Methods to Detect Edge Effected Reductions in Fire Frequency in Simulated Forest Landscapes. ISPRS International Journal of Geo-Information, 8(6): 277.

Wei, Y. et al., 2014. The North American carbon program multi-scale synthesis and terrestrial model intercomparison project–Part 2: Environmental driver data. Geoscientific Model Development, 7(6): 2875-2893.

Welp, L., Randerson, J. and Liu, H., 2007. The sensitivity of carbon fluxes to spring warming and summer drought depends on plant functional type in boreal forest ecosystems. Agricultural and Forest Meteorology, 147(3-4): 172-185.

Weyhenmeyer, G.A. et al., 2012. Selective decay of terrestrial organic carbon during transport from land to sea. Global Change Biology, 18(1): 349-355.

Winterdahl, M., Laudon, H., Lyon, S.W., Pers, C. and Bishop, K., 2016. Sensitivity of stream dissolved organic carbon to temperature and discharge: Implications of future climates. Journal of Geophysical Research: Biogeosciences, 121(1): 126-144.

Worrall, F., Clay, G.D. and May, R., 2013. Controls upon biomass losses and char production from prescribed burning on UK moorland. Journal of Environmental Management, 120: 27-36.

Yang, L. et al., 2018. A new generation of the United States National Land Cover Database: Requirements, research priorities, design, and implementation strategies. ISPRS Journal of Photogrammetry and Remote Sensing, 146: 108-123.

Yin, Y., Liu, H., Liu, G., Hao, Q. and Wang, H., 2013. Vegetation responses to mid-Holocene extreme drought events and subsequent long-term drought on the southeastern Inner Mongolian Plateau, China. Agricultural and Forest Meteorology, 178: 3-9.

Zhang, Q., Shao, M., Jia, X. and Wei, X., 2019. Changes in soil physical and chemical properties after short drought stress in semi-humid forests. Geoderma, 338: 170-177.

Zhao, J. et al., 2019. An evaluation of the flux-gradient and the eddy covariance method to measure CH_4, CO_2, and H_2O fluxes from small ponds. Agricultural and Forest Meteorology, 275: 255-264.

Zhao, M. and Running, S.W., 2010. Drought-induced reduction in global terrestrial net primary production from 2000 through 2009. Science, 329(5994): 940-943.

Zscheischler, J. et al., 2014. Impact of large-scale climate extremes on biospheric carbon fluxes: an intercomparison based on MsTMIP data. Global Biogeochemical Cycles, 28(6): 585-600.

APPENDICES

APPENDIX A. SUPPORTING INFORMATION FOR CHAPTER 2

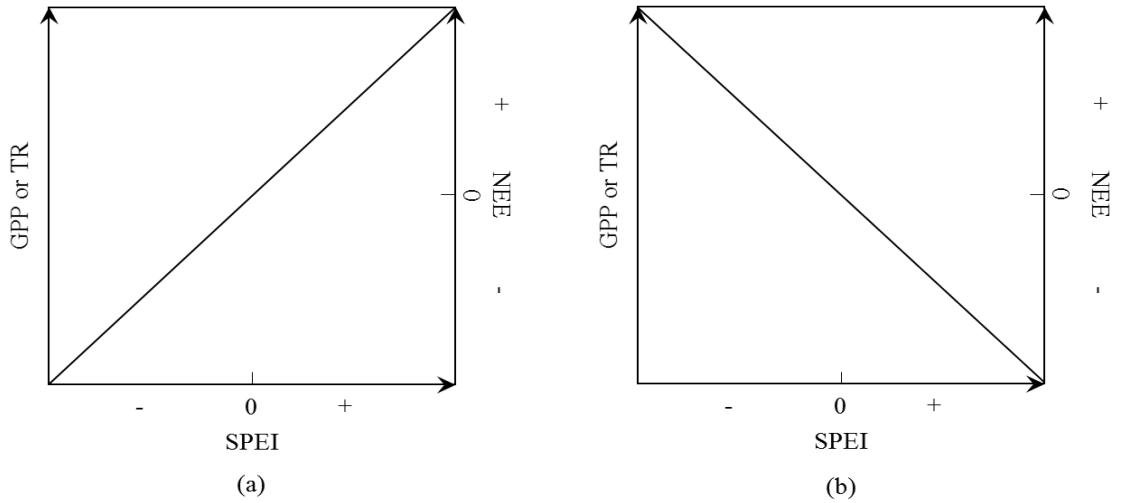

Figure A.1. The relationship between SPEI and carbon fluxes (i.e. GPP, TR, and NEE).

Both GPP and TR are expressed as positive values, while a negative value of NEE represents carbon uptake on land (carbon sink) and a positive value represents carbon release to the atmosphere (source). The positive relationship means that increasing droughts (decreasing value of SPEI) corresponds to a decrease value of GPP, TR or NEE (a), while a negative relationship means that increasing droughts corresponds to an increase in the value of GPP, TR or NEE (b).

APPENDIX B. SUPPORTING INFORMATION FOR CHAPTER 3

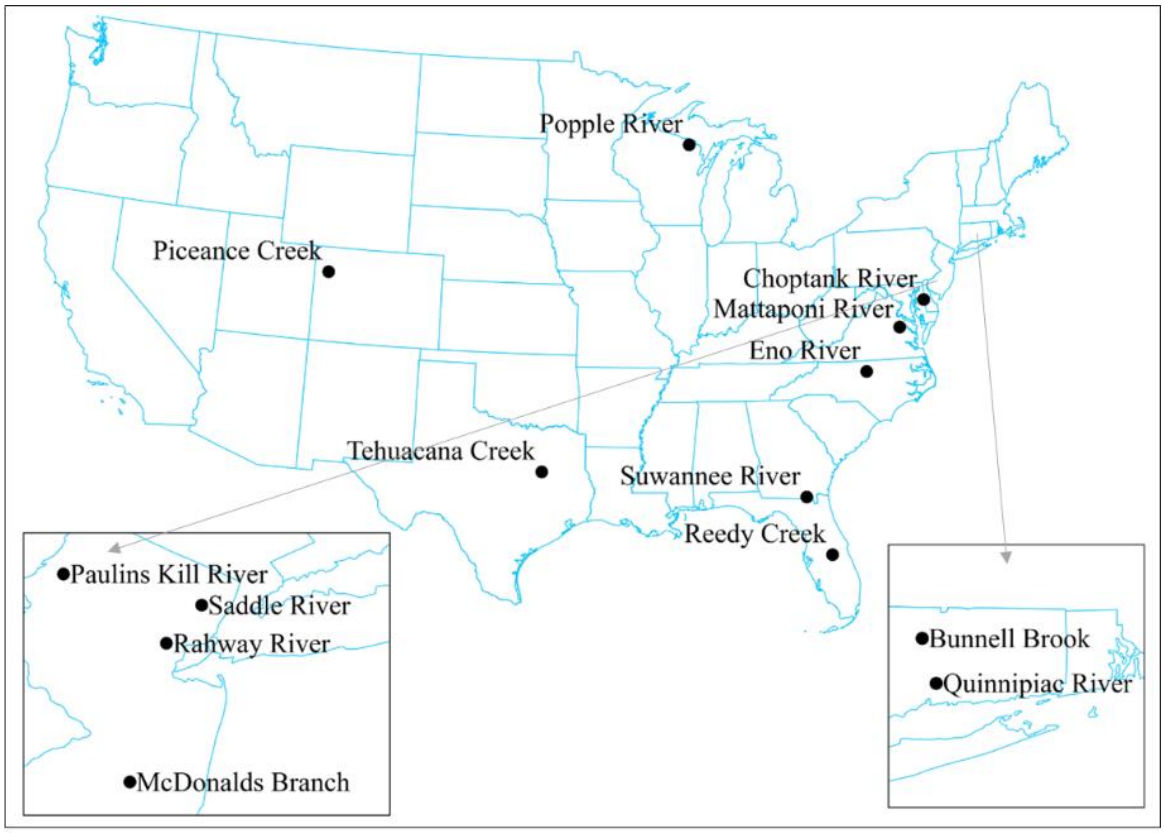

Figure B.1. Locations of the 14 watersheds.

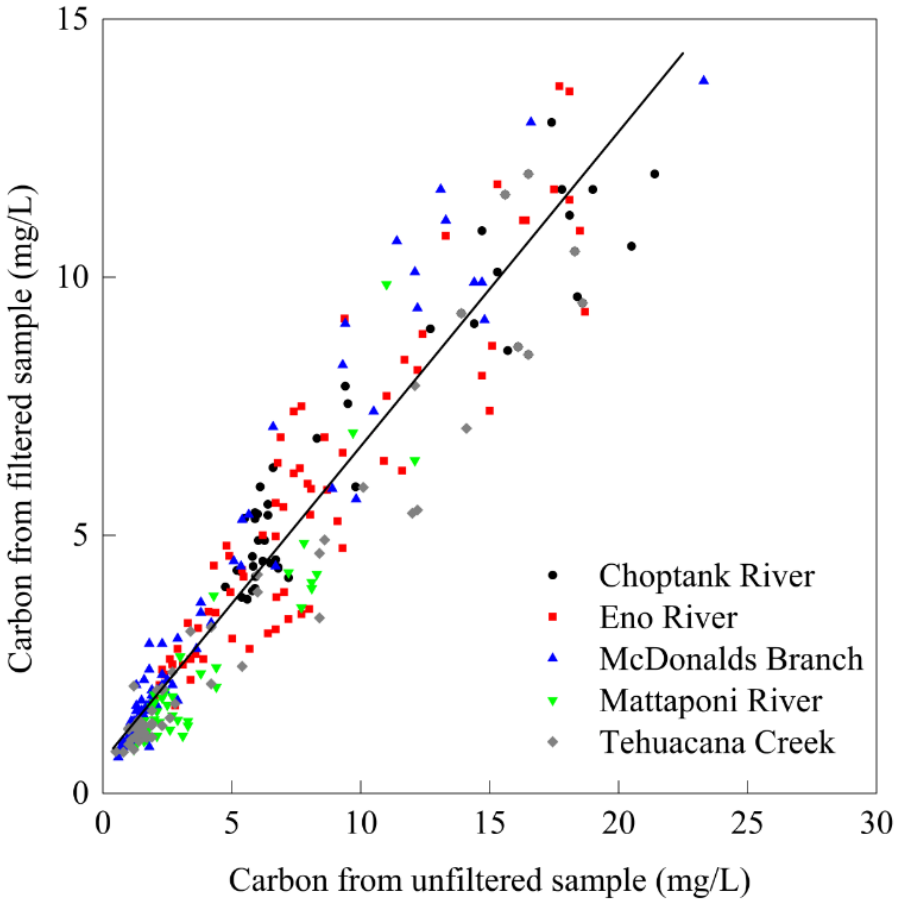

Figure B.2. The model used to modify the DOC concentrations measured from unfiltered waters samples.

To examine the relationship between the organic carbon concentrations measured from the filtered water samples and unfiltered water samples, 300 samples from 5 watersheds that measured the organic carbon from both filtered and unfiltered water samples were used to build a regression model ($y=0.60x+0.63$, $R^2=0.91$).

Table B.1 The hydrologic unit of each watershed and site numbers that used to obtain the discharge and DOC concentration data sets. They are defined by USGS.

Watershed	Hydrologic Unit	Site Number
Bunnell Brook	01080207	1188000
Quinnipiac River	01100004	1196500
McDonalds Branch	02040202	1466500
Paulins Kill River	02040105	1443500
Rahway River	02030104	1394500
Saddle River	02030103	1391500
Choptank River	02060005	1491000
Mattaponi River	02080105	1674500
Eno River	03020201	2085000
Suwannee River	03110201	2314500
Reedy Creek	03090101	2266300, 2266301
Popple River	04030108	4063700
Tehuacana Creek	12030201	8064700
Piceance Creek	14050006	9306200, 9306222

Table B.2. Land cover types.

This study	NLCD 2016
Wetland	Open water; Woody wetlands; Emergent wetland
Shrub	Shrub
Forest	Deciduous forest; Evergreen forest; Mixed forest
Grassland	Herbaceous
Agriculture Land	Hay/Pasture; Cultivated crops
Developed Area	Open space; Barren; Developed low, median, and high

The National Land Cover Database in 2016 (NLCD2016) has 16 land cover classes based on a modified Anderson Level II classification system at a 30-m spatial resolution. In this analysis, we condensed these 16 classes to six land cover types. The proportions of open water of the 14 watersheds ranged from 0.01% (Piceance Creek) to 5.03% (McDonalds Branch) with an average of 1.3%; the land cover 'Open water' was thus assigned to the wetland class. The land cover type 'Perennial ice/Snow' is not included in these watersheds.

APPENDIX C. SUPPORTING INFORMATION FOR CHAPTER 4

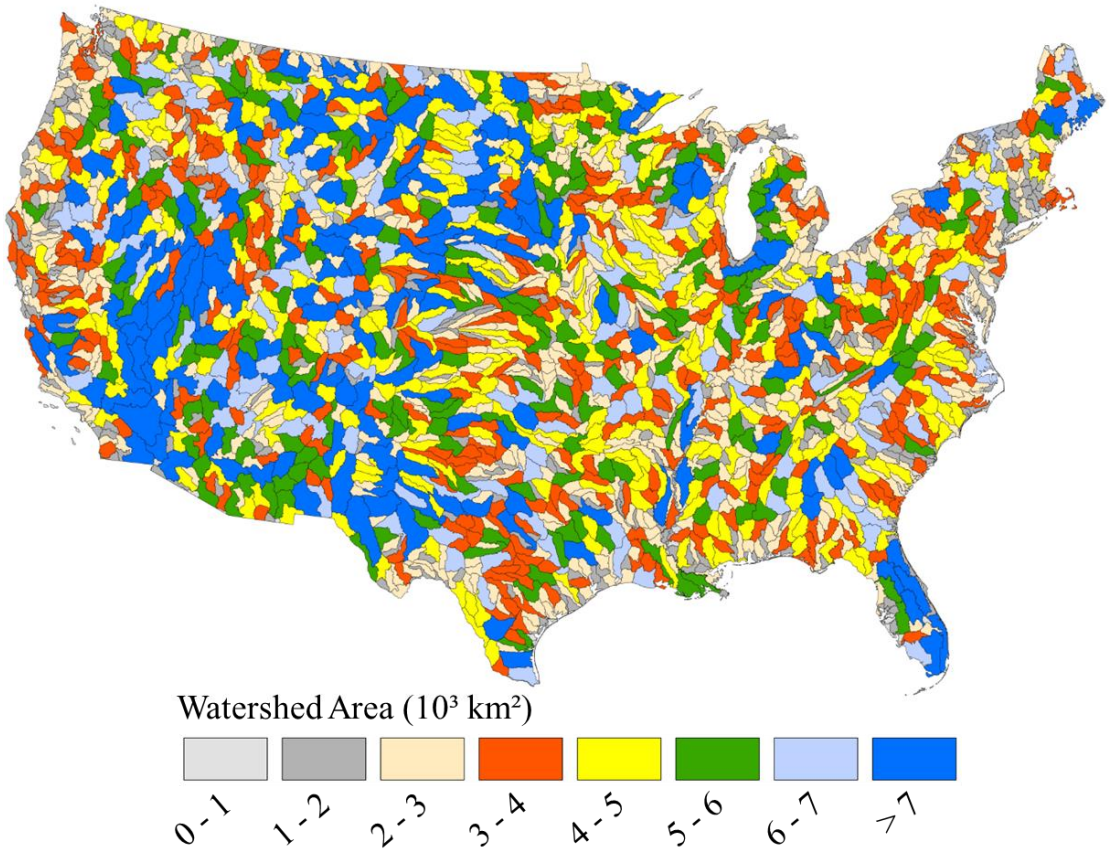

Figure C.1. Size of these 2110 watersheds.

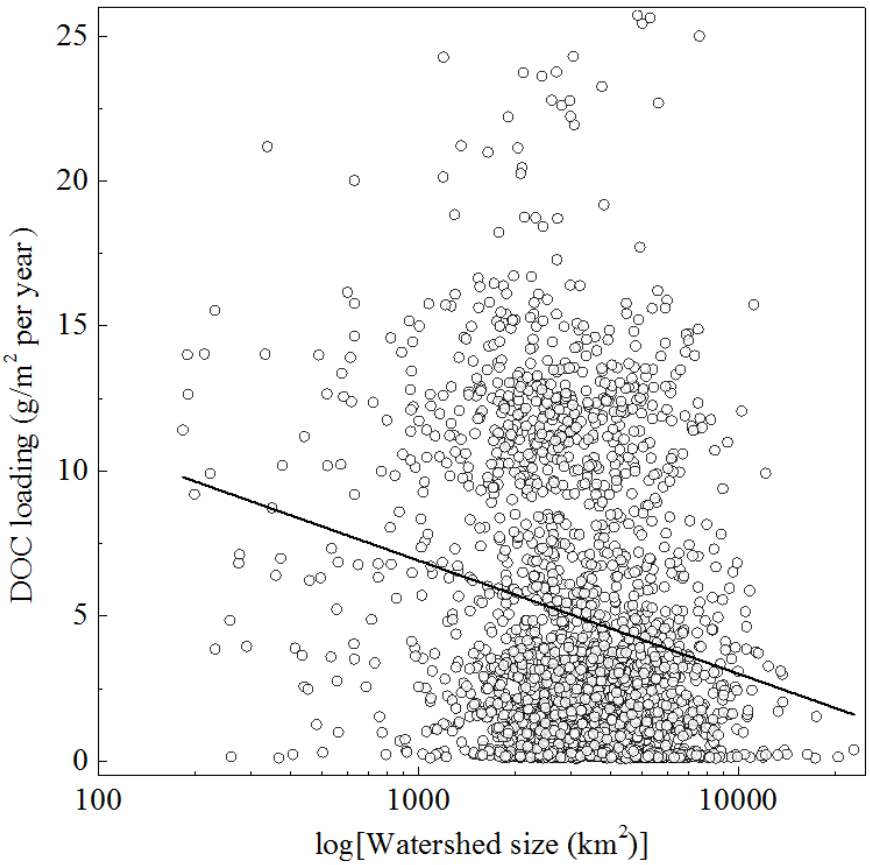

Figure C.2. The relationship between DOC loading from terrestrial to aquatic ecosystems estimated with TAF-DOC and the size of watershed.

The linear regression model is $y=-3.91x+18.63$, $R^2=0.05$.

BIOGRAPHY OF THE AUTHOR

Xinyuan Wei was born and raised in Hebei, China on April 24th, 1990. In 2013, he graduated from Nanjing Forest University and he received a Bachelor of Engineering degree from in Geographic Information System.

In the fall of 2013 Xinyuan was accepted to the University at Buffalo, SUNY as a Master's Student in the Department of Geography.

In summer of 2015 Xinyuan completed his Master's degree and remained in the Department of Geography. He worked as a research assistant for Chris Larsen for nine month.

In the summer of 2016, Xinyuan was accepted to the University of Maine, the School of Forest Resources for a PhD with Daniel Hayes. Xinyuan passed his comprehensive exams and became a candidate for a Doctorate of Philosophy in September 2018.

Xinyuan is a candidate for the Doctor of Philosophy degree in Forest Resources from the University of Maine in August 2020.